The Role of Organic Cation Transporters in the Disposition, Drug-Drug Interactions, and Tissue Toxicity of Amphetamines

David James Wagner

A dissertation

submitted in partial fulfillment of the

requirements for the degree of

Doctor of Philosophy

University of Washington

2018

Reading Committee:

Joanne Wang, Chair

Nina Isoherranen

William Atkins

Program Authorized to Offer Degree:

Pharmaceutics

University of Washington

Abstract

The Role of Organic Cation Transporters in the Disposition, Drug-Drug Interactions, and Tissue Toxicity of Amphetamines

David James Wagner

Chair of the Supervisory Committee:
Professor Joanne Wang
Department of Pharmaceutics

This dissertation research aims to elucidate the roles of organic cation transporters in the disposition, drug-drug interactions, and toxicity of methamphetamine. Work conducted in this dissertation research has elucidated the molecular mechanisms involved in transport and disposition of methamphetamine and its metabolites and provided novel insights into the in vivo significance of OCTs in the disposition, potential drug-drug interactions, and toxicities of this widely used drug of abuse.

In Chapter 2, I showed methamphetamine and its metabolites interact with hOCT1-3 and hMATE1/2-K at clinically relevant concentrations. I further demonstrated that methamphetamine and amphetamine are substrates of hOCT2, hMATE1, and hMATE2-K, suggesting that the hOCT2/hMATEs pathway is involved in renal secretion of methamphetamine and its metabolites.

Following the identification of complex transport kinetics in Chapter 2, Chapter 3 demonstrated that the apparent mechanism of inhibition depends on the substrate transport kinetics and sidedness of the inhibitory interaction. These findings suggest some hOCT2 substrates have spatially distinct binding sites within the binding region and may likely be transported simultaneously.

Chapter 4 determined the pharmacokinetics, tissue exposure, and partition ratios of methamphetamine and major metabolites in various mouse tissues and investigated the impact of Oct3 on the tissue-specific accumulation of *p*-OHMA. The data demonstrated that salivary glands are a novel site of exceedingly high accumulation of methamphetamine, amphetamine, and *p*-OHMA. Furthermore, Chapter 4 identified Oct3 as an important determinant of tissue uptake of and exposure to *p*-OHMA in salivary glands and skeletal muscle. These findings suggest that local tissue accumulation of methamphetamine and/or its metabolites may play a direct role in several of the reported peripheral toxicities of methamphetamine and Oct3 can significantly impact tissue exposure to drugs and drug metabolites independently from their systemic exposure.

This dissertation research has contributed greatly to our understanding of transporter mediated disposition, drug-drug interactions, and toxicity of the drugs of abuse methamphetamine and β-carbolines. Taken together, this research provides useful information that may be considered when prescribing medications to methamphetamine users to mitigate the risk of DDIs that may potentially compromise therapeutic efficacy and drug safety.

TABLE OF CONTENTS

List of Figures v

List of Tables vii

Chapter 1. Introduction 1

1.1 Background 1

1.1.1 Introduction 1

1.1.2 Molecular and Functional Characteristics of Polyspecific Organic Cation Transporters 3

1.1.3 Impact of OCTs and MATEs on Intracellular Levels, Pharmacodynamics, and Toxicity 8

1.1.4 Methamphetamine and the roles of OCTs 12

1.2 Hypothesis and Specific Aims 14

Chapter 2. Interaction and Transport of Methamphetamine and its Primary Metabolites by Organic Cation and Multidrug and Toxin Extrusion Transporters 19

2.1 Introduction 19

2.2 Materials and Methods 21

2.2.1 Materials. 21

2.2.2 Uptake and Inhibition Assays in HEK293 Cells. 22

2.2.3 LC-MS/MS Analysis of Methamphetamine and its Metabolites. 23

2.2.4 Data Analysis. 24

2.3 Results 25

2.3.1 Inhibitory Effect of Methamphetamine and its Metabolites on hOCT1-3 and hMATE1/2-K. 25
2.3.2 Uptake of Methamphetamine and Metabolites by hOCT1-3, hMATE1, and hMATE2-K. 26
2.3.3 Interaction of Methamphetamine and Metabolites with Renal hOAT1 and hOAT3... 27
2.3.4 Methamphetamine and Metabolites Uptake Kinetics by Cation Transporters. 27
2.4 Discussion 28
Chapter 3. Kinetic Evidence for Spatially Distinct Substrate Binding Sites in Organic Cation Transporter 2 49
3.1 Introduction 49
3.2 Materials and Methods 52
3.2.1 Materials. 52
3.2.2 Uptake and Inhibition Assays in HEK293 Cells. 52
3.2.3 Data Analysis. 54
3.3 Results 56
3.3.1 Methamphetamine displays hOCT2 substrate dependent inhibition. 56
3.3.2 Atenolol and metformin display differential substrate affinity (K_m) from inhibition potency (IC_{50}) for hOCT2. 57
3.3.3 Methamphetamine displays differential inhibition mechanisms towards hOCT2-mediated atenolol and metformin transport. 57
3.3.4 Atenolol and metformin display apparent mixed and competitive inhibition of each other. 58
3.3.5 Atenolol mediated hOCT2 transport is noncompetitively inhibited by metformin. 58

3.4 Discussion 60

Chapter 4. Disposition of Methamphetamine and Major Metabolites in Mice: Role of Organic Cation Transporter 3 (Oct3) in Tissue Selective Accumulation of *p*-hydroxymethamphetamine 72

4.1 Introduction 72

4.2 Materials and Methods 75

4.2.1 Materials. 75

4.2.2 Animals. 75

4.2.3 Uptake Experiments. 76

4.2.4 In vivo Pharmacokinetics Studies. 77

4.2.5 LC-MS/MS Analysis of Methamphetamine and its Metabolites. 78

4.2.6 Pharmacokinetic Data Analysis. 78

4.2.7 Statistical Analysis. 79

4.3 Results 80

4.3.1 Transport of Methamphetamine and Metabolites by mOct3 Stably Expressed in HEK-293 Cells. 80

4.3.2 Methamphetamine Pharmacokinetic Studies in $Oct3^{+/+}$ and $Oct3^{-/-}$ Mice. 80

4.3.3 Impact of Oct3 Deletion on Salivary Glands Exposure to Methamphetamine, Amphetamine and p-OHMA. 81

4.3.4 Tissue Distribution of Methamphetamine, Amphetamine, and p-OHMA. 82

4.4 Discussion 83

Chapter 5. Potent Inhibition of Human Organic Cation Transporter 2 (hOCT2) by β-Carboline Alkaloids 96

5.1 Introduction 96
5.2 Materials and Methods 99
5.2.1 Materials 99
5.2.2 Cell Culture 99
5.2.3 β-Carboline Inhibition Studies 100
5.2.4 β-Carbolines Uptake Assay 100
5.2.5 Quantification of β-Carbolines by LC-MS/MS 101
5.2.6 β-Carboline Toxicity Assay 102
5.2.7 Data Analysis 102
5.3 Results 103
5.3.1 β -Carbolines Inhibit hOCT1-3 Mediated ASP+ Uptake 103
5.3.2 Permanently Charged β-carbolines are Substrates of hOCT1-3 104
5.3.3 Impact of hOCT1-3 Expression on β-carboline Cytotoxicity 104
5.4 Discussion 105
Chapter 6. Conclusions and Future Directions 116
Bibliography 120

LIST OF FIGURES

Figure 1-1. Models of organic cation transport in liver hepatocytes (A), kidney proximal tubule cells (B), and salivary gland acini (C). 16
Figure 1-2. Methamphetamine Metabolic Pathways 17
Figure 2-1. Metformin uptake by hOCT1, hOCT2, hOCT3, hMATE1, and hMATE2-K in Flp-in HEK293 cells in the presence or absence of the prototypical inhibitor cimetidine. 34
Figure 2-2. Inhibition by methamphetamine, amphetamine, and *p*-OHMA of hOCT1, hOCT2, hOCT3, hMATE1, and hMATE2-K. 35
Figure 2-3. Replica studies of methamphetamine, amphetamine, and *p*-OHMA inhibition of hOCT1, hOCT2, hOCT3, hMATE1, and hMATE2-K. 36
Figure 2-4. Inhibition of hOCT1 and hOCT2 by methamphetamine and amphetamine fitted to a two binding site model. 37
Figure 2-5. Uptake of 1 μM methamphetamine, amphetamine, and *p*-OHMA by hOCT1, hOCT2, hOCT3, hMATE1, and hMATE2-K. 38
Figure 2-6. Interactions of methamphetamine, amphetamine, and *p*-OHMA with renal hOAT1 and hOAT3. 39
Figure 2-7. Methamphetamine, amphetamine, and *p*-OHMA uptake kinetics by hOCTs. 40
Figure 2-8. Replica studies on methamphetamine, amphetamine, and *p*-OHMA uptake kinetics by hOCTs. 42
Figure 2-9. Methamphetamine and metabolite uptake kinetics by hMATE1 and hMATE2-K. 43
Figure 2-10. Replica studies of methamphetamine (A-D), amphetamine (E-F), and *p*-OHMA (I & J) uptake kinetics by hMATE1 and hMATE2-K. 44
Figure 3-1. Proposed four state and six state models of OCT transport. 65
Figure 3-2. Methamphetamine inhibition of hOCT2 mediated atenolol transport. 66
Figure 3-3. Atenolol and metformin hOCT2 transport and inhibition. 67
Figure 3-4. Methamphetamine inhibition kinetics of hOCT2 mediated metformin and atenolol transport. 68

Figure 3-5. Inhibition kinetics of the hOCT2 substrates atenolol and metformin. 69
Figure 3-6. Metformin and atenolol hOCT2 flux ratios. 70
Figure 3-7. Proposed hOCT2 binding and transport scheme for metformin, atenolol, and methamphetamine. 71
Figure 4-1. Uptake of methamphetamine, amphetamine, and *p* OHMA by vector or mOct3 transfected cells. 89
Figure 4-2. Methamphetamine, amphetamine, and p OHMA plasma concentration-time profiles in *Oct3*$^{+/+}$ and *Oct3*$^{-/-}$ mice. 90
Figure 4-3. Methamphetamine, amphetamine, and *p* OHMA salivary glands concentration-time profiles in Oct3$^{+/+}$ and Oct3$^{-/-}$ mice. 91
Figure 4-4. Methamphetamine, amphetamine, and p OHMA tissue AUC and AUC ratios in Oct3+/+ and Oct3-/- mice. 92
Figure 5-1. Molecular structure of β-carbolines used in the current study and MPP+.. 110
Figure 5-2. Interaction of β-carbolines with hOCT1 3. 111
Figure 5-3. Uptake of 1 μM MPP+ (positive control) and β-carbolines in vector (pcDNA5) or hOCT1 3 stably transfected Flp-in HEK293 cells. 112
Figure 5-4. Concentration-dependent toxicity of MPP+ (positive control) and β-carbolines in vector (pcDNA5) or hOCT1 3 stably transfected Flp-in HEK293 cells. 113

LIST OF TABLES

Table 1-1. Molecular and Functional Characteristics of Major Human Polyspecific Organic Cation Transporters. 18

Table 2-1. IC_{50} and Hill slope values of methamphetamine, amphetamine, and *p*-OHMA for hOCT1-3 and hMATE1/2-K using [^{14}C]metformin as the substrate. 45

Table 2-2. EC_{50} of high-affinity binding site, low-affinity binding site, and P values for statistical comparison of two-binding versus one-binding site. 46

Table 2-3. Kinetic parameters of methamphetamine and metabolites determined from modeling of data in Figure 2-7. 47

Table 2-4. Apparent kinetic transport parameters for methamphetamine, amphetamine, and *p*-OHMA for hMATE1 and hMATE2-K from simultaneously modeling active and passive accumulation. 48

Table 4-1. Methamphetamine plasma pharmacokinetic parameters in *Oct3*$^{+/+}$ and *Oct3*$^{-/-}$ mice 93

Table 4-2. Methamphetamine, amphetamine and *p*-OHMA tissue AUC0-480 (μM×min) in *Oct3*$^{+/+}$ and *Oct3*$^{-/-}$ mice 94

Table 4-3. Methamphetamine, amphetamine, and *p*-OHMA tissue to plasma $AUC_{0\text{-}480}$ ratios in *Oct3*$^{+/+}$ and *Oct3*$^{-/-}$ mice 95

Table 5-1. IC_{50} values of β-carbolines for hOCT1 3 as determined by the ASP+-based uptake assay. 114

Table 5-2. TC_{50} values of β-carboline toxicity towards pcDNA5 (control) and OCT1 3 transfected cells, as determined with the MTT cytotoxicity assay. 115

ACKNOWLEDGEMENTS

I would like to first acknowledge my doctoral advisor, Dr. Joanne Wang. Thank you for giving me the freedom to pursue my own scientific interests and always being there for support.

I must thank my doctoral supervisory committee: Drs. Shen, Atkins, Isoherranen, and Xu for their insights, direction, and assistance over my time at the University of Washington.

My sincerest gratitude goes to the entirety of the Wang lab, past and present. I am honored to have worked with so many great people and scientists.

The whole of the University of Washington Program on Pharmacokinetics of Drugs of Abuse during Pregnancy has helped me in some way. I have appreciated the collaborative nature of our work and the perspectives offered.

The Pharmacological Sciences Training Grant offered an amazing opportunity to discuss and explore science with remarkable colleagues not only in Pharmaceutics but also Medicinal Chemistry and Pharmacology.

I have had a fortunate experience working with remarkable researchers as coauthors. Thank you all for your thoughts, work, and dedication.

I thank the faculty, staff, and students of the departments of Pharmaceutics and Medicinal Chemistry for offering an amazing collaborative environment to learn.

My family has encouraged education and supported me when I needed them while giving me the space to reach this accomplishment. Todd, thank you for sharing a Scotch.

Faith and Savannah, I do not know that I could have made it this far without your help both personally and scientifically. You are amazing people and phenomenal scientists. I am in awe of how far we have come.

Laura, thank you for supporting me in this journey I do not know how you put up with me for this long.

DEDICATION

To my grandparents,

Thank you for showing me the value of education and encouraging me to continue onward. I wish you could have been here to see me complete mine.

Chapter 1. INTRODUCTION

(Part of this chapter was published as "Polyspecific organic cation transporters and their impact on drug intracellular levels and pharmacodynamics." *Pharmacological Research* 111 (2016): 237-246.)

1.1 BACKGROUND

1.1.1 *Introduction*

The ability of a drug molecule to move through cell membranes is a vital property affecting its pharmacokinetic and pharmacodynamics properties. Lipophilic drugs generally have high membrane permeability and their movement across cell membranes occurs primarily through passive diffusion. Hydrophilic drugs, on the other hand, have low membrane permeability, and their efficient uptake into cells and tissues often involve facilitated mechanisms mediated by membrane transporters (also known as carriers). Different from passive diffusion where a drug molecule moves across membranes down its concentration gradient without energy input, carrier-mediated transport can be coupled to a cellular energy source to power uphill transport against the drug concentration gradient. Further, carrier-mediated drug transport is saturable, inhibitable, and highly dependent on the functional characteristics of the membrane transporters expressed in the specific tissues or cell types. In mammalian cells, there are two major types of membrane proteins involved in drug and solute transport: the solute carrier (SLC) and the ATP-binding cassette (ABC) transporters. The past two decades have witnessed an explosion of knowledge in our understandings of the basic biology and pharmacology of various SLC and ABC drug transporters. The *in vivo* roles of these transporters in drug disposition, efficacy, and toxicity are increasingly being appreciated. The clinical significance of transporters as a site of drug-drug interaction and

a source for interindividual variability in drug response is also beginning to be acknowledged (Nishimura and Naito, 2005; Giacomini *et al.*, 2010; DeGorter *et al.*, 2012).

Most drugs are intended to act on targets residing within a specific tissue or cells. While some drugs bind to external cell surface targets (e.g. G protein-coupled receptors), others act on intracellular enzymes and receptors. Thus, it is the unbound drug concentration within the target tissue or cells that is directly responsible for eliciting its pharmacological effect. However, in the clinical setting, direct measurement of drug concentrations in target tissues and cells is difficult to achieve. Measurement of blood or plasma drug concentrations is thus commonly used to establish pharmacokinetic–pharmacodynamic relationships. For drugs that rapidly cross membranes by passive diffusion, unbound plasma concentration is often a good surrogate for unbound tissue concentration because the unbound drug concentration in tissue/cells is at equilibrium with the unbound concentration in plasma at steady state (Smith *et al.*, 2010; Chu *et al.*, 2013). However, if a drug is transported by active uptake and/or efflux drug transporters, such a relationship may no longer exist. For drugs that are substrates of uptake transporters, unbound tissue and/or intracellular drug concentrations can be much higher than drug concentrations in plasma. Conversely, for drugs that are substrates of efflux transporters, unbound concentrations in tissues and cells may be substantially lower than predicted from plasma levels. Increasing evidence suggest that transporters expressed in specific tissues and cells can exert a great impact on local and intracellular drug concentrations, directly influencing their pharmacological and toxicological activities (Smith *et al.*, 2010; Chu *et al.*, 2013).

This thesis work focuses on understanding the role of organic cation transporters in the disposition, drug-drug interactions, and tissue toxicity of methamphetamine, a widely abused drug of significant public health concern. In this chapter, I will first briefly review the molecular and

functional characteristics of major organic cation transporters with a special emphasis on their tissue distribution, cellular localization, and transport mechanisms. The impact of these transporters in controlling tissue and intracellular drug concentrations will be highlighted with resulting consequence on pharmacodynamic response and toxicological effects using several examples from *in vivo* or clinical studies. The background, hypothesis, and specific aims of this thesis work will be presented. Finally, the research focus and overall significance will be summarized.

1.1.2 *Molecular and Functional Characteristics of Polyspecific Organic Cation Transporters*

Organic cations are structurally diverse endogenous compounds (e.g. biogenic amines) and xenobiotics (e.g. drugs, environmental toxins) that carry a net positive charge at physiological pH. About 40% of the commonly prescribed drugs exist as organic cations at physiological pH (Neuhoff *et al.*, 2003). Many organic cations are hydrophilic and rely on transporters to move across cell membranes. In humans and other mammals, there are a number of SLC transporters that appear to have evolved specifically to handle these structurally diverse organic cations. These polyspecific (or multispecific) organic cation transporters include the classic organic cation transporters 1-3 (OCT1-3) from the SLC22 family, the multidrug and toxin extrusion proteins 1-2 (MATE1-2) from the SLC47 family, and the plasma membrane monoamine transporter (PMAT) from the SLC29 family (Engel *et al.*, 2004; Koepsell and Endou, 2004; Wright and Dantzler, 2004; Engel and Wang, 2005; Otsuka *et al.*, 2005; Maeda *et al.*, 2014). The molecular and functional characteristics of the major human polyspecific organic cation transporters are summarized below and in Table 1-1. A variety of clinically used drugs have been identified as the substrates of these transporters, and some selected drug substrates are listed in Table 1-1.

1.1.2.1 Molecular Features of OCTs, MATES, and PMAT

The human OCTs are encoded by the *SLC22* gene family and consist of three closely-related members: OCT1 (*SLC22A1*), OCT2 (*SLC22A2*) and OCT3 (*SLC22A*3). hOCT1 and hOCT2 are 70% identical in protein sequence, whereas hOCT3 shares 50% sequence identity with hOCT1 and hOCT2 (Sala-Rabanal *et al.*, 2013). The OCT proteins contain 542-556 amino acids with 12 predicted α-helical transmembrane domains (TMDs) (Giacomini *et al.*, 2010). The COOH- and NH2-terminal ends of the OCTs are intracellular. One large hydrophilic loop is localized to the extracellular side between TMD1 and TMD2 and contains several N-glycosylation sites. A large intracellular loop is localized between TMD6 and TMD7 with potential protein kinase C-dependent phosphorylation sites (Koepsell *et al.*, 1998).

In excretory organs, OCTs frequently team up with the multidrug and toxin extrusion (MATE) proteins to mediate transepithelial transport of organic cations (Nies *et al.*, 2012). Encoded by the *SLC47A* gene family in humans, MATEs include two members: MATE1 (*SLC47A1*) and MATE2 (*SLC47A2*) (Nies *et al.*, 2012). Human MATE1 has only one isoform with 570 amino acids in length, while human MATE2 has three isoforms: the full length isoform hMATE2 (602 amino acids), hMATE2-K (566 amino acids) and hMATE2-B (220 amino acids) (Otsuka *et al.*, 2005; Masuda *et al.*, 2006). Both hMATE2 and hMATE2-K are functional, whereas hMATE2-B possesses no transport activity (Masuda *et al.*, 2006). Human MATEs are predicted to have 13 TMDs with an extracellular carboxyl terminus and an intracellular amino terminus (Nies *et al.*, 2012; Motohashi and Inui, 2013).

Beside OCTs and MATEs, a newer polyspecific organic cation transporter, the plasma membrane monoamine transporter (PMAT), was recently cloned and characterized by our laboratory (Engel *et al.*, 2004; Engel and Wang, 2005). By gene ontology, PMAT (SLC29A4) belongs to the equilibrative nucleoside transporter (SLC29) family. However, detailed functional

characterization work demonstrated that PMAT functions as a polyspecific organic cation transporter that shares similar substrate specificity and functional characteristics to the OCTs (Engel *et al.*, 2004; Engel and Wang, 2005; Mingyan Zhou *et al.*, 2007; Ho *et al.*, 2011). PMAT is predominantly expressed in the central nervous system and its role in drug disposition and distribution in peripheral tissues may be limited. Research performed in this thesis work is primarily focused on OCT1-3 and MATE1/2-K.

1.1.2.2 Driving Forces of OCTs and MATEs

OCT-mediated organic cation transport is independent of sodium and chloride ions (Koepsell *et al.*, 2003; Koepsell, 2011). OCTs function as electrogenic, facilitative transporters, and the transport direction is dependent on the electrochemical gradient of the transported organic cations (Koepsell and Endou, 2004; Ciarimboli, 2011). In animal cells, the universally existing inside-negative membrane potential is used by the OCTs to drive cellular uptake of the organic cation substrate (Koepsell, 2004). This allows the OCTs to accumulate a substrate with intracellular concentrations much higher (up to 10 fold) than its extracellular concentration (Chien *et al.*, 2015). MATEs, however, are proton/organic cation exchangers (Masuda *et al.*, 2006). They couple a transmembrane proton gradient to drive the transport of organic cations in the opposite direction (Motohashi and Inui, 2013), a process involving an electroneutral exchange of proton for a monovalent organic cation (Wright and Wunz, 1987).

1.1.2.3 Tissue Distribution and Expression of OCTs and MATEs

Despite the similar structure and transport function, tissue distribution of OCT1-3 varies greatly. Oct1, the first OCT isoform identified from rat kidney, is highly expressed in the kidney, liver and small intestine in rodents (Grundemann *et al.*, 1994; Koepsell *et al.*, 2007). In humans, however, OCT1 is mainly found in the liver and localized to the basolateral membrane of

hepatocytes (Motohashi *et al.*, 2002; Nies *et al.*, 2009). Besides, low expression of human OCT1 is also detected in other tissues including small intestine, colon, kidney, lung, brain, heart, skeletal muscle, peripheral leukocytes, adrenal gland, mammary gland, immune cells and adipose tissue (Gorboulev *et al.*, 1997; Zhang *et al.*, 1997; Koepsell *et al.*, 2007). Oct2 was isolated by homology screening from rat kidney and human OCT2 was also cloned later (Okuda *et al.*, 1996; Gorboulev *et al.*, 1997). In humans, OCT2 is predominantly expressed on the basolateral membrane of renal proximal tubule cells in the kidney, and low expression has also been reported in brain, lung, small intestine, thymus, placenta and the inner ear (Gorboulev *et al.*, 1997; Koepsell *et al.*, 2007). Oct3 was independently cloned from rat brain and placenta (Kekuda *et al.*, 1998; Wu *et al.*, 1998), while human OCT3 was cloned from Caki-1 cells and originally identified as an extraneuronal monoamine transporter (Grundemann *et al.*, 1998). Different from hOCT1 and hOCT2, hOCT3 has a broader tissue distribution with relatively high expression in skeletal muscle, placenta, salivary glands, heart, brain, adrenal gland, trachea, small intestine, and uterus (Kekuda *et al.*, 1998; Shang *et al.*, 2003; Koepsell *et al.*, 2007; Duan and Wang, 2010; Lee *et al.*, 2013). The cellular localization of OCT3 is also tissue-specific. For instance, it is expressed on the basolateral membrane of hepatocytes and placental epithelium (Sata *et al.*, 2005; Koepsell *et al.*, 2007), but in the lung, it is localized to the luminal membrane of bronchial epithelial cells (Lips *et al.*, 2005). In salivary glands, the OCT3 protein is localized at both basolateral and apical membranes of the secretory epithelial cells (Lee *et al.*, 2014).

Human MATE1 was first cloned and characterized as an efflux transporter of organic cations (Otsuka *et al.*, 2005). hMATE1 is highly expressed in the liver, kidney, adrenal gland and skeletal muscle (Otsuka *et al.*, 2005), and it is localized to the apical membrane of renal proximal tubule cells and hepatocytes (Li and Shu, 2014). In humans, MATE2 and MATE2-K are mainly expressed

in the kidney, even though they are also detectable in various tissues (Masuda *et al.*, 2006; Komatsu *et al.*, 2011). In the kidney, MATE2 and MATE2-K are also restricted to the apical membrane of renal proximal tubule cells (Komatsu *et al.*, 2011).

1.1.2.4 Models of Organic Cation Transport Across Excretory Epithelia

In secretory organs such as the kidney and liver, the OCTs and MATEs form a functional alliance to mediate organic cation secretion from the body (Figure 1-1). For instance, renal secretion of organic cations consists of two steps. Circulating organic cations in blood are first transported into the renal proximal tubule cells by the basolateral OCT2 driven by negative membrane potential (Budiman *et al.*, 2000). Once inside the tubular cells, organic cations are effluxed into urine by the MATE1 and MATE2-K on the apical membrane (Figure 1-1) (Yin *et al.*, 2015). In the proximal tubule, the Na^+/H^+ exchanger (antiporter) creates a slightly acidic lumen (pH 7.2-6.7) which provides an inwardly-directed proton gradient that can efficiently drive MATE-mediated organic cation efflux (Meijer *et al.*, 1990; Pritchard and Miller, 1993; Bobulescu and Moe, 2009; Hagenbuch, 2010). A similar model has been proposed for organic cation transport in hepatocytes. Located on the basolateral (sinusoidal) membrane of hepatocytes, OCT1, the most abundant OCT isoform in human liver, plays a pivotal role in the uptake of organic cations from blood into the liver (Moule and McGivan, 1990). Once inside the cells, organic cations may be further secreted into the bile by MATE1 on the apical (canalicular) membrane (Figure 1-1) (Otsuka *et al.*, 2005). However, the canalicular pH is 7.2 or higher (Strazzabosco *et al.*, 1991). Without an inwardly directed proton gradient, it is unclear if MATE1-mediated efflux of organic cations across canalicular membrane is likely to occur efficiently or rely on some other transporters at the canaliculi.

1.1.3 *Impact of OCTs and MATEs on Intracellular Levels, Pharmacodynamics, and Toxicity*

1.1.3.1 Impact of OCT1/Oct1 on Hepatic Drug Levels and Action

Located in the sinusoidal membrane of hepatocytes, OCT1 has been identified as a main organic cation transporter in the liver and is responsible for the uptake of basic compounds in hepatocytes (Koepsell *et al.*, 2007; Giacomini *et al.*, 2010; Hillgren *et al.*, 2013; Koepsell, 2013). Although OCT3 and MATE1 are also expressed in hepatocytes, their roles in hepatic drug disposition and elimination have not been well established as compared to OCT1 (Koepsell *et al.*, 2007; Hillgren *et al.*, 2013; Staud *et al.*, 2013; Zamek-Gliszczynski, Bao, *et al.*, 2013). MATE1 appears to mediate some biliary excretion but its activity with *in vivo* probes is generally low and appears to be significantly less than in the kidney (Scheen, 1996; Ito *et al.*, 2010; Graham *et al.*, 2011; Zamek-Gliszczynski, Bao, *et al.*, 2013). The apparent low activity of MATE1 was thought to be due to the lack of a significant pH gradient between hepatocytes and bile (Kirpichnikov *et al.*, 2002), which is necessary to drive MATE1-mediated organic cation efflux as a proton/organic cation antiporter (Zamek-Gliszczynski, Bao, *et al.*, 2013). The importance of OCT1 in influencing liver intracellular concentrations and pharmacodynamics can be best appreciated with studies on the antidiabetic drug, metformin (Wang *et al.*, 2002; Shu *et al.*, 2007; Takane *et al.*, 2008; Minuesa *et al.*, 2009; Gong *et al.*, 2012; Choi *et al.*, 2013; Jung *et al.*, 2013).

Shu et al. first demonstrated OCT1 regulates hepatic uptake and response to metformin (Shu *et al.*, 2007). They showed that metformin hepatic concentration was 4.2-fold greater in wildtype Oct1 (*Oct1*$^{+/+}$) mice than in *Oct1* knockout (*Oct1*$^{-/-}$) mice while metformin concentrations in the plasma and other organs were similar between *Oct1*$^{+/+}$ and *Oct1*$^{-/-}$ mice. The role of OCT1 in metformin pharmacokinetics and pharmacodynamics in humans was then investigated in a pharmacogenetics study in healthy volunteers carrying either the normal reference OCT1 allele or

variant alleles (OCT1-R61C, -G401S, -G465R, and 420del) that showed reduced metformin transport activity *in vitro*. After metformin treatment, volunteers carrying the OCT1 polymorphisms had significantly higher plasma glucose levels than those carrying the reference allele in OGTT (Shu *et al.*, 2008). These results are consistent with the data from the mice, further supporting that OCT1 is a critical determinant of liver concentrations of metformin, which then directly affects the therapeutic response.

The impact of hepatic OCT1 on liver drug disposition and action highlighted the fact that pharmacodynamic responses do not always correlate with plasma drug concentration data (i.e. pharmacokinetics). Rather, drug concentrations in target tissues are more relevant to therapeutic activity. As discussed, a decreased pharmacodynamic response of metformin was observed in *Oct1*$^{-/-}$ mice without a corresponding change in plasma exposure (Shu *et al.*, 2007). In contrast, this decreased pharmacodynamic response in *Oct*$^{-/-}$ mice corroborated with a substantial reduction in metformin concentrations in the liver. A decreased response to metformin was observed in volunteers carrying OCT1 polymorphisms in spite of an increased metformin systemic exposure (Shu *et al.*, 2007, 2008). These studies clearly demonstrated the ability of locally expressed uptake transporters to impact intracellular drug concentrations at the site of action, and thus directly influencing the pharmacological activity of a medication.

1.1.3.2 Impact of OCT2/MATEs on Renal Drug Clearance, Accumulation and Nephrotoxicity

In human kidneys, OCT2 is the primary blood-facing organic cation uptake transporter (Wright and Dantzler, 2004; Koepsell *et al.*, 2007; Koepsell, 2013; Morrissey *et al.*, 2013). The luminal-facing MATE1 and MATE2-K work in concert with OCT2 to mediate active renal secretion of basic drugs (Lai *et al.*, 2010; Hillgren *et al.*, 2013; Müller *et al.*, 2013; Yin *et al.*, 2015) (Figure 1-1). The roles of OCT2 and the MATE transporters in renal elimination of organic cations

are well established (Wang *et al.*, 2008; Higgins *et al.*, 2012; Ito *et al.*, 2012; Yoon *et al.*, 2013). Many cationic drugs, such as metformin and atenolol, are eliminated by active renal secretion by the OCT2/MATE pathway (Song *et al.*, 2008; Wang *et al.*, 2008; Gong *et al.*, 2012). Due to the role of OCT2 in the elimination of drugs, inhibition of OCT2 can lead to decreased renal clearance, increased exposure, and possibly toxicity by the victim drug in vivo (Yin and Wang, 2016; Ivanyuk *et al.*, 2017). In vitro inhibition assessments are recommended to predict the potential for clinically relevant drug-drug interactions with OCT2 (European Medicines Agency, 2012; Zamek-Gliszczynski, Lee, *et al.*, 2013; Food and Drug Administration, 2017). Furthermore, an imbalance between OCT2-mediated uptake and MATE-mediated efflux may result in drug accumulation in proximal tubule cells, leading to drug-induced nephrotoxicity and kidney injury (Yin *et al.*, 2016). This scenario can occur clinically and is thought to underlie the differential nephrotoxicity of platinum-based anticancer agents (Yonezawa and Inui, 2011).

1.1.3.3 Impact of OCT3/Oct3 on Drug Accumulation and Secretion in Salivary Glands

OCT3 is broadly expressed in a number of tissues including the placenta, salivary glands, heart, brain, and intestine in both human and rodents (Wu *et al.*, 2000; Koepsell *et al.*, 2007; Lee *et al.*, 2013, 2014; Chen *et al.*, 2015). Our laboratory previously reported that OCT3 is highly expressed in human parotid, submandibular, and sublingual salivary glands (Lee *et al.*, 2014). Other polyspecific organic cation transporters, including OCT1, 2, MATEs, and PMAT, are minimally expressed in human or rodent salivary glands. OCT3 protein is localized at both basolateral (blood-facing) and apical (saliva-facing) membranes of salivary gland acinar cells. OCT3 appears to mediate both epithelial uptake and efflux of organic cations in the secretory cells of salivary glands, where the OCT3-mediated drug uptake is likely to be facilitated by the inside

negative membrane potential and the efflux is dependent on the electrochemical potential of the substrate (Figure 1-1).

Using a mouse model of targeted deletion of *Oct3,* our laboratory previously showed that OCT3 is responsible for the accumulation and secretion of metformin in salivary glands (Lee *et al.*, 2014). When dosed to wild-type mice, metformin was actively transported into the salivary glands and achieved very high level of accumulation. In contrast, active uptake and accumulation of metformin in salivary glands were substantially attenuated in *Oct3*$^{-/-}$ mice, and the salivary exposure was reduced by more than 50% in *Oct3*$^{-/-}$ mice as compared with wildtype mice. In addition to the salivary gland, Oct3 was shown to play a role in uptake to the heart and skeletal muscle in mice (Lee *et al.*, 2014). Conversely, OCT3 generally does not play a major role in the elimination of drugs as other transporters appear to play a larger role in eliminating organs. For example, OCT2 is highly expressed in the kidney and no differences in clearance of metformin were observed when administered IV to wild type and Oct3 knockout mice (Shirasaka *et al.*, 2016).

The salivary glands play an important role in oral health, nutrient digestion, and immunity to microbial infection (Holsinger and Bui, 2007). Dysfunction of the salivary glands can lead to xerostomia and dysgeusia (Ackerman and Kasbekar, 1996). Although xerostomia has many origins (Cassolato and Turnbull, 2003), excessive accumulation of foreign chemicals in salivary glands may lead to tissue toxicity and dysfunction of the salivary glands. Previous studies from our laboratory demonstrated a critical role of OCT3 in the salivary glands' drug accumulation and secretion. The high levels of drug accumulation achieved in salivary tissue are alarming with respect to potential tissue-specific adverse effects.

1.1.4 *Methamphetamine and the roles of OCTs*

Methamphetamine is a widely abused illicit drug with approximately 1.2 million reported users in the United States (Maxwell and Rutkowski, 2008; Volkow *et al.*, 2010; Panenka *et al.*, 2013; Volkow, 2013). Also known as "meth", "crystal", “speed” or "ice", methamphetamine is a potent and highly addictive central nervous stimulant that acts by inhibition and reversal of neurotransmitter transporters of dopamine, norepinephrine, and serotonin (Carvalho *et al.*, 2012; Panenka *et al.*, 2013). High or repeated doses of methamphetamine can affect multiple organ systems, leading to profound neurotoxicity, cardiotoxicity, acute renal failure, and pulmonary toxicity (Volkow *et al.*, 2010; Carvalho *et al.*, 2012). High levels of methamphetamine abuse have been reported in individuals receiving drug therapies for HIV, hepatitis, or other conditions, raising the concern of potential drug-drug interactions (Bracchi *et al.*, 2015).

Following oral, inhalation, or intranasal administration, methamphetamine is well-absorbed into the bloodstream (Harris *et al.*, 2003; Schep *et al.*, 2010) and is distributed into many organs with the highest uptake occurring in lungs, liver, brain, and kidneys (Volkow *et al.*, 2010). Methamphetamine is initially metabolized by the polymorphic enzyme cytochrome P450 2D6 to the circulating metabolites amphetamine and *p*-hydroxymethamphetamine (*p*-OHMA) (Figure 1-2) (Lin *et al.*, 1997; Shima *et al.*, 2008). Micromolar circulating concentrations of amphetamine and *p*-OHMA have been reported in opportunistic studies of methamphetamine abusers (Shima *et al.*, 2008). Amphetamine is also psychoactive with similar pharmacology to methamphetamine (Panenka *et al.*, 2013). *p*-OHMA is not psychoactive but is a vasoconstrictor and at least one case study has implicated it in fatal intoxication (Römhild *et al.*, 2003). In vitro metabolism of methamphetamine by Flavin-containing monooxygenase (FMO) 3 has also been reported although metabolites formed by FMO3 do not appear to circulate at appreciable levels (Cashman *et al.*,

1999). Concurrent use of CYP2D6 substrates or inhibitors with methamphetamine and related designer drugs represents a risk of potential drug interactions leading to toxicity (Wu *et al.*, 1997; Pritzker *et al.*, 2002; Newton *et al.*, 2005).

Renal excretion is another major elimination pathway for methamphetamine and its metabolites. Approximately 37–54% of methamphetamine is recovered unchanged in the urine although more may be eliminated renally in CYP2D6 poor metabolizers (Kim *et al.*, 2004). The renal excretion rate of methamphetamine is highly dependent on urinary pH (Beckett and Rowland, 1965c; b, Cook *et al.*, 1992, 1993). The fraction unbound of methamphetamine (f_u) is about 0.8 (de la Torre *et al.*, 2004). The reported renal clearance of methamphetamine is highly variable (e.g. 67-371 mL/min) and much larger than glomerular filtration rate (GFR) in some individuals, suggesting that the drug is actively secreted by the kidney (Beckett and Rowland, 1965b; c; Kim *et al.*, 2004). PET imaging also revealed that methamphetamine is highly accumulated in the kidney (Volkow *et al.*, 2010). Both metabolites, *p*-OHMA and amphetamine, also undergo urinary excretion with a possible active secretion component (Shima *et al.*, 2006).

Methamphetamine is considered one of the most toxic drugs of abuse with both central nervous system (CNS) and peripheral toxicities (Volkow *et al.*, 2010). Methamphetamine neurotoxicity is relatively well understood with long-term neurological injuries primarily targeting the dopaminergic and serotonergic neurons, where methamphetamine is highly concentrated by the monoamine transporters (Schep *et al.*, 2010; Panenka *et al.*, 2013). Additionally, nephrotoxicity, cardiotoxicity, muscle, and salivary gland toxicities are major concerns but with poorly understood mechanisms (Carvalho *et al.*, 2012). The peripheral toxicity colloquially known "meth mouth", xerostomia (dry mouth) and rampant dental caries, is one of the most widely known injuries that is publicized in many anti-drug campaigns (Shaner *et al.*, 2006).

Little is currently known about the involvement of drug transporters in the elimination and distribution of methamphetamine and its metabolites. With a pKa of ~9.9, methamphetamine and its primary metabolites exist predominantly as protonated cations at physiological pH (de la Torre *et al.*, 2004). Several in vitro and in vivo studies have indicated that amphetamines may interact with organic cation transporters (Kitaichi *et al.*, 2003; Amphoux *et al.*, 2006; Zhu *et al.*, 2010). However, the inhibition potency, substrate specificity, and transport kinetics of methamphetamine and metabolites towards organic cation uptake and efflux transporters have not been comprehensively characterized. Furthermore, the specific roles of OCTs and MATEs in systemic disposition, tissue-specific accumulation, drug-drug interactions, and peripheral tissue toxicities are essentially unknown.

1.2 Hypothesis and Specific Aims

The overall goal of my research project is to understand the roles of organic cation transporters in the disposition, drug-drug interactions, and toxicity of drugs of abuse with a focus on methamphetamine. The overarching hypothesis is that methamphetamine and its metabolites interact with OCTs and MATEs and these transporters are involved in the disposition, DDIs, tissue-specific accumulation, and toxicity of methamphetamine.

The specific aims are:

Specific Aim 1: Determine if methamphetamine and metabolites are inhibitors and substrates of hOCT1-3 and hMATE1/2-K.

Specific Aim 2: Characterize the complex inhibition kinetics of methamphetamine towards hOCT2.

Specific Aim 3: Determine if Oct3 is involved in the PK, tissue accumulation, and salivary gland toxicity of methamphetamine and/or its metabolites using a mouse model.

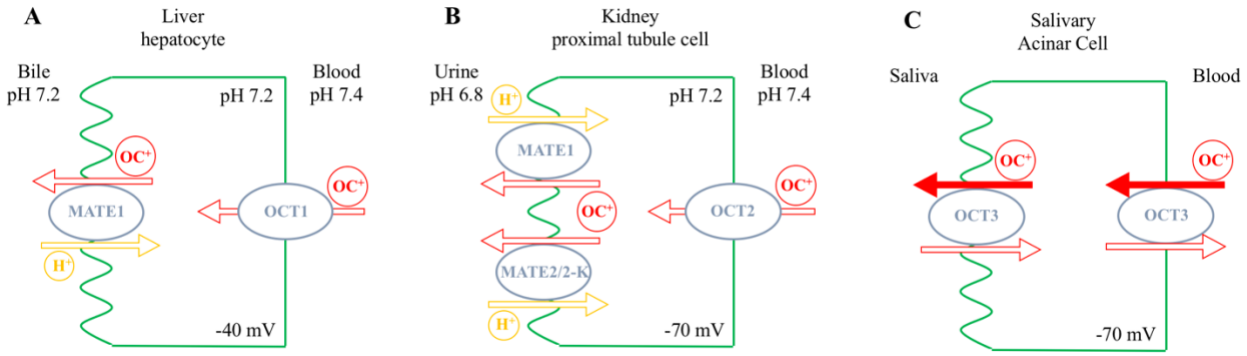

Figure 1-1. Models of organic cation transport in liver hepatocytes (A), kidney proximal tubule cells (B), and salivary gland acini (C).

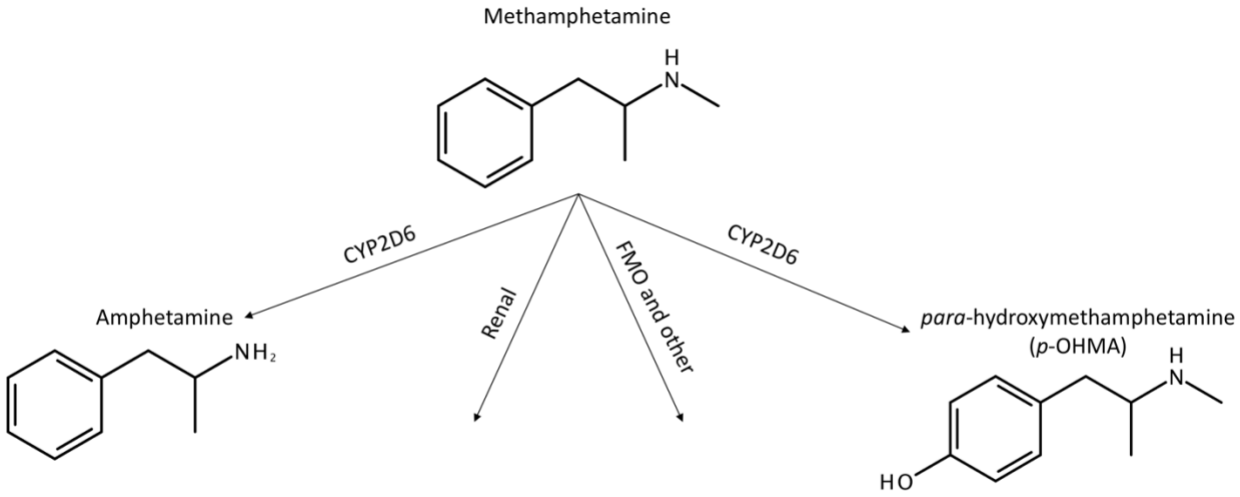

Figure 1-2. Methamphetamine Metabolic Pathways

Table 1-1. Molecular and Functional Characteristics of Major Human Polyspecific Organic Cation Transporters.

Transporters	Gene	Transport Mode	Tissue Distribution	Selected Drug Substrates	Reference
OCT1	*SLC22A1*	Electrogenic	Liver, small intestine, kidney, lung, brain, heart, skeletal muscle, placenta, mammary gland, adrenal gland, immune cells, adipose tissue	Acyclovir, atenolol, debrisoquine, furamidine, ganciclovir, lamivudine, lamotrigine, metformin, oxaliplatin, pentamidine, picoplatin, tropisetron, zalcitabine	(Iwai *et al.*, 2011; Nies *et al.*, 2011; Saadatmand *et al.*, 2012; Koepsell, 2013; Yin *et al.*, 2015)
OCT2	*SLC22A2*	Electrogenic	Kidney, brain, lung, small intestine, thymus, placenta	Amantadine, amiloride, atenolol, cimetidine, cisplatin, famotidine, ifosfamide, lamivudine, memantine, metformin, oxaliplatin, picoplatin	(Nies *et al.*, 2011; Ishiguro *et al.*, 2013; Koepsell, 2013; Yin *et al.*, 2015)
OCT3	*SLC22A3*	Electrogenic	Liver, skeletal muscle, heart, placenta, brain, kidney, small intestine, urinary bladder, cornea, mammary gland, lung	Cisplatin, etilefrine, lamivudine, lidocaine, metformin, oxaliplatin, pramipexole, quinidine	(Yonezawa *et al.*, 2006; Nies *et al.*, 2011; Koepsell, 2013)
MATE1	*SLC47A1*	Electroneutral (H^+/OC^+ exchange)	Liver, kidney, skeletal muscle, adrenal gland	Acyclovir, atenolol, cimetidine, cisplatin, fexofenadine, guanidine, metformin, oxaliplatin, procainamide, topotecan	(Tanihara *et al.*, 2007; Yokoo *et al.*, 2007; Ohta *et al.*, 2009; Ciarimboli, 2011; Yin *et al.*, 2015)
MATE2/2-K	*SLC47A2*	Electroneutral (H^+/OC^+ exchange)	Kidney	Atenolol, cimetidine, cisplatin, guanidine, metformin, oxaliplatin, procainamide, topotecan	(Masuda *et al.*, 2006; Tanihara *et al.*, 2007; Ciarimboli, 2011; Yin *et al.*, 2015)
PMAT	*SLC29A4*	Electrogenic pH sensitive	Brain, heart, small intestine, kidney, liver	Metformin, ritonavir	(Engel *et al.*, 2004; Engel and Wang, 2005; M Zhou *et al.*, 2007; Xia *et al.*, 2007; Itagaki *et al.*, 2012)

Chapter 2. INTERACTION AND TRANSPORT OF METHAMPHETAMINE AND ITS PRIMARY METABOLITES BY ORGANIC CATION AND MULTIDRUG AND TOXIN EXTRUSION TRANSPORTERS

(A version of this chapter was published in *Drug Metabolism and Disposition* 45.7 (2017): 770-778.)

2.1 INTRODUCTION

Methamphetamine is a widely abused illicit drug with approximately 1.2 million reported users in the United States (Volkow, 2013). Also known as "meth", "crystal", "speed" or "ice", methamphetamine is a potent and highly addictive central nervous stimulant that acts by inhibition and reversal of neurotransmitter transporters of dopamine, norepinephrine, and serotonin (Carvalho *et al.*, 2012; Panenka *et al.*, 2013). Illicit methamphetamine is sold as either a racemic mixture or the *d*-methamphetamine isomer since the dextro isomer is much more psychoactive (de la Torre *et al.*, 2004). High or repeated doses of methamphetamine can affect multiple organ systems, leading to profound neurotoxicity, cardiotoxicity, acute renal failure, and pulmonary toxicity (Volkow *et al.*, 2010; Carvalho *et al.*, 2012).

Following oral, inhalation, or intranasal administration, methamphetamine is well-absorbed into the bloodstream (Harris *et al.*, 2003; Schep *et al.*, 2010) and is distributed into many organs with the highest uptake occurring in lungs, liver, brain, and kidneys (Volkow *et al.*, 2010). Methamphetamine is eliminated by both hepatic metabolism and renal excretion. In the liver, it is metabolized by the polymorphic enzyme cytochrome P450 2D6 to the *p*-hydroxylation metabolite,

p-hydroxymethamphetamine (*p*-OHMA), and the N-demethylation product, amphetamine (Lin *et al.*, 1997; Shima *et al.*, 2008). Both metabolites have been reported to circulate in plasma of methamphetamine abusers up to the micromolar range (Shima *et al.*, 2008). Amphetamine is also highly psychoactive and addictive with a mechanism of action similar to methamphetamine (Panenka *et al.*, 2013). *p*-OHMA is not psychoactive but acts as a cardiovascular agent with hypertensive and adrenergic effects (Römhild *et al.*, 2003). Concurrent use of CYP2D6 substrates or inhibitors with methamphetamine and related designer drugs represents a risk of potential drug interactions leading to toxicity (Wu *et al.*, 1997; Pritzker *et al.*, 2002; Newton *et al.*, 2005).

Renal excretion is another major elimination pathway for methamphetamine and its metabolites. Approximately 37–54% of methamphetamine is recovered unchanged in the urine although more may be eliminated renally in CYP2D6 poor metabolizers (Kim *et al.*, 2004). The renal excretion rate of methamphetamine is highly dependent on urinary pH (Beckett and Rowland, 1965c; b, Cook *et al.*, 1992, 1993). The fraction unbound of methamphetamine (f_u) is about 0.8 (de la Torre *et al.*, 2004). The reported renal clearance of methamphetamine is highly variable (e.g. 67-371 mL/min) and much larger than glomerular filtration rate (GFR) in some individuals, suggesting that the drug is actively secreted by the kidney (Beckett and Rowland, 1965b; c; Kim *et al.*, 2004). PET imaging also revealed that methamphetamine is highly accumulated in the kidney (Volkow *et al.*, 2010). Both metabolites, *p*-OHMA and amphetamine, also undergo urinary excretion with a possible active secretion component (Shima *et al.*, 2006).

Little is currently known about the involvement of drug transporters in renal elimination and tissue distribution of methamphetamine and its metabolites. With a pKa of ~9.9, methamphetamine and its primary metabolites exist predominantly as protonated cations at physiological pH (de la Torre *et al.*, 2004). The reported or calculated LogD of methamphetamine,

amphetamine and *p*-OHMA at 7.4 is -0.38, -0.62, and -1.11, respectively (Fowler *et al.*, 2007), suggesting a low passive membrane diffusion for the protonated species. In rats, methamphetamine renal clearance was significantly reduced by cimetidine, a classic inhibitor of renal organic cation secretion system (Kitaichi *et al.*, 2003). *In vitro* studies have indicated that amphetamine is an inhibitor of human organic cation transporters (OCT) (Amphoux *et al.*, 2006; Zhu *et al.*, 2010). However, the inhibition potency, substrate specificity, and transport kinetics of methamphetamine and metabolites towards renal organic cation uptake and efflux transporters have not been comprehensively characterized. This information is important for understanding the mechanisms involved in the disposition and potential drug-drug interaction of methamphetamine. The goals of this study were to characterize the interaction of methamphetamine and its major metabolites with human OCT1-3 and multidrug and toxin extrusion (MATE) transporter 1 and 2-K (hMATE1/2-K) and to identify the major transporters involved in renal secretion of methamphetamine, amphetamine and *p*-OHMA.

2.2 Materials and Methods

2.2.1 *Materials.*

d-Methamphetamine, *d*-amphetamine, and *p*-OHMA were purchased from Sigma-Aldrich (St. Louis, MO) and were of analytical grade. Currently, there is no evidence that organic cation transporters have stereo-selective interaction with cationic substrates (Yin *et al.*, 2015). We focused our study on the dextro isoforms of methamphetamine and amphetamine because they are the psychoactive forms. In all our studies, methamphetamine and amphetamine refer to the dextro isoforms unless specified otherwise. Methamphetamine-D_{11} and amphetamine-D_{11} were purchased from Cerilliant Corporation (Round Rock, TX). [^{14}C]metformin (98 mCi/mmol) was purchased from Moravek Biochemicals, Inc. (Brea, CA). [^{3}H]estrone sulfate (50 Ci/mmol), and

[^{3}H]*para*-aminohippurate (PAH) (3 Ci/mmol) were purchased from American Radiolabeled Chemicals, Inc. (St. Louis, MO). Optima grade acetonitrile, water, and formic acid were purchased from Fisher Scientific (Waltham, MA). Cell culture media and reagents were purchased from Invitrogen (Carlsbad, CA). All other chemicals were commercially available and of analytical grade or higher.

2.2.2 *Uptake and Inhibition Assays in HEK293 Cells.*

Flp-in HEK293 cells stably expressing hOCT1, hOCT2, hOCT3, hMATE1, hMATE2-K, hOAT1, and hOAT3 were previously generated in our laboratory (Duan and Wang, 2010; Duan *et al.*, 2015; Yin *et al.*, 2015). The cells were cultured in high glucose DMEM media with 10% FBS, 1 mM L-glutamine, 100 U/mL penicillin, 100 μg/mL streptomycin, and 150 μg/mL hygromycin B supplementation at 37°C with 5% CO_2 and high humidity. All cell culture plastic surfaces were coated with 0.01% poly-D-lysine to improve cell attachment. Uptake and inhibition assays were performed as previously described with modification for analysis of methamphetamine and its metabolites by LC-MS/MS (Duan and Wang, 2010; Duan *et al.*, 2015; Yin *et al.*, 2015). Briefly, cells were seeded in 96-well plates at 100,000 cells/well and grown overnight. Prior to incubation initiation, cells were washed with pre-warmed Hanks balanced salt solution (HBSS) and allowed to acclimate for 10 minutes at 37°C or pre-incubated with HBSS containing 30 mM ammonium chloride for 20 minutes for MATE experiments in order to acidify the intracellular compartment and drive MATE uptake (Tanihara *et al.*, 2007). Media was removed and incubation initiated by addition of 100 μL of HBSS at pH 7.4 containing a substrate with or without inhibitor. Uptake was stopped by removal of media and washing the cells three times with ice cold HBSS. Cells were either lysed with 100 μL of 1 M NaOH and neutralized with 100 μL of 1 M HCl for incubations containing a radiolabeled substrate for measurement by liquid scintillation counting

(LSC) (PerkinElmer, Tri-Carb B3110TR, Waltham, MA) or permeabilized with 100 μL of methanol containing 100 nM stable labeled internal standard for analysis by LC-MS/MS. Protein content in the lysate in each well was measured by the BCA Protein Assay Kit (Pierce Chemical, Rockford, IL) and the uptake in cells was normalized to their total protein concentrations. The inhibitory effect of methamphetamine, amphetamine, and *p*-OHMA on hOCT1, hOCT2, hOCT3, hMATE1, and hMATE2-K was assessed in transporter-expressing HEK293 cells using [^{14}C]metformin, a well-established and clinically relevant probe substrate for these transporters (European Medicines Agency, 2012; Food and Drug Administration, 2012b; Hillgren *et al.*, 2013). The concentration of metformin in inhibition experiments (11 μM, 1 μCi/mL) was selected to be much lower than its K_m values (780-1500 μM) for the transporters tested (Koepsell *et al.*, 2007; Tanihara *et al.*, 2007). Inhibition and kinetic experiments were performed during the initial rate period using a short incubation time as specified in figure legends. Transport experiments were performed in triplicate and repeated three times independently. Uptake was performed in both empty vector- and transporter-transfected cells; and transporter specific uptake was calculated by subtracting uptake in vector-transfected cells.

2.2.3 *LC-MS/MS Analysis of Methamphetamine and its Metabolites.*

Methamphetamine, amphetamine, and *p*-OHMA levels were quantified using an LC-MS/MS system consisting of an AB-Sciex API 4500 triple quadrupole mass spectrometer (Foster City, CA) coupled with an LC-20AD ultra-fast liquid chromatography system (Shimadzu Co., Kyoto, Japan). The Turbo Ion Spray interface was operated in positive ion mode. Ten microliters of cell lysate was injected onto an Agilent Eclipse Plus C18 column (1.8 μm; 4.6x50 mm) running with an isocratic method consisting of 0.28 ml/min 0.2% formic acid in water and 0.12 ml/min acetonitrile. Mass transitions (*m/z*) were 150→119, 136→91, 166→135, 161→97, and 147→98

for methamphetamine, amphetamine, *p*-OHMA, methamphetamine-d_{11}, and amphetamine-d_{11}, respectively. Data was analyzed using Analyst software version 1.6.2 (AB Sciex). Assay accuracy and precision were within 15% (20% for the lower limit of quantification).

2.2.4 *Data Analysis.*

Transport experiments were performed in triplicate and repeated three times independently. Data representation and replicates with specific n numbers are detailed in each figure legend. Transport kinetics were fitted using GraphPad Prism 6.0 (GraphPad Software, Inc., La Jolla, CA) for inhibitory interactions and uptake kinetics of hOCT1-3. WinNonLin Phoenix 6.4.0 (Certara, Princeton, NJ) was used for fitting hMATE apparent transport kinetics. The IC50 values were calculated by fitting the Log inhibitor concentration versus the transporter specific uptake normalized to the vehicle control using the equation:

$$v = \text{Bottom} + \frac{\text{Top}-\text{Bottom}}{1+10^{(\text{LogIC}_{50}-\text{I})*\text{H}}} \quad (2\text{-}1)$$

where V is the rate of uptake in the presence of the inhibitor, Bottom is the residual baseline value, Top is the rate of uptake in the absence of inhibitor, I is the inhibitor concentration, and H is the Hill coefficient. Two site inhibition data was fitted using the equation:

$$v = \text{Bottom} + (\text{Top} - \text{Bottom})\left(\frac{\text{Fraction1}}{1+10^{\text{I}-\text{LogEC}_{50,1}}} + \frac{1-\text{Fraction1}}{1+10^{\text{I}-\text{LogEC}_{50,2}}}\right) \quad (2\text{-}2)$$

One and two site inhibition equations were compared by an extra sum of squares F test using the data from all three independent experiments modeled simultaneously. Apparent hMATE1/2-K K_m and V_{max} values were obtained by simultaneously fitting the data to the Michaelis-Menten equation with a passive diffusion component in transporter transfected cells and only the passive diffusion component in vector transfected cells (Brouwer *et al.*, 2013):

$$v = \frac{V_{max}*S}{K_m+S} + P_{diff} * S \quad (2\text{-}3)$$

where V is the velocity of uptake, V_{max} is the maximum velocity of uptake, S is the substrate concentration, K_m is the Michaelis-Menten constant, and P_{dif} is the nonsaturable passive diffusion rate constant. Sigmoidal saturation kinetics of *p*-OHMA hOCT2 transport were obtained by fitting transporter mediated uptake to the Michaelis-Menten equation with a Hill slope for the substrate concentration and half maximal transport concentration ($K_{1/2}$ in place of K_m) after inspection of the Eadie-Hofstee plot (Copeland, 2000):

$$v = \frac{V_{max} * S^H}{K_{1/2}{}^H + S^H} \quad (2\text{-}4)$$

Amphetamine hOCT2 specific uptake kinetics were fit to a biphasic Michaelis-Menten equation:

$$v = \frac{V_{max1} * S}{K_{m1} + S} + \frac{V_{max2} * S}{K_{m2} + S} \quad (2\text{-}5)$$

2.3 RESULTS

2.3.1 *Inhibitory Effect of Methamphetamine and its Metabolites on hOCT1-3 and hMATE1/2-K.*

The transport activities of hOCT1, hOCT2, hOCT3, hMATE1, and hMATE2-K in the Flp-in HEK293 expression systems were first confirmed with metformin uptake in the presence or absence of the prototypical inhibitor cimetidine (Figure 2-1). Methamphetamine, amphetamine, and *p*-OHMA inhibited metformin uptake by hOCT1-3 and hMATE1/2-K in a concentration-dependent manner (Figure 2-2 and Figure 2-3). The IC_{50} values were summarized in Table 2-1. Methamphetamine and amphetamine were 4-20 fold more potent for hOCT1 and hOCT2 than for hOCT3, hMATE1, and hMATE2-K, with hOCT2 showing the greatest sensitivity to both psychostimulants (hOCT2 IC_{50} of 15.0 ± 6.8 and 20.3 ± 16.9 μM, respectively). *p*-OHMA was a more potent inhibitor of hOCT1 than other transporters. Addition of the 4-hydroxyl group to the aromatic phenyl ring (*p*-OHMA) greatly increased binding to hOCT3 but decreased its potency toward hOCT2 as compared with methamphetamine. Interestingly, the Hill slope of

methamphetamine and amphetamine inhibition of hOCT1 and hOCT2 was approximately 0.5 (Table 2-1). Conversely, the Hill slope of *p*-OHMA against hOCT2 was approximately 1.5. hMATE2-K also had steep Hill slopes ranging between 1.6 and 1.9 for methamphetamine and its metabolites. These Hill slopes suggest more complex interactions than simple competitive inhibition may be occurring with these transporters.

Inspection of methamphetamine and amphetamine dose-dependent inhibition of hOCT1 and hOCT2 revealed biphasic inhibition characteristics (Figure 2-4). A two-site inhibition model was compared with a one site inhibition model using extra sum of squares F test and a cutoff significance value of 0.05 by simultaneously fitting the data from three independent experiments each run in triplicate. The two-binding site model fit significantly better for methamphetamine inhibition of hOCT1 and hOCT2 as well as amphetamine inhibition of hOCT2 ($p<0.0001$) but not hOCT1 (Table 2-2). The high-affinity EC_{50} values were in the low micromolar range (0.72-5.29 μM) while the apparent low affinity interactions appeared to be in the high micromolar range (58.2-400 μM) for these transporters.

2.3.2 *Uptake of Methamphetamine and Metabolites by hOCT1-3, hMATE1, and hMATE2-K.*

The substrate potential of methamphetamine, amphetamine, and *p*-OHMA was assessed by measuring the uptake of these compounds (1 μM) in control cells and transporter expressing cells (Figure 2-5). After a 5-minute incubation, methamphetamine and amphetamine showed approximately 2-fold greater uptake in cells expressing hOCT2, hMATE1, and hMATE2-K. *p*-OHMA accumulated extensively in hOCT1, hOCT2, hOCT3, and to a lesser degree hMATE1 but not at all in hMATE2-K transfected cells when compared to control cells (Figure 2-5). These data suggest that renal secretion of methamphetamine and its primary metabolites may involve the hOCT2/hMATEs pathway.

2.3.3 *Interaction of Methamphetamine and Metabolites with Renal hOAT1 and hOAT3.*

While hOCT2 and hOAT1/3 respectively mediate renal secretion of organic cations and organic anions, some substrate and inhibitor overlap between hOCT and hOATs has been reported (Lai *et al.*, 2010). We then investigated if methamphetamine and metabolites interact with hOAT1 and hOAT3 (Figure 2-6 A and B). hOAT1- and hOAT3-mediated PAH or ES uptake was completely suppressed by the reference inhibitor probenecid. In contrast, methamphetamine and amphetamine showed no inhibitory effect on hOAT1 or hOAT3 at 1 mM. Only *p*-OHMA showed a significant inhibition of hOAT1 and hOAT3 at 1 mM with 47 ± 17 and 38 ± 28% inhibition, respectively. Uptake studies showed that none of the compounds were substrates of hOAT1 or hOAT3 (Figure 2-6 C-E), suggesting a primary role of the hOCT2/hMATEs pathway in active renal secretion of these compounds.

2.3.4 *Methamphetamine and Metabolites Uptake Kinetics by Cation Transporters.*

The kinetics of hOCT1, hOCT2, hOCT3, hMATE1, and hMATE2-K in transporting methamphetamine, amphetamine, and *p*-OHMA was assessed by determining concentration-dependent transport rates. The specific uptake was obtained for hOCT1-3 by subtracting uptake in the control cells and Eadie-Hofstee plots were evaluated to identify the type of interaction. Due to high passive diffusion at high concentrations, methamphetamine kinetics can only be accurately determined at a low concentration range (0-15 μM). Within this range, methamphetamine displayed saturable kinetics with a K_m of 2.09 ± 0.88 μM (Figure 2-7A, Figure 2-8, Table 2-2), which is very close to the high affinity half-inhibitory concentration (1.21 ± 0.19 μM) observed in Figure 2-4B. For amphetamine, we were able to cover a wider concentration range (0-600 μM). As shown in Figure 2-7B, biphasic transport kinetics were observed, and the K_m values for the

apparent high and the low affinity binding sites were determined to be 0.830 ± 0.55 μM and 534 ± 350 μM, respectively. Interestingly, *p*-OHMA displayed sigmoidal kinetics for hOCT2 as clearly revealed by the Eadie-Hofstee plot (Figure 2-7D). The *p*-OHMA hOCT2 half maximal transport concentration ($K_{1/2}$) is 31.8 ± 9.3 μM and the Hill slope is 1.64 ± 0.15. For *p*-OHMA transport by hOCT1 and hOCT3, no apparent sigmodal or biphasic pattern was observable in the Eadie-Hofstee plot. Fitting to a standard Michaelis-Menten equation yielded apparent K_m values of 14.5 ± 8.7 and 53.3 ± 6.2 μM for hOCT1 and hOCT3, respectively (Figure 2-7, Figure 2-8, and Table 2-3).

hMATE1/2-K transport studies were conducted after intracellular acidification to provide an outwardly directed proton gradient to drive substrate uptake because the MATE transporters function as proton/organic cation exchangers. Under this condition, we observed very high uptake of methamphetamine and metabolites in vector-transfected cells, likely due to a pH effect on passive diffusion. The high uptake in vector-transfected cells makes it difficult to discern transporter-specific uptake at high substrate concentrations. We therefore fitted the concentration-dependent uptake in transporter-expressing cells to a Michaelis-Menten equation with a nonsaturable passive diffusion component (Figure 2-9, Figure 2-10, and Table 2-4). This simultaneous fitting of both carrier-mediated and noncarrier-mediated uptake allowed for an estimate of the apparent K_m values for hMATE1/2-K in the presence of a high passive permeability component (Table 2-3).

2.4 DISCUSSION

In spite of the major role of renal clearance in methamphetamine disposition the molecular mechanisms underlying the tubular secretion of methamphetamine and its major metabolites had

not been fully elucidated (Caldwell *et al.*, 1972; Kim *et al.*, 2004; Carvalho *et al.*, 2012). Here we showed methamphetamine and its metabolites interact with hOCT1-3 and hMATE1/2-K at clinically relevant concentrations (Melega *et al.*, 2007; Shima *et al.*, 2009). We further demonstrated that methamphetamine and amphetamine are substrates of hOCT2, hMATE1, and hMATE2-K, but not hOCT1or hOCT3. Interestingly, *p*-OHMA was a substrate of hOCT1-3 as well as hMATE1, but not hMATE2-K. Methamphetamine and its metabolites do not interact with renal organic anion transporters hOAT1 or hOAT3. Methamphetamine and its metabolites demonstrated complex inhibitory and substrate kinetics with hOCT2. Our data suggest that the hOCT2/hMATEs pathway is involved in renal secretion of methamphetamine and its metabolites, and that inhibition of hOCT2 and hMATEs by methamphetamine may lead to potential DDIs for drugs that are eliminated by the hOCT2/hMATE pathway.

The importance of renal elimination of methamphetamine has long been known; however, the exact molecular mechanisms of renal secretion had not been identified (Beckett and Rowland, 1965c; Caldwell *et al.*, 1972). Here we identified the hOCT2/hMATE pathway as being involved in the active renal secretion of methamphetamine and amphetamine. Methamphetamine may be a potential victim of DDIs by inhibitors (e.g. cimetidine, zalcitabine, dolutegravir) of OCT2 and/or MATE transporters which could reduce its renal clearance and increase exposure (Jung *et al.*, 2008; Reese *et al.*, 2013). Located at the apical membrane of renal proximal tubule cells, the MATE transporters function as proton/organic cation exchangers, which rely on the transmembrane proton gradient to drive organic cation secretion into the urine (Otsuka *et al.*, 2005). The pH dependence of methamphetamine and amphetamine renal excretion rates has long been known, where urine acidification increases renal excretion while urine alkalization has an opposite effect (Beckett and Rowland, 1965a, c; b). The effect of urinary pH on methamphetamine

or amphetamine renal excretion has been mostly attributed to the pH effect on ionization and membrane partitioning, which affects tubular reabsorption of these weak bases (Beckett and Rowland, 1965a, c; b). Here, our data suggest that renal secretion of methamphetamine and amphetamine involves the pH-dependent MATE transporters. Therefore, the increased excretion rates observed with acidic urine could be due to a combined effect of acidic pH in reducing partition-mediated reabsorption along with increasing MATE-mediated tubular secretion.

The liver is the major site of methamphetamine metabolism. Intriguingly, methamphetamine and amphetamine were not substrates of hOCT1, the major OCT isoform responsible for hepatic uptake of organic cations. Therefore, hepatic uptake of methamphetamine and amphetamine may be facilitated by other transporters yet to be identified or be driven by passive diffusion. Interestingly, *p*-OHMA was transported by hOCT1, suggesting that the para hydroxyl group may be important for OCT1 transport selectivity of substituted amphetamines. hOCT1 may thus be involved in hepatic transport of *p*-OHMA.

In this study, we used metformin as the probe substrate because it is recommended as an *in vitro* and *in vivo* probe substrate for evaluating hOCT2, hMATE1, and hMATE2-K interaction studies by the International Transporter Consortium (ITC), Food and Drug Administration (FDA), and European Medicines Agency (EMA) (European Medicines Agency, 2012; Food and Drug Administration, 2012b; Hillgren *et al.*, 2013). Substrate dependent inhibition has previously been demonstrated for OCTs with a number of substrates and inhibitors (Moaddel *et al.*, 2005; Gorbunov *et al.*, 2008; Minuesa *et al.*, 2009; Hacker *et al.*, 2015; Yin *et al.*, 2016). For example, inhibition potencies of several clinical drugs towards hOCT2 were reported to be approximately 10-fold more potent when atenolol was used as the substrate as compared to metformin (Yin *et al.*, 2016). Due to the observed complex interactions, the apparent inhibition potencies of

amphetamines may be highly dependent on the substrate. As an illicit drug, abusers may use methamphetamine while taking prescription medications. Testing the inhibition potencies with the specific hOCT substrate drugs used by methamphetamine abusers may be warranted to determine the likelihood of clinically relevant interactions.

Particularly high levels of methamphetamine abuse are reported in individuals receiving treatment for HIV and hepatitis who may be receiving multiple medications for treatment. (Panenka *et al.*, 2013; Volkow, 2013; Bracchi *et al.*, 2015). Importantly, numerous antiretrovirals (e.g. lamivudine, zalcitabine) interact with OCTs and rely on these transporters for cellular uptake into HIV-infected CD4 cells (Zhou *et al.*, 2006; Jung *et al.*, 2008). Methamphetamine and its metabolites inhibited the active transport of the probe substrate metformin by hOCT1-3 and hMATE1/2-K (Table 2-1) within the concentration range reported in abusers of methamphetamine (Melega *et al.*, 2007; Shima *et al.*, 2009). The free plasma concentrations of methamphetamine in some abusers have been reported to be in the tens of micromolar range and even 130 μM in one individual, indicating the potential to reach inhibitory concentrations of hOCT1-3 and hMATE1/2-K *in vivo* (de la Torre *et al.*, 2004; Shima *et al.*, 2008). Inhibition of hOCT1 and hOCT2 may reduce intracellular levels of some antiretrovirals in HIV-infected CD4 cells, reducing their effective concentration and efficacy at the site of action (Minuesa *et al.*, 2008, 2009; Wagner *et al.*, 2016). These potential distributional DDIs are of particular concern with drugs of abuse as patients may not be willing to reveal their use of illicit drugs.

Methamphetamine and its metabolites demonstrated complex interactions with hOCT1 and hOCT2, suggesting they may have multiple binding sites on these transporters. The structural basis of the complex kinetic interactions between amphetamines and hOCTs is currently unclear as the crystal structures of these transporters have not been obtained. Amphetamine showed

biphasic hOCT2 uptake kinetics with an apparent high (0.830 ± 0.55 μM) and low affinity (534 ± 350 μM) aligning with the observed high and low affinity inhibitory interactions. Conversely, *p*-OHMA had a relatively steep hOCT2 inhibition Hill slope (1.55 ± 0.32) and demonstrated sigmoidal uptake kinetics (Table 2-3,Figure 2-7). Sigmoidal uptake kinetics may be characteristic of homotropic activation (Segel, 1976; Atkins, 2005). Both a large binding pocket in the outward facing cleft allowing for spatially distinct binding as well as a distal allosteric binding site have been proposed for OCTs based on kinetics and biochemical analyses (Gorboulev *et al.*, 1999; Harper and Wright, 2012; Koepsell, 2015). The possible distal allosteric binding site has demonstrated very high affinity interactions with no transport observed in the concentrations range (e.g. 6-41 pM for MPP+) (Moaddel *et al.*, 2005; Gorbunov *et al.*, 2008; Minuesa *et al.*, 2009; Koepsell, 2015). Binding within the transportable region is generally a lower affinity interaction (e.g. 0.87-12.3 μM for MPP+) with known substrates (Moaddel et al., 2005; Gorbunov et al., 2008; Minuesa et al., 2009; Koepsell, 2015). Recent developments have also suggested the possibility of simultaneous binding of two substrates within the transport site (Harper and Wright, 2012; Koepsell, 2015). The apparent affinities observed for methamphetamine and metabolites across their transportable concentration ranges suggest that both binding sites may reside within the transport region. More studies are needed to understand the complex kinetic behaviors of the OCTs and their structure-function relationships.

In summary, our study determined the molecular mechanisms involved in transport and disposition of methamphetamine and its metabolites. Moreover, our studies showed that methamphetamine has the potential to inhibit hOCT and hMATE transporters at clinically relevant concentrations. Finally, we identified complex kinetic interactions between amphetamines and hOCT2. Our findings provide useful information that may be considered when prescribing

medications to methamphetamine users to mitigate the risk of DDIs that may potentially compromise therapeutic efficacy and drug safety.

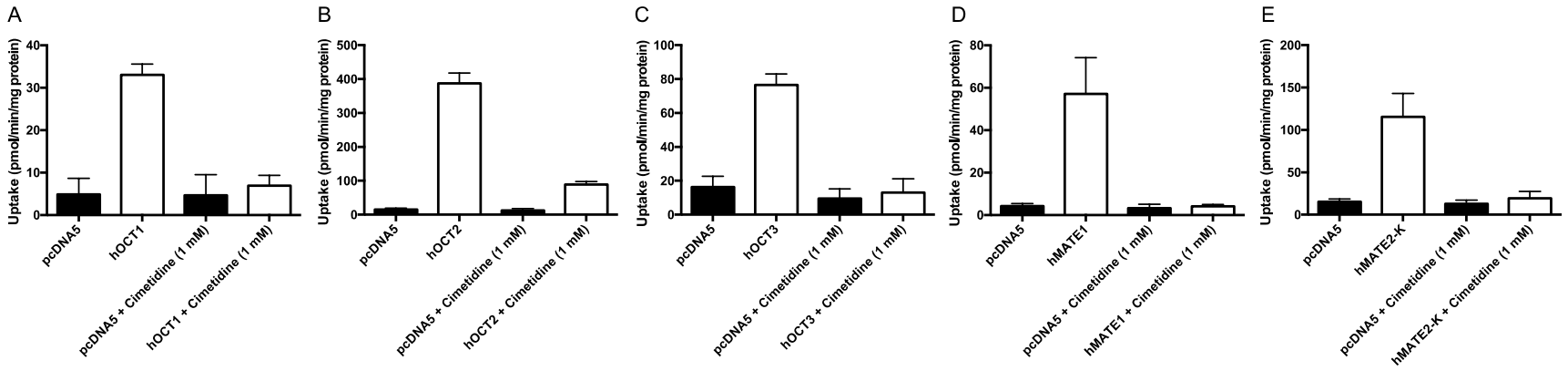

Figure 2-1. Metformin uptake by hOCT1, hOCT2, hOCT3, hMATE1, and hMATE2-K in Flp-in HEK293 cells in the presence or absence of the prototypical inhibitor cimetidine.

Incubations for of hOCT1 (A), hOCT2 (B), hOCT3 (C), hMATE1 (D), and hMATE2-K (E) were within the linear initial rate of uptake.

Each data point represents the mean ± S.D. from three independent experiments.

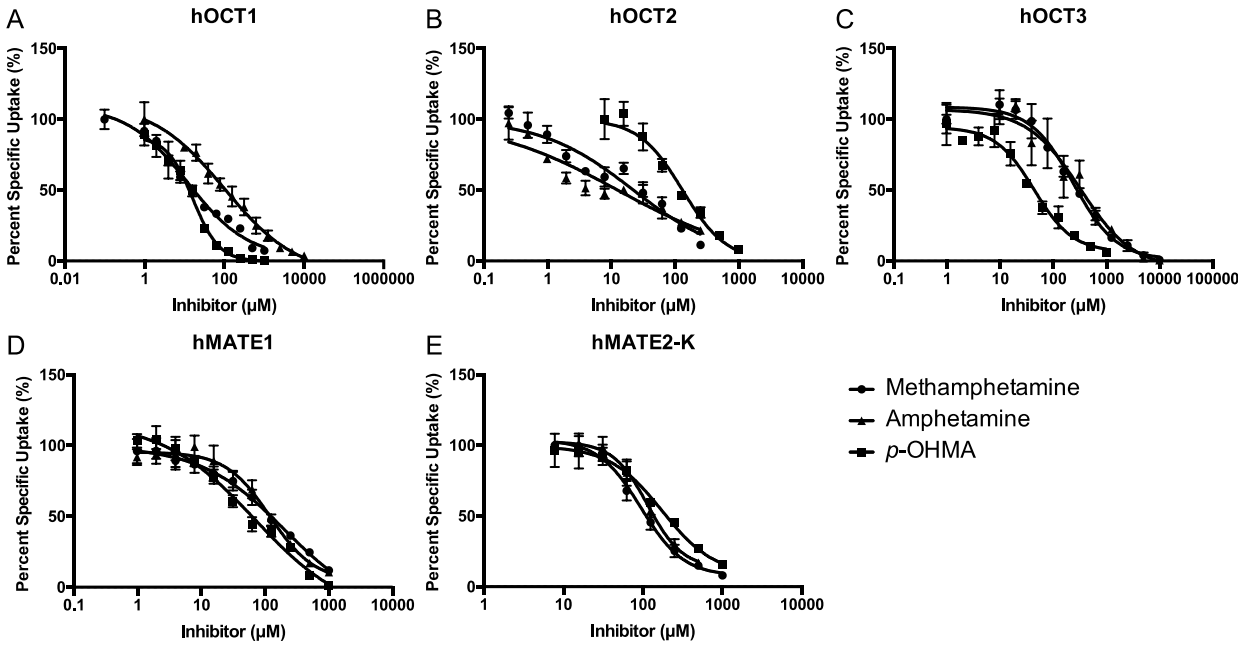

Figure 2-2. Inhibition by methamphetamine, amphetamine, and *p*-OHMA of hOCT1, hOCT2, hOCT3, hMATE1, and hMATE2-K.

Uptake of [^{14}C]metformin (11μM) in the absence and presence of inhibitor was measured in both transporter expressing and control HEK cells. Transporter-specific uptake was obtained by subtracting the uptake in vector-transfected cells from the uptake in transporter-expressing cells. Incubations were performed at 2, 0.5, 2, 5, and 0.5 minutes for of hOCT1 (A), hOCT2 (B), hOCT3 (C), hMATE1 (D), and hMATE2-K (E), respectively, which are within the linear initial rate of uptake. Activity in the absence of inhibitor (100%) corresponds to 28.2, 373, 60.2, 52.9, and 100 pmol/min/mg protein for hOCT1, hOCT2, hOCT3, hMATE1, and hMATE2-K, respectively. Each data point represents the mean ± S.D. from one representative experiment in triplicate. Curves from two additional independent repeats are displayed in Figure 2-3. The IC_{50} values shown in Table 2-1 are mean ± S.D. of the IC_{50} values from the three independent experiments.

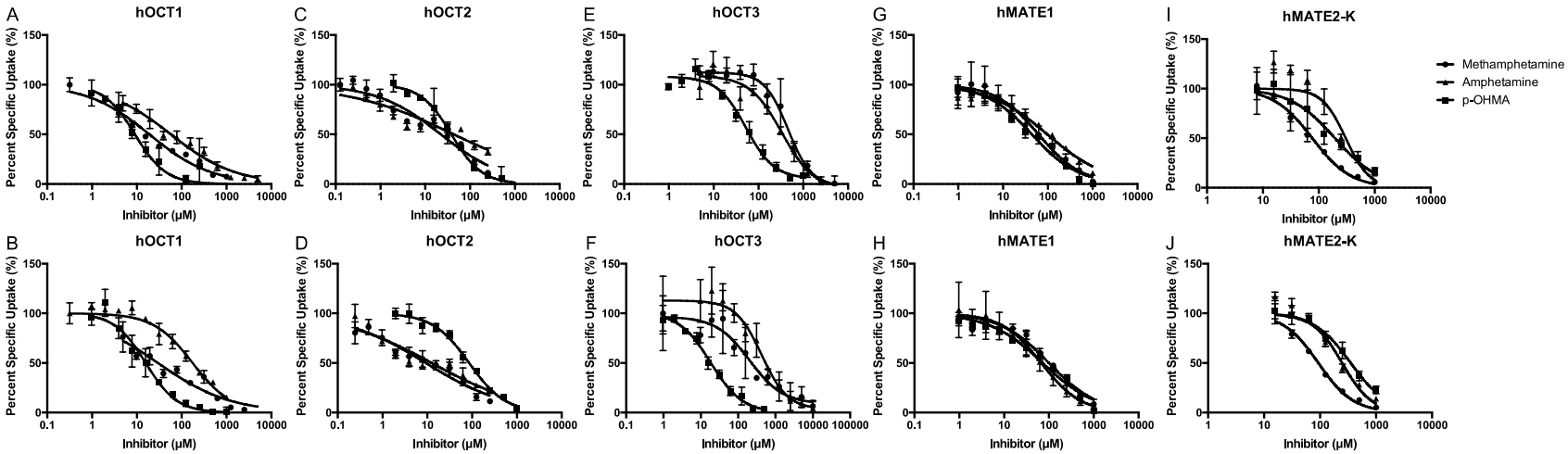

Figure 2-3. Replica studies of methamphetamine, amphetamine, and *p*-OHMA inhibition of hOCT1, hOCT2, hOCT3, hMATE1, and hMATE2-K.

Uptake of [^{14}C]metformin (11μM) in the absence and presence of inhibitor was measured in both transporter expressing and control HEK cells. Incubations were performed at 2, 0.5, 2, 5, and 0.5 minutes for of hOCT1 (A & B), hOCT2 (C & D), hOCT3 (E & F), hMATE1 (G & H), and hMATE2-K (I & J), respectively, which are within the linear initial rate of uptake. The top and bottom rows represent the second and third sets of experiments repeated independently. Each data point represents the mean ± S.D. from one experiment performed in triplicate.

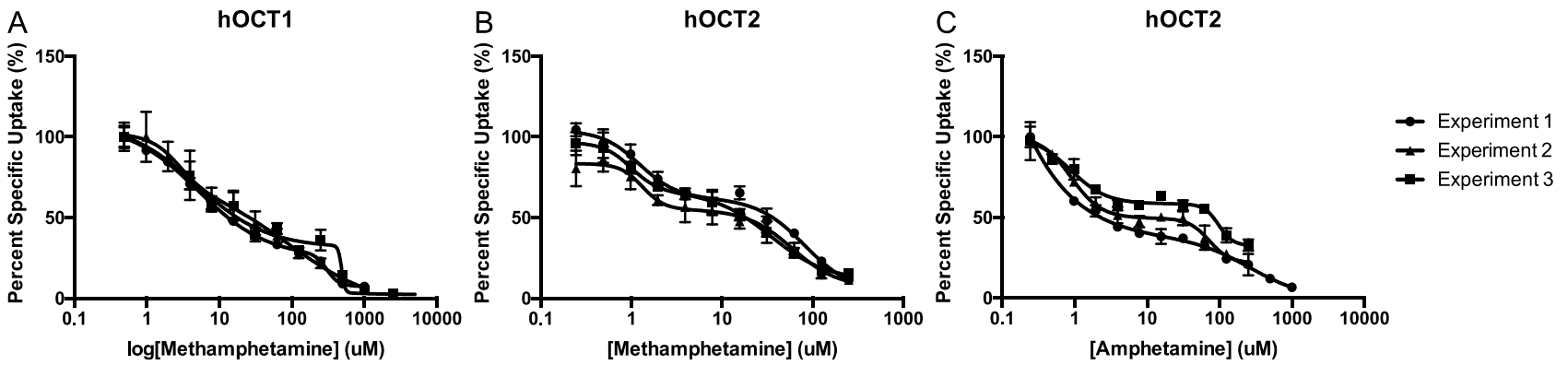

Figure 2-4. Inhibition of hOCT1 and hOCT2 by methamphetamine and amphetamine fitted to a two binding site model.

Uptake of 11 μM [^{14}C]metformin in the absence and presence of inhibitor was measured in both transporter-expressing and control (vector-transfected) HEK cells. Transporter-specific uptake was obtained by subtracting the uptake in control cells from the uptake in transporter-expressing cells. Data was fit to the two-site inhibition model (Eq. 2) for methamphetamine inhibition of hOCT1 (A), methamphetamine inhibition of hOCT2 (B), and amphetamine inhibition of hOCT2 (C). Each data point represents the mean ± S.D. from one of three independent experiments performed in triplicate.

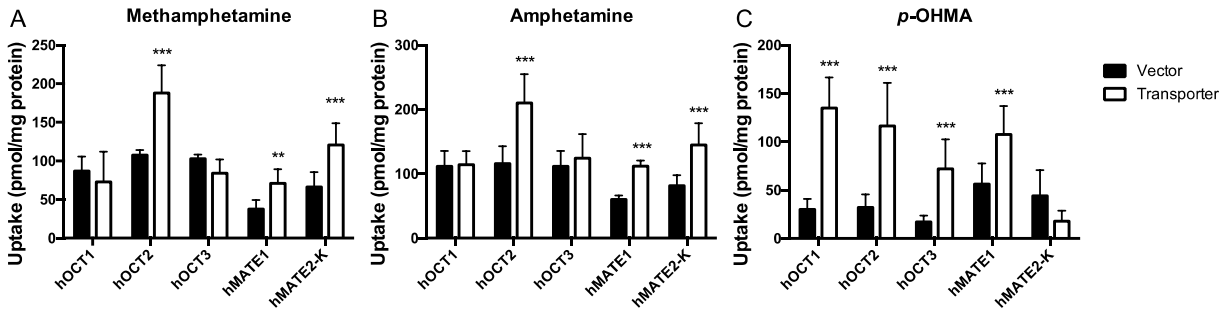

Figure 2-5. Uptake of 1 μM methamphetamine, amphetamine, and *p*-OHMA by hOCT1, hOCT2, hOCT3, hMATE1, and hMATE2-K.

Uptake was measured after a 5-minute incubation at 37°C. Data are illustrated as the mean ± S.D. from three independent experiments performed in triplicate. Uptake in transporter-expressing cells was compared with that in control cells (**P<0.01; ***P<0.001).

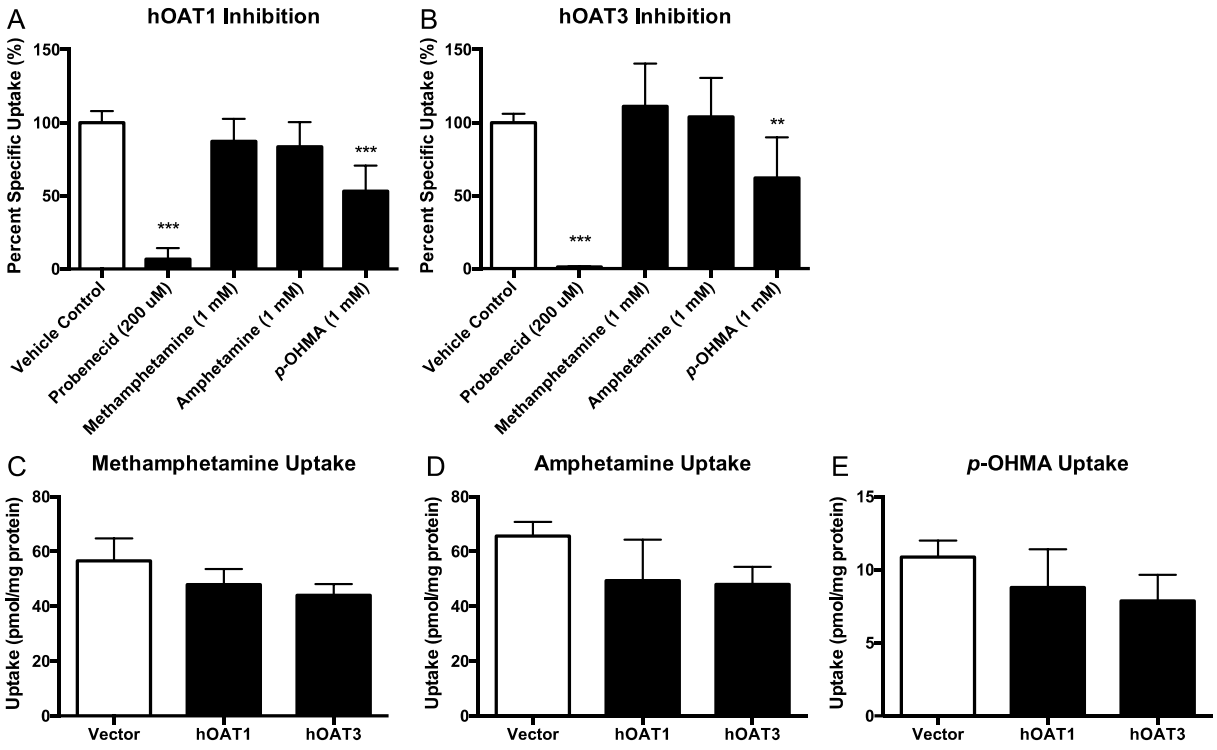

Figure 2-6. Interactions of methamphetamine, amphetamine, and *p*-OHMA with renal hOAT1 and hOAT3.

Effect of methamphetamine, amphetamine, and *p*-OHMA on PAH (1 µM) uptake by hOAT1 (A) and estrone sulfate (0.06µM) uptake by hOAT3 (B) was measured at 1 minute after incubation at 37°C. Transporter-specific uptake was obtained by subtracting the uptake in vector-transfected cells from the uptake in transporter-expressing cells. The classic OAT inhibitor probenecid was used as control. Activity in the absence of an inhibitor (100%) corresponded to 36.6 and 2.1 pmol/min/mg protein for PAH and estrone sulfate uptake, respectively. Uptake of methamphetamine (C), amphetamine (D), and *p*-OHMA (E) by hOAT1 and hOAT3 was measured after a 5-minute incubation at 37°C. Data are illustrated as the mean ± S.D. from three independent experiments performed in triplicate. Uptake in transporter-expressing cells was compared with that in control cells (**P<0.01; ***P<0.001).

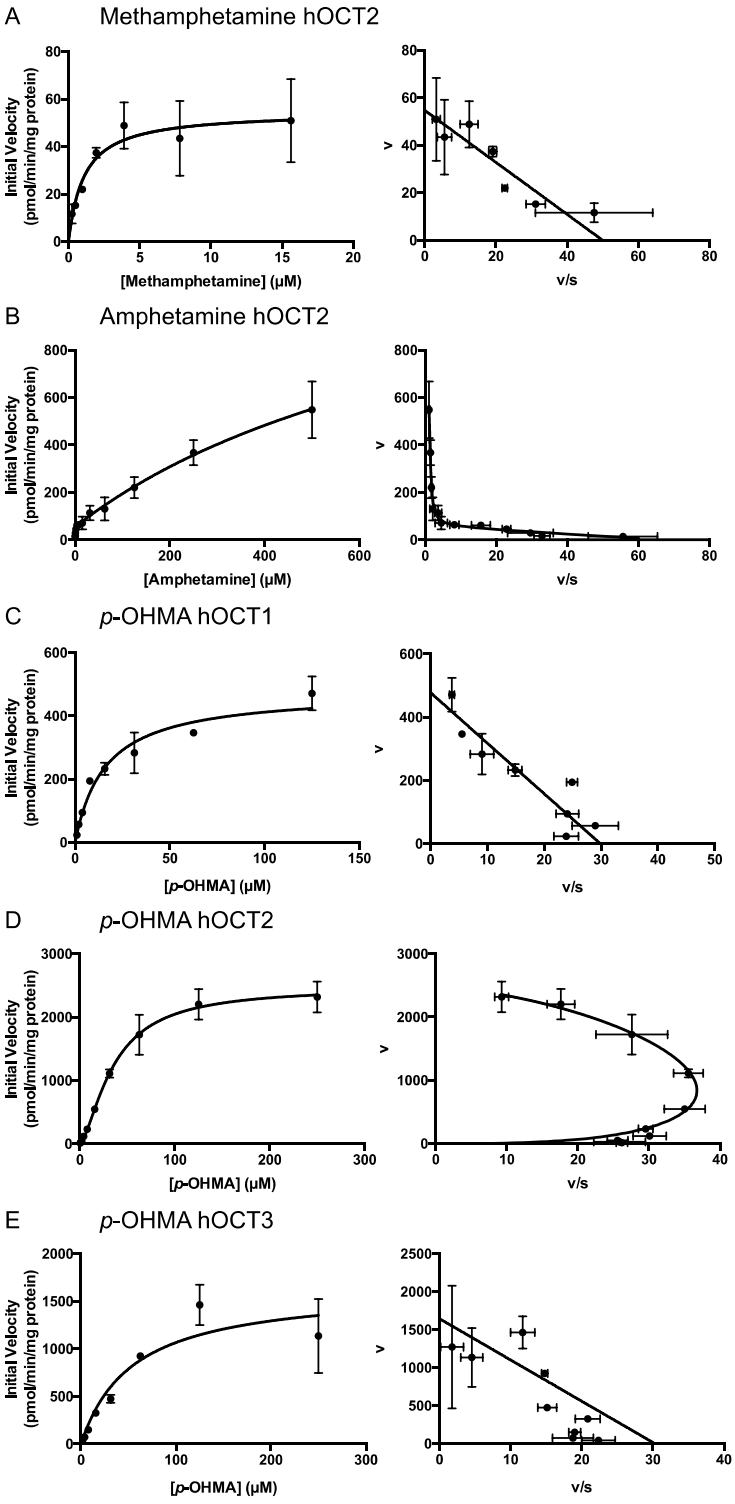

Figure 2-7. Methamphetamine, amphetamine, and *p*-OHMA uptake kinetics by hOCTs. Concentration-dependent uptake of substrate was measured in both transporter-expressing and control cells at 37°C after 1 minute incubations. Transporter-specific uptake was obtained by

subtracting the uptake in vector-transfected cells from the uptake in transporter-expressing cells. Panes display saturation curves (v vs. s) and Eadie-Hofstee transformations (v vs. v/s) for the kinetic data. Based on the Eadie-Hofstee plots, kinetics for hOCT2-mediated methamphetamine transport (A) and hOCT- and hOCT3-mediated *p*-OHMA transport (C and E) were fitted with the standard Michaelis-Menten equation. hOCT2-mediated amphetamine transport (B) was fitted to a biphasic Michaelis-Menten equation (Eq. 2-5). hOCT2-mediated *p*-OHMA transport (D) was fitted to the Michaelis-Menten equation with a Hill slope (Eq. 2-4). Each data point represents the mean ± S.D. from one representative experiment in triplicate. Curves from two additional independent repeats are displayed in Figure 2-8. The kinetic parameters in Table 2-2 are mean ± S.D. of the values from three independent experiments.

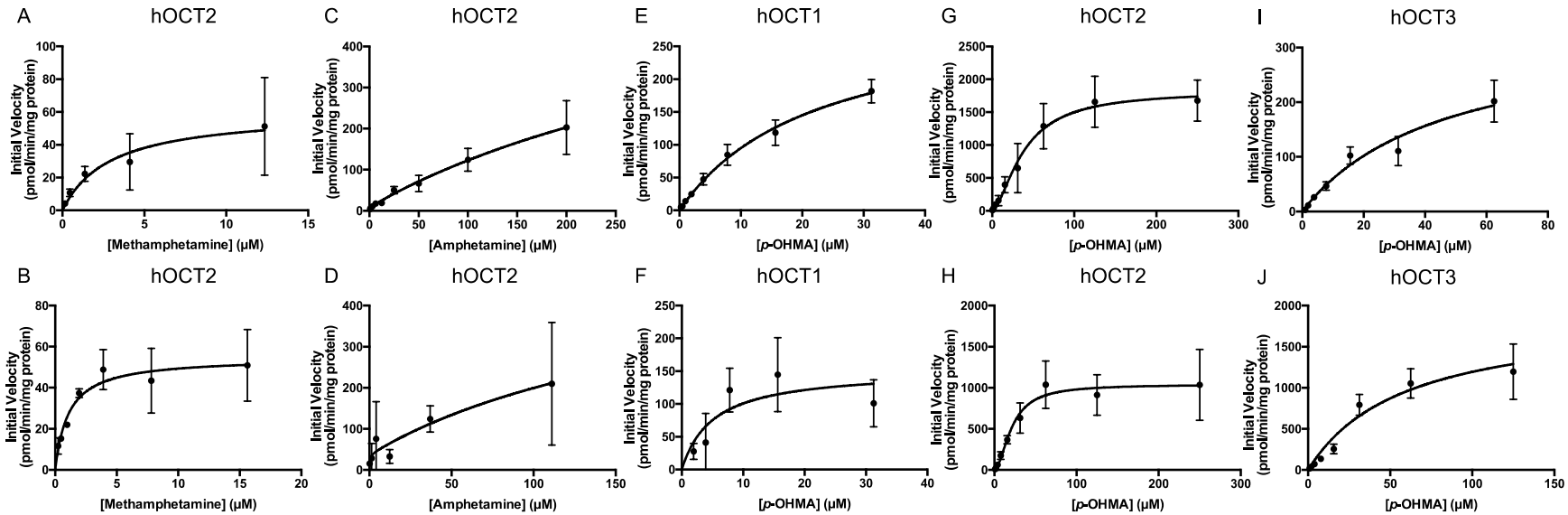

Figure 2-8. Replica studies on methamphetamine, amphetamine, and *p*-OHMA uptake kinetics by hOCTs.

Concentration-dependent uptake of substrate was measured in both transporter-expressing and control (vector-transfected) cells at 37°C after 1 minute incubations. Transporter-specific uptake was obtained by subtracting the uptake in control cells from the uptake in transporter-expressing cells. Kinetics for hOCT2-mediated methamphetamine transport and hOCT1- and hOCT3-mediated *p*-OHMA transport were fitted with the standard Michaelis-Menten equation. hOCT2-mediated amphetamine transport was fitted to a biphasic Michaelis-Menten equation (Eq. 5). hOCT2-mediated *p*-OHMA transport was fitted to the Michaelis-Menten equation with a Hill slope (Eq. 4). Each data point represents the mean ± S.D. from one of three independent experiments each run in triplicate. The top and bottom rows of panes represent the second and third sets of experiments repeated independently.

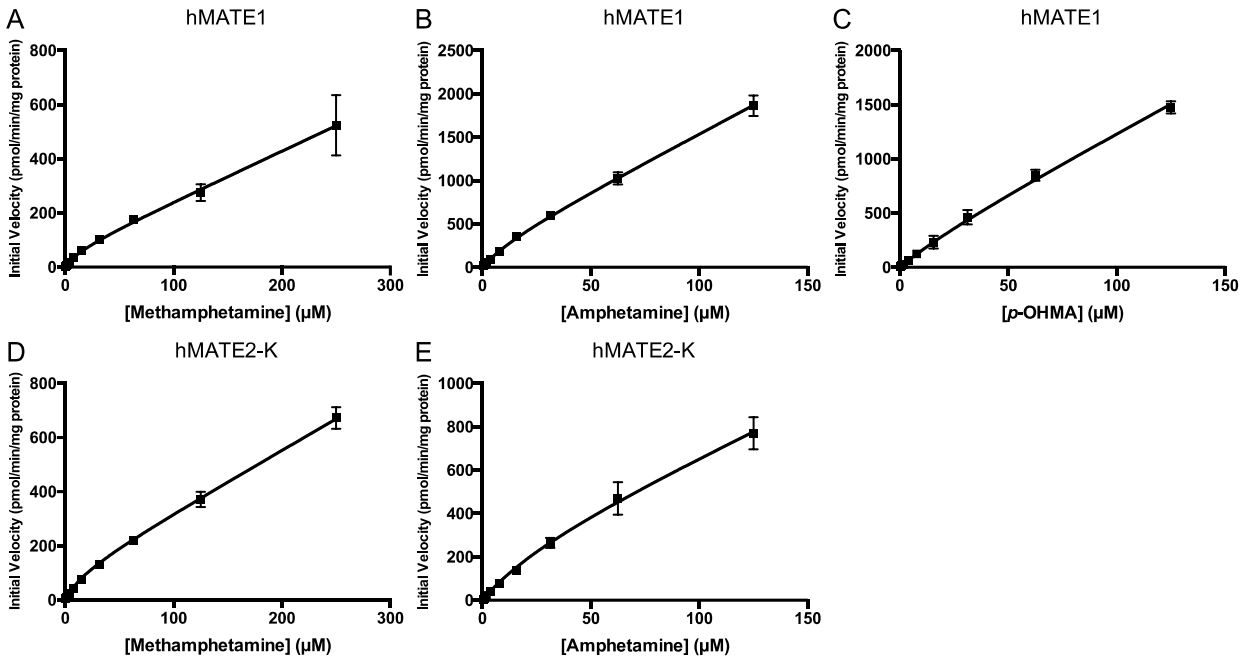

Figure 2-9. Methamphetamine and metabolite uptake kinetics by hMATE1 and hMATE2-K.

Methamphetamine, amphetamine and *p*-OHMA uptake in hMATE1-expresing cells was performed during initial linear uptake time at 5, 2, and 2 min respectively (A-C). Methamphetamine and amphetamine hMATE2-expresing cells was performed during initial linear uptake time at 5 min (D and E). Incubations were performed at 37°C and data were fitted with a Michaelis-Menten equation with a nonsaturable passive diffusion component (Eq. 2-3). Each data point represents the mean ± S.D. from one representative experiment in triplicate. Curves from two additional independent repeats are displayed in Figure 2-10. The kinetic parameters in Table 2-3 are mean ± S.D. of the values from three independent experiments.

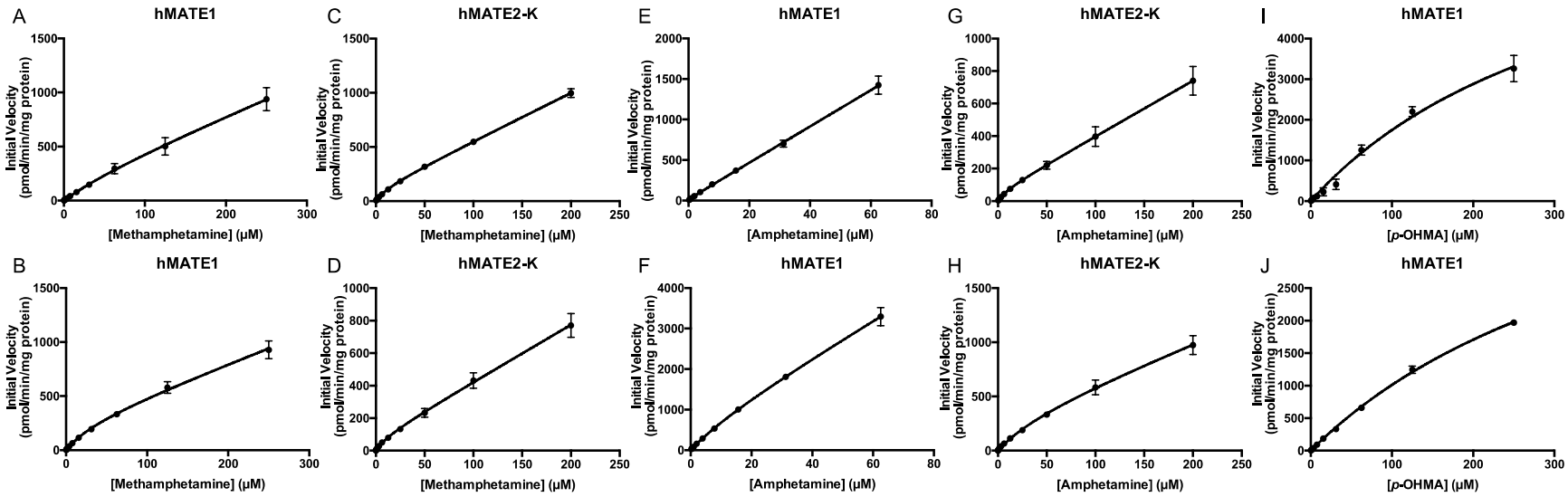

Figure 2-10. Replica studies of methamphetamine (A-D), amphetamine (E-F), and *p*-OHMA (I & J) uptake kinetics by hMATE1 and hMATE2-K.

Uptake in hMATE1-expresing cells was performed during initial linear uptake time at 5, 2, and 2 min, respectively. Incubations were performed at 37°C and data were fitted with a Michaelis-Menten equation with a nonsaturable passive diffusion component (Eq. 3). Each data point represents the mean ± S.D. from one of three independent experiments each performed in triplicate. The top and bottom rows of panes represent the second and third sets of experiments repeated independently.

Table 2-1. IC_{50} and Hill slope values of methamphetamine, amphetamine, and *p*-OHMA for hOCT1-3 and hMATE1/2-K using [^{14}C]metformin as the substrate.

Transporter	Methamphetamine		Amphetamine		*p*-OHMA	
	IC_{50} (μM)	Hill Slope	IC_{50} (μM)	Hill Slope	IC_{50} (μM)	Hill Slope
hOCT1	21.1 ± 8.8	0.55 ± 0.02	96.7 ± 37	0.61 ± 0.28	12.0 ± 3.4	1.17 ± 0.14
hOCT2	15.0 ± 6.8	0.56 ± 0.07	20.3 ±16.9	0.44 ±0.1	83.8 ± 22.3	1.55 ± 0.32
hOCT3	300 ± 139	1.42 ± 0.68	363 ± 56.4	1.1 ±0.2	44.4 ± 25.5	1.1 ±0.26
hMATE1	107 ± 38	0.79 ±0.09	94.0 ± 25.3	0.89 ±0.2	59.1 ± 14.3	0.84 ±0.12
hMATE2-K	84.3 ±12.9	1.63 ±0.14	158 ±48	1.9 ±0.6	234 ± 86.8	1.21 ± 0.11

Results represent mean ± S.D. of three independent experiments each run in triplicate.

Table 2-2. EC_{50} of high-affinity binding site, low-affinity binding site, and P values for statistical comparison of two-binding versus one-binding site.

Inhibitor	Transporter	High-Affinity EC_{50} (μM)	Low-Affinity EC_{50} (μM)	Model Comparison: Two-Binding vs. One-Binding Site
Methamphetamine	hOCT1	5.29 ± 0.66	400 ± 229	P<0.0001
	hOCT2	1.21 ± 0.19	58.2 ± 23.4	P<0.0001
Amphetamine	hOCT1	NA	NA	P=0.55
	hOCT2	0.72 ± 0.29	145 ±104	P<0.0001

EC_{50} values were obtained by fitting inhibition data in Figure 2-5 using equation 2-2 described in Materials and Methods. The last column lists the P value from comparing equation 2-1 and equation 2-2 by an extra sum of squares F test. Results represent Mean ± S.D. of three independent experiments each run in triplicate. NA: Not Applicable.

Table 2-3. Kinetic parameters of methamphetamine and metabolites determined from modeling of data in Figure 2-7.

Compound	Transporter	K_{m1} (μM)	V_{max1} (pmol/mg/min)	K_{m2} (μM)	V_{max2} (pmol/mg/min)
Methamphetamine	hOCT2	2.09 ± 0.88	49.7 ± 12.2	ND	ND
Amphetamine	hOCT2	0.830 ± 0.55	34.6 ± 23.7	534 ± 350	853 ± 474
p-OHMA	hOCT1	14.5 ± 8.7	312 ± 163	NA	NA
	hOCT2	$K_{1/2}$: 31.8 ± 9.3 h: 1.64 ± 0.15	1780 ± 718	NA	NA
	hOCT3	53.3 ± 6.2	1290 ± 830	NA	NA

Models were chosen based on examination of Eadie-Hofstee plots. Methamphetamine was fit to a standard Michaelis-Menten equation. Amphetamine uptake kinetics were fit to a biphasic Michaelis-Menten equation (Eq. 2-5). *p*-OHMA hOCT1 and hOCT3 mediated transport were fit to a standard Michaelis-Menten equation. Sigmoidal kinetics of hOCT2-mediated *p*-OHMA transport were obtained by fitting transporter mediated uptake to the Michaelis-Menten equation with a hill slope (Eq. 2-5) for the substrate concentration and half maximal transport concentration ($K_{1/2}$ in place of K_m). Results represent Mean ± S.D. of three independent experiments each run in triplicate. ND: Not determined due to high diffusion. NA: Not Applicable

Table 2-4. Apparent kinetic transport parameters for methamphetamine, amphetamine, and *p*-OHMA for hMATE1 and hMATE2-K from simultaneously modeling active and passive accumulation.

Transporter	Methamphetamine		Amphetamine		*p*-OHMA	
	K_m (μM)	V_{max} (pmol/mg/min)	K_m (μM)	V_{max} (pmol/mg/min)	K_m (μM)	V_{max} (pmol/mg/min)
hMATE1	20.6 ± 4.5	86.6 ± 54	14.1 ± 4.9	238 ± 141	49.8 ± 26	257 ± 190
hMATE2-K	18.1 ± 11	97.7 ± 25.3	16.4 ± 12.2	92.9 ± 8.5	NA	NA

Results represent Mean ± S.D. of three independent experiments each run in triplicate. NA: Not Applicable.

Chapter 3. KINETIC EVIDENCE FOR SPATIALLY DISTINCT SUBSTRATE BINDING SITES IN ORGANIC CATION TRANSPORTER 2

3.1 INTRODUCTION

Organic cation transporter (OCT) 2 mediates the first step in the active renal secretion of cationic drugs by moving them out of the blood and into the proximal tubule cell (Yin *et al.*, 2015; Wagner *et al.*, 2016; Miners *et al.*, 2017). Due to the role of OCT2 in the elimination of drugs, inhibition of OCT2 can lead to decreased renal clearance and increased exposure and possibly toxicity by the victim drug in vivo (Yin and Wang, 2016; Ivanyuk *et al.*, 2017). In vitro inhibition assessments are recommended to predict the potential for clinically relevant drug-drug interactions with OCT2 (European Medicines Agency, 2012; Zamek-Gliszczynski, Lee, *et al.*, 2013; Food and Drug Administration, 2017). Predictive models that compare the clinical concentrations of the perpetrator drug with its in vitro IC_{50} or K_i value for a drug transporter is used to assess the likelihood of an in vivo drug-drug interaction (European Medicines Agency, 2012; Zamek-Gliszczynski, Lee, *et al.*, 2013; Food and Drug Administration, 2017). These in vitro to in vivo predictions have been complicated by many groups observing substrate dependent inhibition of OCT2 activity in vitro where the apparent potency of an inhibitor (i.e. IC_{50} or K_i) is vastly dissimilar when different substrates are used (Moaddel *et al.*, 2005; Gorbunov *et al.*, 2008; Minuesa *et al.*, 2009; Belzer *et al.*, 2013; Thévenod *et al.*, 2013; Hacker *et al.*, 2015; Yin *et al.*, 2016). Further complicating extrapolation of in vitro inhibitory potencies are our and others' observations of atypical inhibition kinetics including biphasic inhibition (Minuesa *et al.*, 2009; Wagner *et al.*, 2017).

Our laboratory previously demonstrated that apparent inhibition potencies of several clinical drugs towards hOCT2 were approximately 10-fold greater when atenolol was used as the substrate as compared to metformin (Yin *et al.*, 2016). These differences in potency also lead to disagreement in predicting the in vivo relevance of inhibition based on simple static models. The drug metabolizing enzyme cytochrome P450 (CYP450) 3A has also been shown to display substrate dependent inhibition and atypical kinetics (Kenworthy *et al.*, 1999). A wealth of information from crystal structures and enzyme kinetics has led to an improved understanding of CYP3A4 substrate dependent inhibition (Atkins, 2006). Current best practices for dealing with CYP3A inhibition include using at least two substrates known to behave differently and any clinically relevant substrates of concern (European Medicines Agency, 2012; Food and Drug Administration, 2017).

Currently, the structural basis of the complex kinetic interactions underpinning substrate dependent inhibition with OCT2 is unclear as a crystal structure is not available. Mutagenesis studies have suggested OCTs have a large outward facing binding cleft with partially overlapping binding regions for different substrates and inhibitors (Gorboulev *et al.*, 1999; Popp *et al.*, 2005; Koepsell *et al.*, 2007). Binding and inhibition studies have provided evidence that two of the same substrate or inhibitor may bind to the outward conformation simultaneously (Gorbunov *et al.*, 2008; Minuesa *et al.*, 2009; Wagner *et al.*, 2017). We previously showed that methamphetamine and amphetamine display biphasic transport and inhibition kinetics with hOCT2, suggesting multiple binding sites (Wagner *et al.*, 2017). The simultaneous transport of two substrate molecules was proposed based on substrate binding experiments for OCTs (Koepsell, 2015), indicating that OCTs may function according to a six-state transport model in addition to the originally proposed typical four-state model for carriers (Figure 3-1) (Koepsell, 2015).

The four-state model for a carrier, or Iso Uni Uni kinetics, originally proposed for OCTs highlights the complexities of translocation of a substrate across a membrane as opposed to a typical enzyme reaction that can be adequately described by Michaelis-Menten kinetics (Segel, 1976; Stein, 1986; Budiman *et al.*, 2000; Stein and Litman, 2014). OCTs typically function as electrogenic facilitative transporters with the direction of transport dependent on the electrochemical gradient of the substrate (Koepsell *et al.*, 2007; Wagner *et al.*, 2016). Alternatively, OCTs may also function as electroneutral antiporters when a sufficient concentration of counter ion substrate is on the opposing membrane side (i.e. trans) in vitro (Budiman *et al.*, 2000). The asymmetrical distribution of inward and outward facing conformations of OCTs is driven by the electric potential in the absence of substrate but can be altered in the presence of a substrate (Budiman *et al.*, 2000; Gorbunov *et al.*, 2008). These conformational changes and movement across the cell membrane are incorporated into the four-state carrier model (Figure 3-1) (Stein, 1986; Stein and Litman, 2014). The addition of membrane sidedness is also built into the constants that make up the apparent K_m and V_{max} of a transporter. For example, the transporter turn over number (k_{cat}) is a combination of the rates of translocation across the membrane as well as return to the original outward facing transporter conformation for the next round of transport (Stein, 1986; Stein and Litman, 2014).

The four-state model for a carrier also has implications for the models of inhibition used (Krupka and Devés, 1983). Notably, inhibition of a carrier can lead to non-intuitive changes in victim substrate kinetics due to the multiple steps being required for the translocation of the substrate across the membrane (Krupka and Devés, 1980; Deves and Krupka, 1990; Deves, 1991). To date, simple enzyme kinetic models have typically been applied to understanding the substrate and inhibition kinetics of OCTs. However, mounting reports suggesting more complicated

substrate and inhibitor interactions with OCTs led us to more mechanistically investigate the inhibition kinetics within the context of the carrier model. Our observed substrate dependent inhibition of hOCT2 mediated atenolol and metformin transport as well as the biphasic methamphetamine inhibition of hOCT2 provided excellent opportunities for deeper evaluation of hOCT2 interactions (Yin *et al.*, 2016; Wagner *et al.*, 2017). We theorized that atenolol may bind to a spatially unique site from metformin within the hOCT2 transportable area and that methamphetamine's high and low affinity binding interactions may overlap differently with atenolol and metformin. The goals of this study were to characterize the complex interactions previously observed with methamphetamine and determine the inhibition mechanisms for prototypical OCT2 substrates with each other in vitro.

3.2 Materials and Methods

3.2.1 *Materials.*

Metformin and atenolol were purchased from Sigma-Aldrich (St. Louis, MO) and were of analytical grade. [^{14}C]metformin (115 mCi/mmol) and [^{3}H]atenolol (3.5 Ci/mmol) were purchased from Moravek Biochemicals, Inc. (Brea, CA). Cell culture media and reagents were purchased from Invitrogen (Carlsbad, CA). All other chemicals were commercially available and of analytical grade or higher.

3.2.2 *Uptake and Inhibition Assays in HEK293 Cells.*

Flp-in HEK293 cells stably expressing, hOCT2 were previously generated in our laboratory (Duan *et al.*, 2015). The cells were cultured in high glucose DMEM media with 10% FBS, 1 mM L-glutamine, 100 U/mL penicillin, 100 μg/mL streptomycin, and 150 μg/mL hygromycin B

supplementation at 37°C with 5% CO_2 and high humidity. All cell culture plastic surfaces were coated with 0.01% poly-D-lysine to improve cell attachment. Uptake and inhibition assays were performed as previously described with modification for flux ratio experiments (Duan and Wang, 2010; Duan *et al.*, 2015; Yin *et al.*, 2015; Wagner *et al.*, 2017). Briefly, cells were seeded in 96-well plates at 100,000 cells/well and grown overnight. Prior to incubation initiation, cells were washed with pre-warmed Hanks balanced salt solution (HBSS) and allowed to acclimatize for 10 minutes at 37°C. Media was removed and incubation initiated by addition of 100 μL of HBSS at pH 7.4 containing a substrate with or without inhibitor. Uptake was stopped by removal of media and washing the cells three times with ice cold HBSS. Cells were lysed with 100 μL of 1 M NaOH and neutralized with 100 μL of 1 M HCl for measurement by liquid scintillation counting (LSC) (PerkinElmer, Tri-Carb B3110TR, Waltham, MA). Protein content in the lysate in each well was measured by the BCA Protein Assay Kit (Pierce Chemical, Rockford, IL) and the uptake in cells was normalized to their total protein concentrations.

Flux ratios are a comparison of zero-trans and infinite-trans uptake rates and represent a comparison of the rate of conformational change of the bound transporter across the membrane versus the rate for the unbound transporter. (Krupka and Devés, 1983; Deves and Krupka, 1990). Zero-trans uptake experiments are performed with no pre-loading of substrate assuming effectively zero substrate in the trans compartment at the start. Infinite-trans uptake experiments are performed with pre-loading of saturating ($>>K_m$) substrate concentrations assuming effectively infinite substrate in the trans compartment at the start. Based on the four state transporter model proposed for OCTs (Budiman *et al.*, 2000), a flux ratio of 1 indicates the rate of conformational change of the transporter from one side to the other is similar for the transporter when it is bound to a substrate or not bound to a substrate (Krupka and Devés, 1983; Deves and Krupka, 1990).

Flux ratios greater than one indicate the rate of conformational change of a transporter bound with substrate is faster than without a substrate. Conversely, a flux ratio less than one indicates a poor substrate with a rate of translocation that is slower when the transporter is bound to the substrate. For infinite-trans experiments, cells were pre-loaded with saturating substrate concentrations (10 mM metformin or 2 mM atenolol) approximately 5 to 10-fold higher than their apparent K_m for 10 minutes at 37°C (Koepsell *et al.*, 2007; Harper and Wright, 2012; Yin *et al.*, 2015). Pilot experiments had indicated equilibrium was reached by 10 minutes.

The concentration of radiolabeled metformin (9 μM, 1 μCi/mL) and atenolol (390 nM, 1 μCi/mL) in IC_{50} and flux experiments was selected to be much lower than their apparent hOCT2 K_m (Koepsell *et al.*, 2007; Yin *et al.*, 2015, 2016). Inhibition and kinetic experiments were performed during the initial linear rate period using a short incubation time as specified in figure legends. IC_{50} and flux transport experiments were performed in triplicate and repeated three times independently. Due to the number of substrate and inhibitor concentrations required to fully characterize inhibition, K_i experiments were performed in duplicate and repeated three times independently. Uptake was performed in both empty vector- and transporter-transfected cells; and transporter specific uptake was calculated by subtracting uptake in vector-transfected cells.

3.2.3 *Data Analysis.*

Transport experiments were performed in triplicate and repeated three times independently. Data representation and replicates with specific n numbers are detailed in each figure legend. Transport kinetics were fitted using GraphPad Prism 6.0 (GraphPad Software, Inc., La Jolla, CA) for inhibitory interactions and uptake kinetics. The IC_{50} values were calculated by fitting the Log inhibitor concentration versus the transporter specific uptake normalized to the vehicle control using the equation:

$$v = \text{Bottom} + \frac{\text{Top}-\text{Bottom}}{1+10^{(\text{LogIC}_{50}-I)*H}} \quad (3\text{-}1)$$

where V is the rate of uptake in the presence of the inhibitor, Bottom is the residual baseline value, Top is the rate of uptake in the absence of inhibitor, I is the inhibitor concentration, and H is the Hill coefficient.

The likely model structure was selected based on examining the changes in apparent substrate K_m and V_{max} across inhibitor concentrations (e.g. Lineweaver-Burke and Lineweaver-Burke secondary replots). The final inhibition models were selected based on nonlinear regression and comparison with simpler nested models using an extra sum-of-squares *F* test ($P<0.05$ was considered significantly different).

Apparent competitive inhibition kinetics were fit to the following equation:

$$v = \frac{V_{max}[S]}{[S]+K_m\left(1+\frac{[I]}{K_i}\right)} \quad (3\text{-}2)$$

where V_{max} is the maximal rate of uptake, [S] is the substrate concentration, K_m is the apparent Michaelis-Menten constant, [I] is the inhibitor concentration and K_i is the apparent inhibitor constant (Segel, 1976; Copeland, 2000).

Apparent mixed inhibition kinetics ("intersecting, linear noncompetitive inhibition") were fit to the following equation:

$$v = \frac{[S]V_{max}}{K_m\left(1+\frac{[I]}{K_i}\right)+[S]\left(1+\frac{[I]}{\alpha K_i}\right)} \quad (3\text{-}3)$$

where α is the effect that I has on K_m (Segel, 1976).

The complex methamphetamine inhibition of metformin kinetic values were obtained by fitting transporter mediated uptake to a solved two site inhibition model with apparent partial

noncompetitive high affinity and apparent low affinity competitive interactions after typical examination of secondary and tertiary Lineweaver-Burk plots and comparison with simpler nested models (Segel, 1976):

$$v = \frac{V_{max}\left(\frac{[S]}{K_m}+\frac{\beta[S][I]}{\alpha K_{i,1}K_s}\right)}{1+\frac{[S]}{K_m}+\frac{[S][I]}{\alpha K_{i,1}K_s}+\frac{[I]}{K_{i,1}}+\frac{[I]^2}{\alpha K_{i,1}K_{i,2}}+\frac{[I]}{K_{i,2}}} \quad (3\text{-}4)$$

where $K_{i,1}$ is the high affinity inhibitor constant, $K_{i,2}$ is the low affinity inhibitor constant, and β is the effect the inhibitor has on the V_{max} of the IES complex. Initial values for $K_{i,1}$ and $K_{i,2}$ were based on the high and low affinity EC_{50} values previously observed for methamphetamine inhibition of metformin. Initial values for metformin substrate kinetics (V_{max} and K_s) were from separate experiments run in the absence of inhibitor.

3.3 RESULTS

3.3.1 *Methamphetamine displays hOCT2 substrate dependent inhibition.*

We previously showed that the inhibition kinetics of hOCT2 mediated metformin uptake by methamphetamine followed biphasic kinetics with a high affinity EC_{50} of 1.2 μM and low affinity EC_{50} of 58 μM (Wagner et al., 2017). Intriguingly, when atenolol was used as the substrate, inhibition of hOCT2 by methamphetamine was monophasic with an IC_{50} of 2.3 ± 0.2 μM and Hill slope of 1.1 ± 0.1 (Figure 3-2). The IC_{50} for atenolol transport is similar to our previously reported apparent K_m of methamphetamine (2.09 μM) at the high affinity binding site (Wagner et al., 2017). These data demonstrate that methamphetamine inhibition of hOCT2 is substrate-dependent and the inhibition mechanisms of hOCT2 may differ when atenolol or metformin is used.

3.3.2 *Atenolol and metformin display differential substrate affinity (K_m) from inhibition potency (IC_{50}) for hOCT2.*

If metformin and atenolol binding to hOCT2 do not overlap with each other, their apparent inhibition potency for each other (IC_{50}) may be different than their apparent affinity for hOCT2 (K_m). To test this, we determined and compared the apparent affinities and inhibition potencies of atenolol and metformin towards each other (Figure 3-3). Initial rate studies showed that atenolol had an apparent K_m of 178 ± 12 μM and V_{max} of 865 ± 100 pmol/min/mg protein and metformin had a K_m of 1,560 ± 310 μM and V_{max} of 55,000 ± 15,000 pmol/min/mg protein. These values are similar to those previously generated in our laboratory and reported by others (Koepsell *et al.*, 2007; Yin *et al.*, 2015) Mutual inhibition studies showed that metformin inhibited hOCT2 mediated atenolol uptake with an IC_{50} value of 470 ± 120 μM, which is about 3-folder than metformin's K_m. Remarkably, atenolol inhibited hOCT2 mediated uptake of metformin with an IC_{50} value of 2,500 ± 500 μM, which is more than 10-fold higher than atenolol's apparent K_m.

3.3.3 *Methamphetamine displays differential inhibition mechanisms towards hOCT2-mediated atenolol and metformin transport.*

The similarities in the methamphetamine high affinity K_m and its IC_{50} value for atenolol (Figure 3-2) suggested the high affinity methamphetamine binding site may overlap with atenolol's binding site. Conversely, the biphasic methamphetamine inhibition of metformin (Figure 3-2) suggests that more complicated interactions involving multiple binding sites may be involved. Enzyme inhibition models that do not explicitly take into account the transporter specific model were fit to the data. The complex methamphetamine inhibition of metformin kinetic values were obtained by fitting transporter mediated uptake to a solved two site inhibition model with apparent partial noncompetitive high affinity and apparent low affinity competitive interactions

(Figure 3-4). The methamphetamine inhibition of metformin showed apparent mixed ("partial noncompetitive") high affinity ($K_{i,1}$=2.1 ± 1.3 μM, α=1.5 ± 0.17, β= 0.62 ± 0.14) and apparent low affinity ($K_{i,2}$=22 ± 3.1 μM) competitive mechanisms (Figure 3-4). Methamphetamine displayed only apparent competitive inhibition (Figure 3-3) of atenolol transport with a K_i of 2.4 ± 0.5 μM (Figure 3-4). The apparent competitive inhibition of atenolol by methamphetamine with a K_i (2.4 μM) corresponds with methamphetamine's high affinity apparent K_m (2.09 μM) suggests the high affinity methamphetamine binding site may overlap with atenolol's binding site.

3.3.4 *Atenolol and metformin display apparent mixed and competitive inhibition of each other.*

The difference between the IC_{50} value of atenolol inhibiting metformin transport and the methamphetamine inhibition kinetics provided evidence that atenolol and metformin may have discrete binding sites in the hOCT2 binding region. In order to gain a more mechanistic understanding of how atenolol and metformin interact with hOCT2, zero-trans K_i experiments were performed to identify the apparent mechanism of inhibition of each other. Enzyme inhibition models were fit to the data. Atenolol demonstrated apparent mixed inhibition of metformin transport with an apparent K_i of 1,100 ± 510 μM (Figure 3-5) which is similar to the IC_{50} value obtained (Figure 3-3). Unexpectedly, metformin displayed apparent competitive inhibition of atenolol transport with an apparent K_i of 360 ± 52 μM (Figure 3-5) similar to the IC_{50} value obtained (Figure 3-3).

3.3.5 *Atenolol mediated hOCT2 transport is noncompetitively inhibited by metformin.*

Krupka and Devés previoulsy demonstrated that the apparent mechanism of noncompetitive zero-trans inhibition can differ from the true mechanism of inhibition if the flux ratio of the substrate, which is the ratio of zero-trans and infinite-trans uptake rates, deviates from unity

(Krupka and Devés, 1983; Deves and Krupka, 1990). In order to be able to identify the true mechanism of inhibition, we compared zero-trans and infinite-trans uptake and calculated flux ratios of metformin and atenolol. Metformin had significantly higher hOCT2 specific uptake in the infinite-trans uptake experiments than in zero-trans uptake experiments with a calculated flux ratio of 1.7 ± 0.21 (Figure 3-6 A & B). Conversely, atenolol showed a significantly lower rate of infinite-trans uptake than zero-trans uptake with a calculated flux ratio of 0.17 ± 0.03 (Figure 3-6 A & B).

Flux experiments in the presence of an inhibitor can sometimes be used in conjunction with K_i experiment to determine the mechanism and sidedness of the inhibitory interaction (Krupka and Devés, 1983; Deves and Krupka, 1990). Atenolol flux experiments were conducted with and without the presence of 10 mM metformin in order to identify the true mechanism metformin inhibited hOCT2 with and which side of the membrane the inhibitory interaction impacts. The flux ratio of atenolol was significantly reduced from 0.13 ± 0.01 to 0.03 ± 0.03 in the presence of 10 mM metformin suggesting the inhibition of atenolol transport by metformin is actually driven by a noncompetitive interaction impacting an intracellular transport step of hOCT2 transport (Figure 3-6 C). The concentration of 5 μM methamphetamine was selected to minimize any confounding low affinity interactions. Methamphetamine slightly increased atenolol's flux ratio from 0.127 ± 0.076 to 0.173 ± 0.091, although the difference was not significant (P=0.54) (Figure 3-6 D). The flux ratio of atenolol would only be expect to not change if a noncompetitive inhibitor is acting both internally and externally but the apparent mechanism of inhibition in a zero-trans uptake experiment would be expected to appear noncompetitive (Krupka and Devés, 1983; Deves and Krupka, 1990).

3.4 DISCUSSION

Substrate dependent inhibition and atypical kinetics of OCTs has gained increasing attention recently as it has significant implications for quantitative prediction of transporter-mediated drug clearance and DDIs. While many have identified substrate dependent transporter inhibition (Moaddel *et al.*, 2005; Gorbunov *et al.*, 2008; Minuesa *et al.*, 2009; Belzer *et al.*, 2013; Thévenod *et al.*, 2013; Hacker *et al.*, 2015; Yin *et al.*, 2016), there is currently little kinetic or mechanistic understanding of the underlying causes for substrate dependent inhibition of OCTs. This study determined the mutual inhibition mechanisms of two prototypical hOCT2 substrates and applied this understanding to characterize the complex interaction with methamphetamine. Our data demonstrated that a substrate can inhibit hOCT2 with apparent K_i values drastically different from its apparent K_m for hOCT2 (Figure 3-3). Furthermore, the inhibition mechanism determined by fitting data to classic enzyme inhibition models (i.e. competitive or noncompetitive) may not reflect the true nature of substrate-inhibitor interaction but rather depends on the substrate transport kinetics (e.g. flux ratio) and sidedness of the inhibitory interaction (Figure 3-5 and Figure 3-7). Our analyses suggest metformin and atenolol have spatially distinct binding sites within the hOCT2 binding region and may be transported simultaneously.

Methamphetamine was able to completely inhibit atenolol transport through a high affinity interaction (K_i= 2.4 ± 0.5 μM) while only partially inhibiting metformin transport in this concentration range (Figure 3-2 & Figure 3-5). The complete inhibition of atenolol transport is also highlighted by the monophasic IC_{50} (Figure 3-2). We observed both high ($K_{i,1}$=2.1 ± 1.3 μM) and low affinity inhibition ($K_{i,2}$=22 ± 3.1 μM) of metformin. The biphasic inhibition curve (Figure 3-2) and apparent high affinity mixed inhibition suggests the high affinity methamphetamine interaction only partially reduces metformin transport while the low affinity inhibition is able to

completely block metformin transport (Figure 3-6 & Figure 3-7). The large hOCT2 binding region that can accommodate multiple substrates bound simultaneously provides the potential for a truly noncompetitive substrate to not impact the transport of another substrate (Krupka and Devés, 1983; Popp *et al.*, 2005; Gorbunov *et al.*, 2008). OCT binding pockets may be able to accommodate two of the same substrate as is supported by binding studies and biphasic uptake kinetics (Gorbunov *et al.*, 2008; Wagner *et al.*, 2017). It has been mathematically theorized that a truly noncompetitive good substrate may not impact the transport of another substrate (e.g. six-state model of transport) (Krupka and Devés, 1983). In these experiments, both atenolol and metformin inhibited the others' hOCT2 mediated transport (Figure 3-3). The IC_{50} (2,500 μM) for atenolol inhibiting hOCT2 mediated metformin transport was more than 10-fold higher than atenolol's apparent K_m, suggesting the inhibitory interaction may not be simple competition of the outward facing conformation of the transporter. The disconnect between atenolol and metformin inhibition potencies against each other and their apparent transport K_m values provided additional evidence that they may not competitively inhibit each other.

In enzyme kinetics, the mechanism of inhibition is determined by analyzing changes in substrate kinetics in the presence of varying concentrations. By performing these studies and fitting data to various enzyme inhibition models, the apparent mechanism of atenolol inhibition of metformin transport was found to be mixed (Figure 3-3). Surprisingly, metformin appeared to competitively inhibit atenolol transport (Figure 3-3). While enzyme kinetics have been used to model transporter interactions with substrates and inhibitors, these models do not explicitly take into account the unique features of a transport cycle across the membrane. For example, if the substrate-bound transporter reorients faster than the unbound transporter (flux ratio >1), the transporter will exist mainly in the inward facing conformation at high substrate concentrations

which is inaccessible to the inhibitor. The apparent inhibition pattern for a noncompetitive inhibitor in this situation would be expected to not appear as only noncompetitive but will have an apparent competitive aspect in the inhibition kinetics with changes in the apparent K_m of the victim substrate (e.g. apparent mixed inhibition) (Deves, 1991).

The possibility that the apparent mechanism of inhibition could differ from the true mechanism lead us to perform transport flux experiments to better understand the substrate kinetics of metformin and atenolol within the framework of the four-state transporter model. Metformin exhibited a flux ratio greater than one but atenolol has a flux ratio less than one (Figure 3-6). Based on the atenolol flux ratio being less than unity (Figure 3-6 A & B), the apparent competitive inhibition of hOCT2 mediated atenolol transport by metformin (Figure 3-3) could be explained by either competitive inhibition on the outside or noncompetitive inhibition impacting an intracellular step in translocation (Krupka and Devés, 1983). These data indicated the true mechanism of inhibition could be different than the apparent mechanisms of inhibition we observed.

In order to identify the true mechanism by which metformin inhibited hOCT2-mediated atenolol transport, we performed atenolol flux experiments with and without the presence of metformin. Flux experiments in the presence of an inhibitor can sometimes be used in conjunction with K_i experiment to determine the mechanism and sidedness of the inhibitory interaction (Krupka and Devés, 1983; Deves and Krupka, 1990). Due to the flux ratio of metformin being greater than one, we cannot confirm the true mechanism of methamphetamine or atenolol inhibition using flux experiments. However, changes to atenolol's flux ratio in the presence of an inhibitor would provide additional information about mechanisms of inhibition. Apparent competitive inhibition of the uptake of a substrate with a flux ratio less than one is expected by either competitive inhibition outside or noncompetitive inhibition inside the membrane (Krupka

and Devés, 1983). A decrease in atenolol flux ratio is expected if noncompetitive inhibition impacts an intracellular transport step while an increase in flux ratio is expected from competitive inhibition (Deves and Krupka, 1990). The significant decrease in the atenolol flux ratio from 0.13 ± 0.01 to 0.03 ± 0.03 suggests the inhibition of atenolol transport by metformin may be driven by a noncompetitive interaction impacting an intracellular step in hOCT2-mediated atenolol transport. One possible explanation is that metformin may drive the distribution of hOCT2 towards the inward confirmation as a substrate with a flux ratio greater than one, effectively stabilizing the inward conformation in a noncompetitive manner. Alternatively, when atenolol and metformin are both bound, it adds an additional intracellular step to release metformin, which slows the net translocation of atenolol (Figure 3-7). It should be noted that while the step in atenolol transport impacted by metformin appears to be intracellular, it is possible this interaction is initiated by metformin binding extracellularly (Deves and Krupka, 1990). Atenolol has a flux ratio less than one and a comparatively lower V_{max} than metformin (atenolol V_{max}: 865 pmol/min/mg protein; metformin V_{max}: 55,000 pmol/min/mg protein) suggesting that the translocation time of hOCT2 with atenolol from outward to inward is relatively slow. Atenolol may inhibit metformin transport by slowing the translocation rate from the outside to the inside. Taken together these data suggest the high affinity methamphetamine and atenolol binding sites overlap and are distinct from the binding site of metformin (Figure 3-7). However, we have no evidence to support if metformin and the low affinity methamphetamine binding site truly interact competitively due to the kinetic properties of metformin. Based on methamphetamine's low affinity apparent competitive and complete inhibition of metformin transport (Figure 3-4), it is likely the low affinity methamphetamine binding site does overlap with metformin's binding site.

This study relied solely on transport kinetics to provide support for spatially distinct binding within the hOCT2 binding region. We believe this is the simplest explanation of our results but cannot rule out other possibilities. A distal allosteric binding site has been proposed for OCTs and could partially explain some of these results (Gorbunov *et al.*, 2008). Unfortunately, traditional kinetic experiments are also unable to conclusively demonstrate the stoichiometry of transporter. Our cell-based test system adds a number of complexities and assumptions to interpreting substrate transport. Additional orthogonal studies like stoichiometric binding measurements or crystallography may facilitate a greater understanding of the mechanisms of OCT transport and inhibition.

In spite of these limitations, this study determined the inhibition mechanisms for prototypical hOCT2 substrates with each other and applied this understanding to characterize the complex interaction with methamphetamine. Our data demonstrated that hOCT2 substrates can inhibit other substrates with apparent K_i values different from their apparent K_m values. Furthermore, the apparent mechanism of inhibition (i.e. competitive or noncompetitive) depends on the substrate transport kinetics (e.g. flux ratio) and sidedness of the inhibitory interaction. Our findings suggest metformin and atenolol have spatially distinct binding sites within the hOCT2 binding region and may be transported simultaneously.

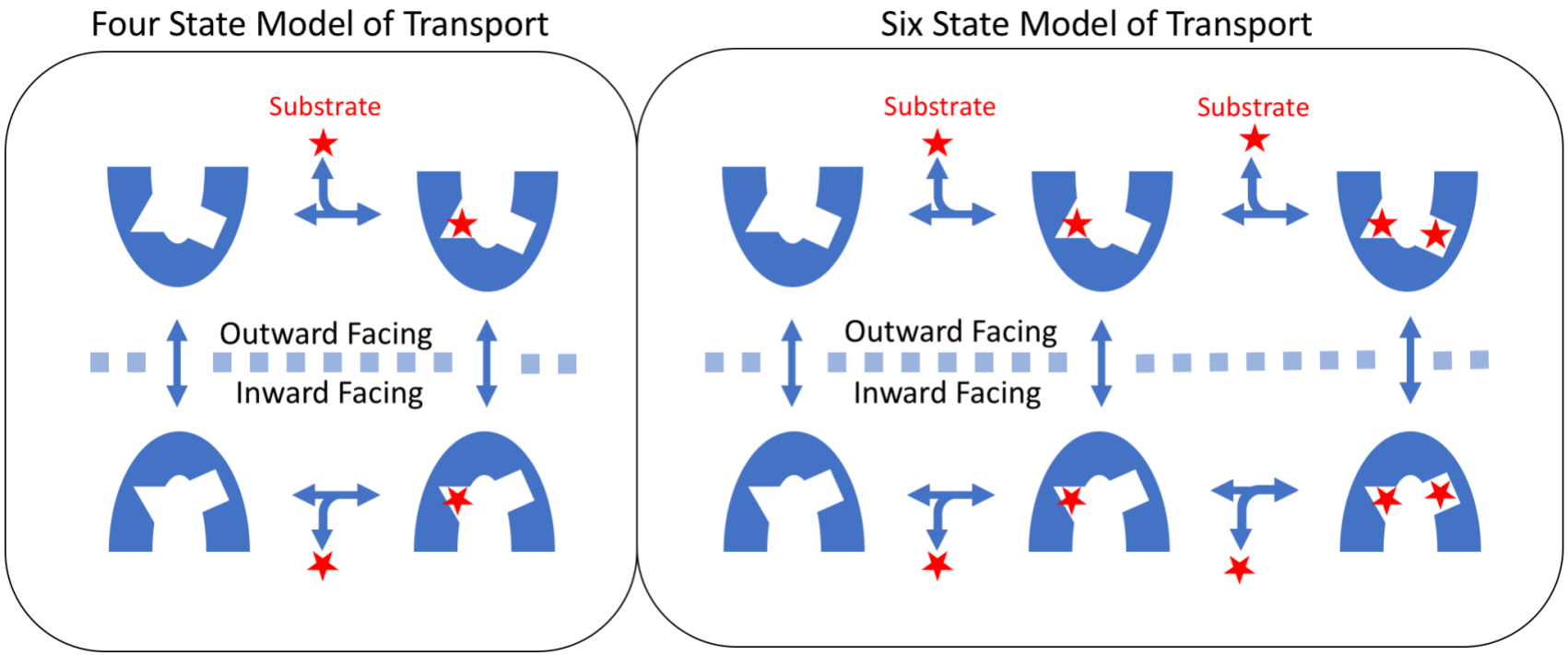

Figure 3-1. Proposed four state and six state models of OCT transport.

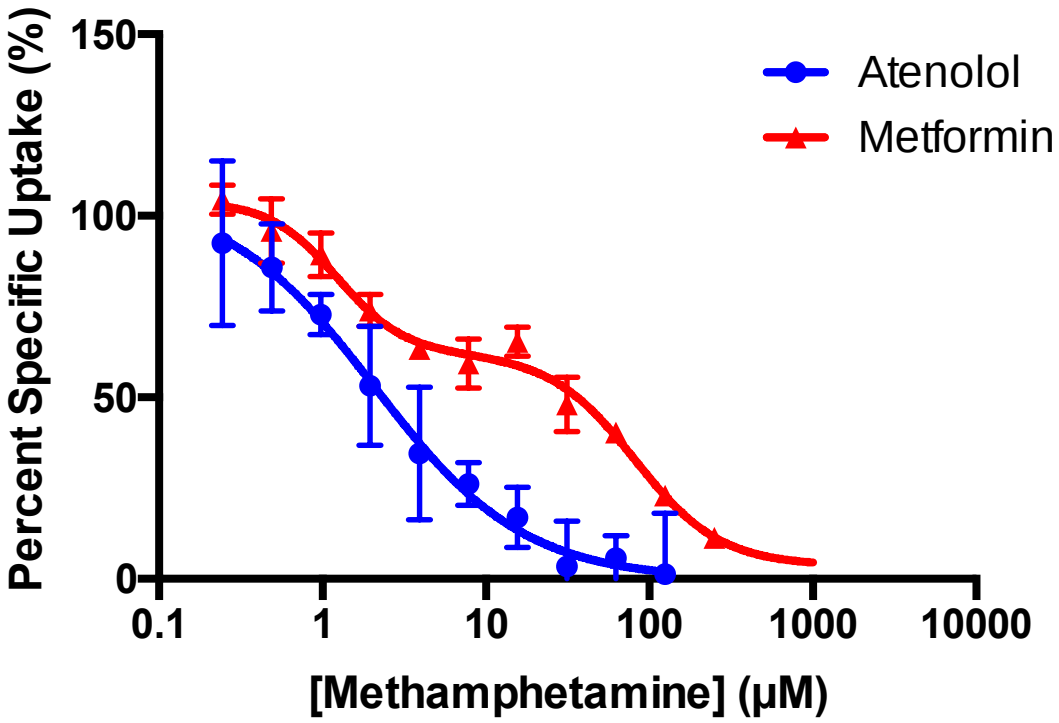

Figure 3-2. Methamphetamine inhibition of hOCT2 mediated atenolol transport. Uptake of [^{3}H]atenolol (390 nM, 1 μCi/mL) in the absence and presence of the inhibitor methamphetamine was measured in both transporter expressing and control HEK cells. Transporter-specific uptake was obtained by subtracting the uptake in vector-transfected cells from the uptake in transporter-expressing cells. Incubations were performed at 2 minutes for atenolol. Each data point represents the mean and standard deviation from one representative experiment in triplicate. Inhibition of metformin is graphed as a comparison for illustration purposes and was previously published (Wagner *et al.*, 2017).

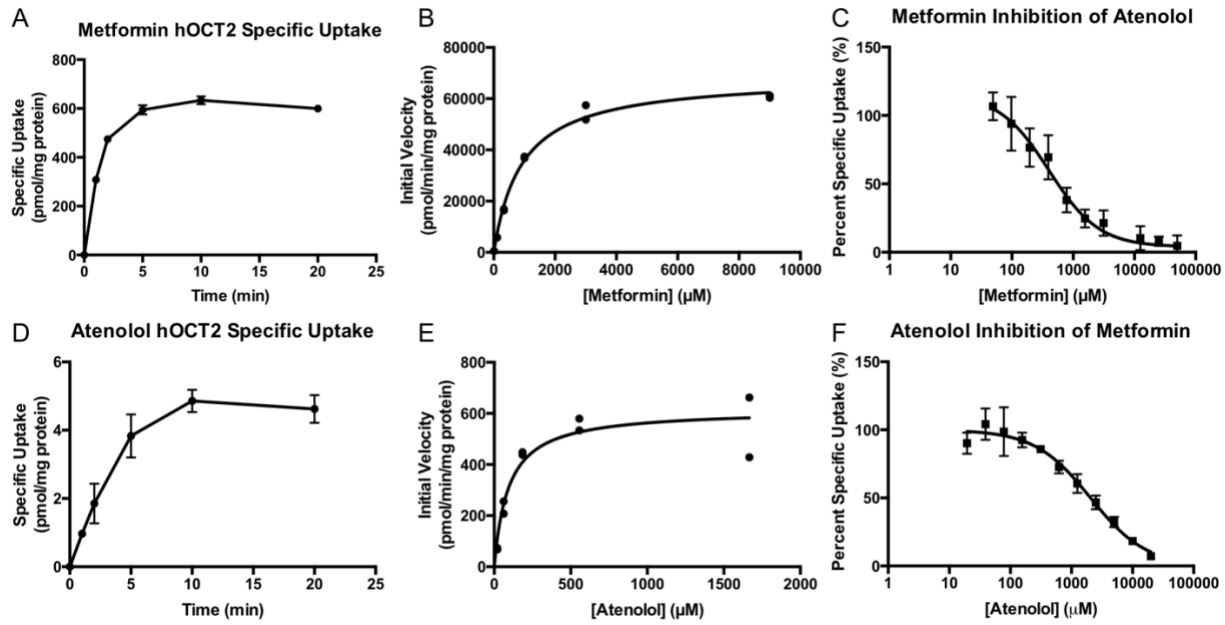

Figure 3-3. Atenolol and metformin hOCT2 transport and inhibition.

Metformin time dependent uptake (9 μM, 1 μCi/mL) (A), transport kinetics (B), and inhibition of hOCT2 mediated atenolol transport were characterized. Atenolol time dependent uptake (9 μM, 1 μCi/mL) (A), transport kinetics (B), and inhibition of hOCT2 mediated metformin transport were characterized. Transporter-specific uptake was obtained by subtracting the uptake in vector-transfected cells from the uptake in transporter-expressing cells. Incubations were performed at 2 and 1 minutes for the substrates atenolol and metformin respectively. Each data point represents the mean ± S.D. from one representative experiment in triplicate (A, C, D, and F) or each of the duplicate values (B and F). Atenolol had an average apparent K_m of 178 ± 12 μM and V_{max} 865 ± 100 pmol/min/mg protein across three experiments. Metformin had an average apparent K_m of 1560 ± 310 μM and V_{max} 55000 ± 15000 pmol/min/mg protein across five experiments. The average IC_{50} values from three independent experiments were 470 ± 120 μM and 2500 ± 500 μM for metformin and atenolol inhibition of hOCT2, respectively.

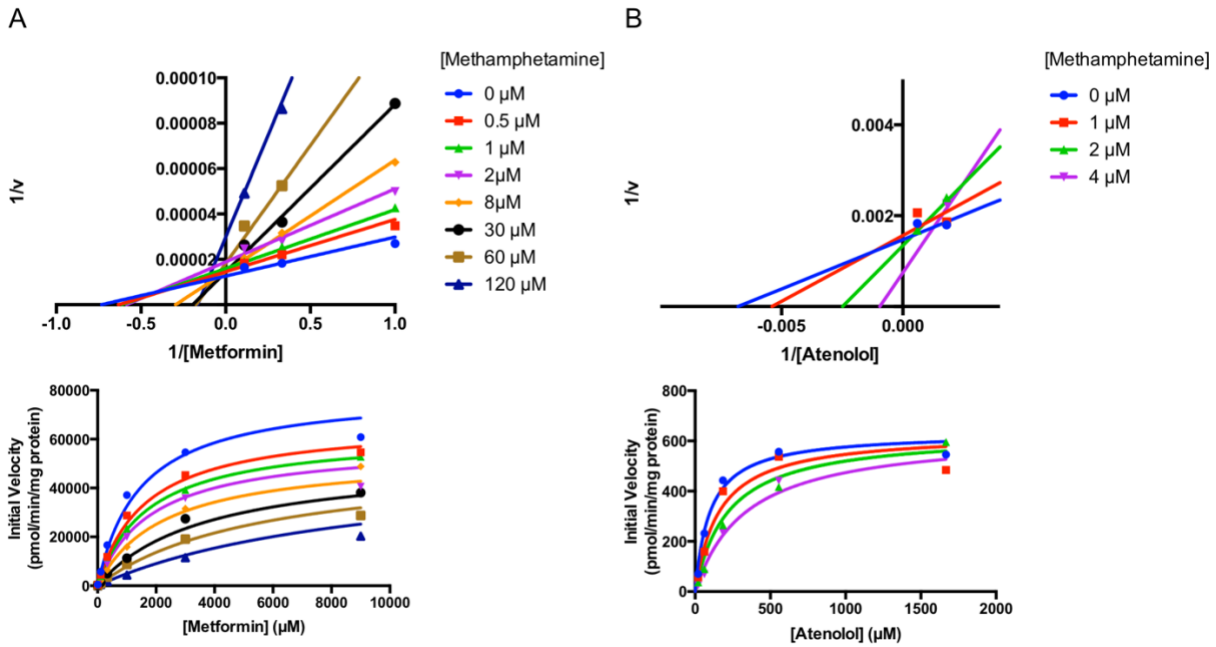

Figure 3-4. Methamphetamine inhibition kinetics of hOCT2 mediated metformin and atenolol transport.

Uptake of various concentrations of metformin (A) or atenolol (B) in the absence and presence of the inhibitor methamphetamine was measured in both transporter expressing and control HEK cells. Transporter-specific uptake was obtained by subtracting the uptake in vector-transfected cells from the uptake in transporter-expressing cells. Incubations were performed at 1 and 2 minutes for the substrates metformin and atenolol, respectively, which are within the linear initial rate of uptake. Each data point represents the mean from one representative experiment in duplicate. The mean values of the kinetic data were used to transform data into Lineweaver-Burk plots. The full untransformed kinetic data fit to corresponding inhibition models are displayed in the bottom half of each pane. Across three experiments, methamphetamine inhibition of metformin showed apparent mixed ("partial noncompetitive") high affinity ($K_{i,1}$=2.1 ± 1.3 µM, α=1.5 ± 0.17, β= 0.62 ± 0.14) and apparent low affinity ($K_{i,2}$=22 ± 3.1 µM) competitive mechanisms (Eq.3-4). Methamphetamine displayed only apparent competitive inhibition of atenolol transport with a K_i of 2.4 ± 0.5 µM across three experiments.

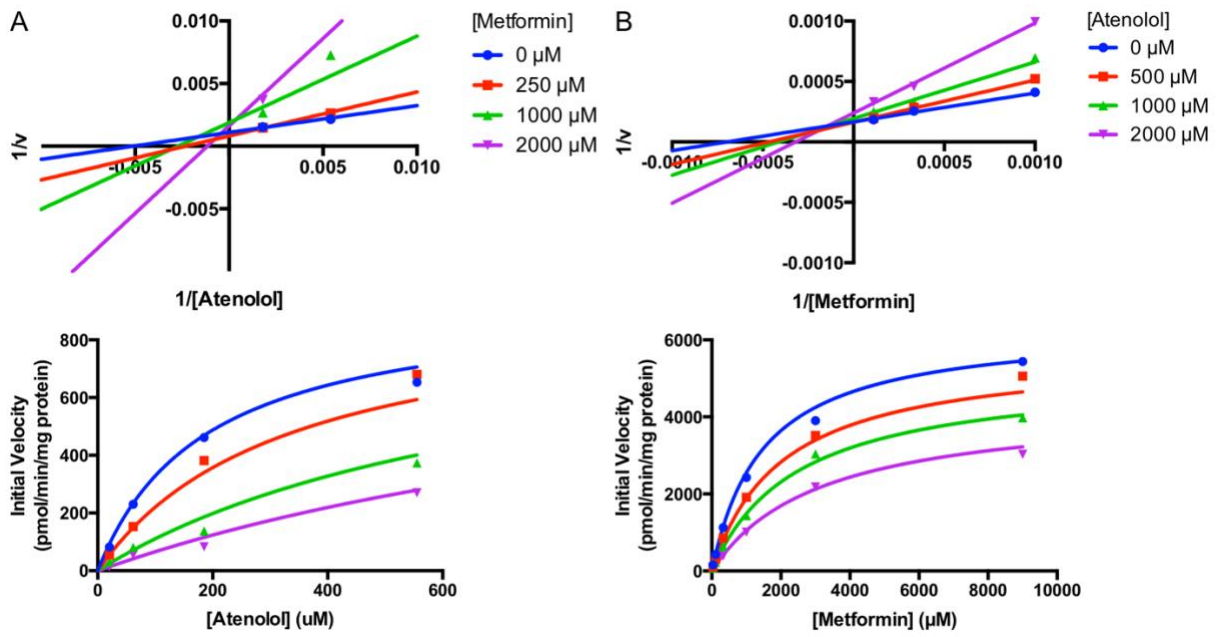

Figure 3-5. Inhibition kinetics of the hOCT2 substrates atenolol and metformin.

Uptake of [^{3}H]atenolol or [^{14}C]metformin in the absence and presence of inhibitor was measured in both transporter expressing and control HEK cells. Transporter-specific uptake was obtained by subtracting the uptake in vector-transfected cells from the uptake in transporter-expressing cells. Incubations were performed at 2 and 1 minutes for the substrates (A) atenolol and (B) metformin, respectively. Each data point represents the mean from one representative experiment in duplicate. The mean values of the kinetic data were used to transform data into Lineweaver-Burk plots. The full untransformed kinetic data fit to corresponding inhibition models are displayed in the inset. Atenolol demonstrated apparent mixed inhibition of metformin transport with an average apparent K_i of 1100 ± 510 µM from three independent experiments. Metformin displayed apparent competitive inhibition of atenolol transport with an average apparent K_i of 360 ± 52 µM from three independent experiments.

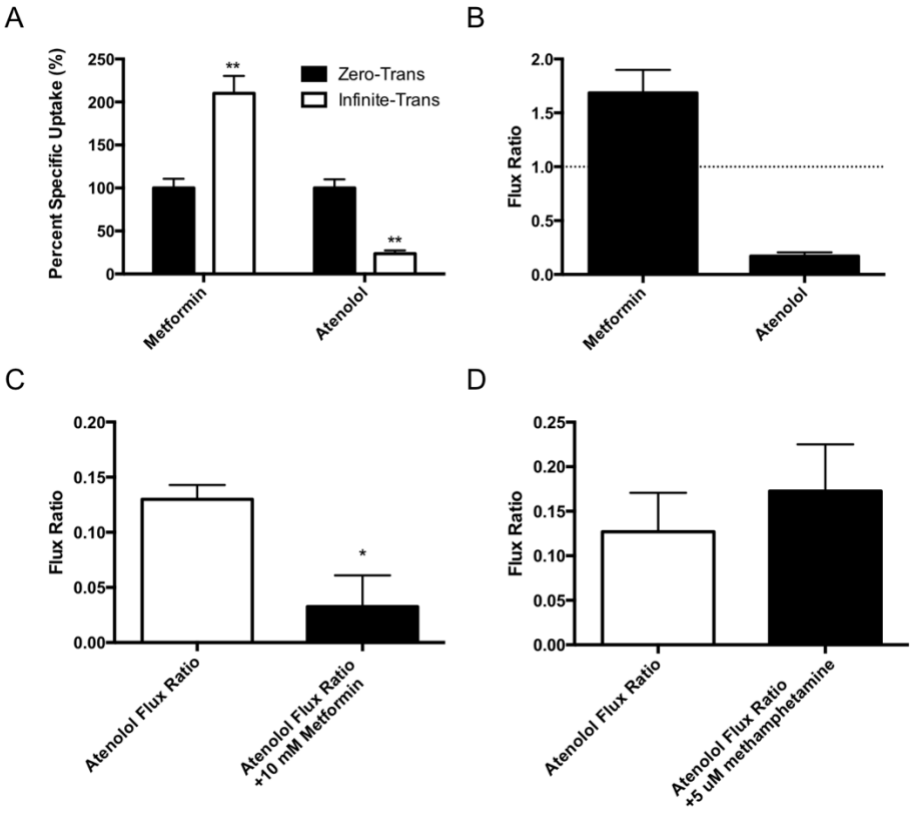

Figure 3-6. Metformin and atenolol hOCT2 flux ratios.

Zero-trans and infinite-trans uptake of [^{14}C]metformin (9 μM, 1 μCi/mL or [^{3}H]atenolol (390 nM, 1 μCi/mL) was measured in both transporter expressing and control HEK cells (A). Flux ratios were calculated by dividing the infinite-trans uptake by the zero-trans uptake (B). Atenolol flux ratios in the presence or absence of 10 mM cis metformin (C) or 5 μM cis methamphetamine (D) were compared. Transporter-specific uptake was obtained by subtracting the uptake in vector-transfected cells from the uptake in transporter-expressing cells. Incubations were performed at 1 and 2 minutes for the substrates metformin and atenolol respectively. Each data point represents the mean ± SE from three independent experiments each run in triplicate. Uptake in zero-trans experiments was compared with infinite-trans uptake and flux ratios in the absence or presence of inhibitor were compared using a Student's t-test and correct for multiple comparisons with the Bonferroni method (*P<0.05; **P<0.01).

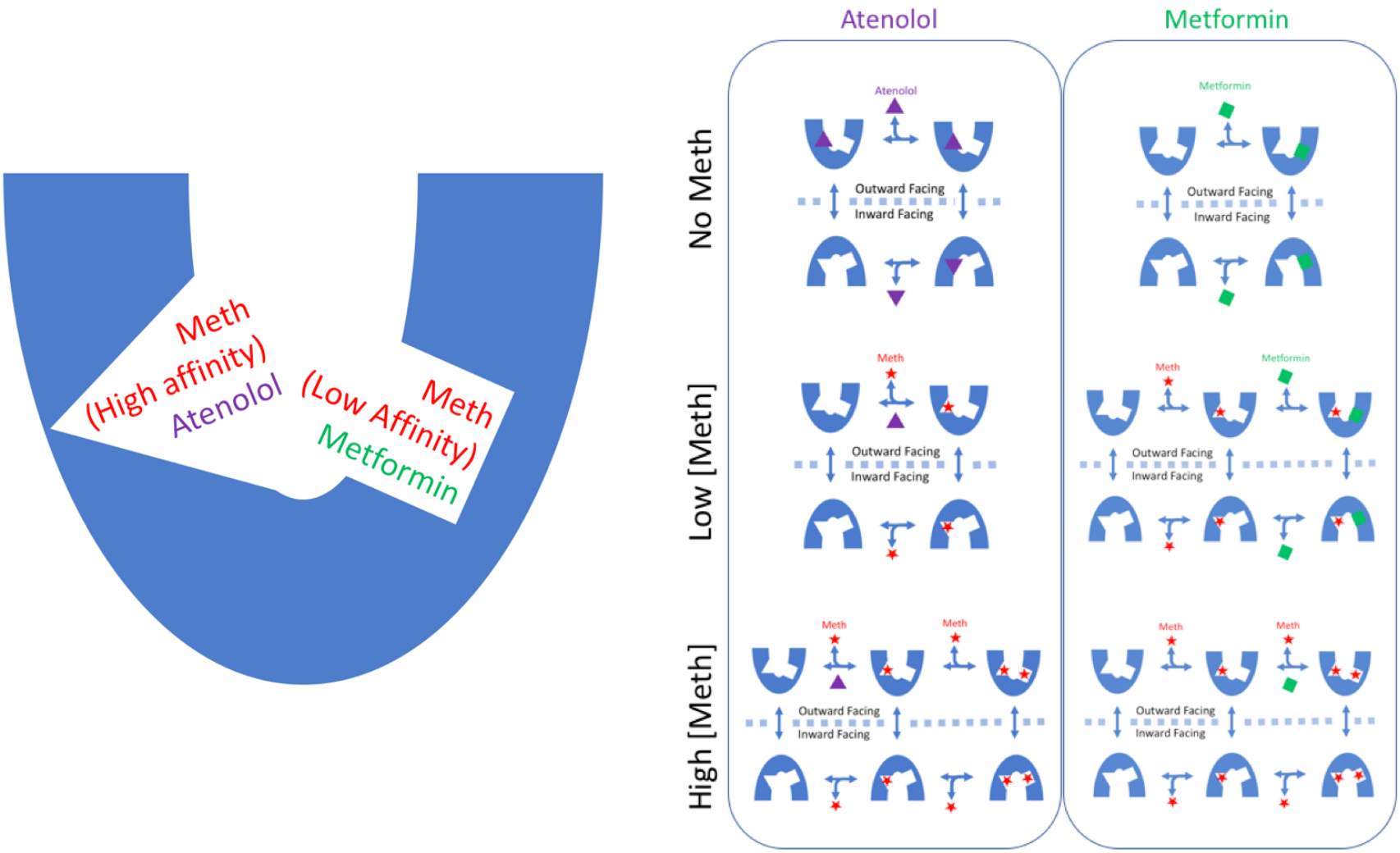

Figure 3-7. Proposed hOCT2 binding and transport scheme for metformin, atenolol, and methamphetamine.

Chapter 4. DISPOSITION OF METHAMPHETAMINE AND MAJOR METABOLITES IN MICE: ROLE OF ORGANIC CATION TRANSPORTER 3 (OCT3) IN TISSUE SELECTIVE ACCUMULATION OF *P*-HYDROXYMETHAMPHETAMINE

(A version of this chapter was accepted for publication in *Drug Metabolism and Disposition*.)

4.1 INTRODUCTION

Methamphetamine is one of the most widely abused and toxic illicit drugs (Volkow *et al.*, 2010; Volkow, 2013). Methamphetamine or "meth" is a potent and highly addictive central nervous stimulant that acts by inhibiting and reversing the dopamine transporter (DAT), norepinephrine transporter (NET), and serotonin transporter (SERT) (Carvalho *et al.*, 2012; Panenka *et al.*, 2013). In vivo, methamphetamine is metabolized to two major primary metabolites, amphetamine *and para*-hydroxymethamphetamine (*p*-OHMA) (Lin *et al.*, 1997; Shima *et al.*, 2008). Amphetamine has similar psychoactive and addictive properties as methamphetamine (Carvalho *et al.*, 2012; Panenka *et al.*, 2013). *p*-OHMA is not psychoactive but has cardiovascular activity with hypertensive and adrenergic activity (Römhild *et al.*, 2003).

Methamphetamine is considered one of the most toxic drugs of abuse with both central nervous system (CNS) and peripheral toxicities (Volkow *et al.*, 2010). Methamphetamine neurotoxicity is relatively well understood with long-term neurological injuries primarily targeting the dopaminergic and serotonergic neurons, where methamphetamine is highly concentrated by the monoamine transporters (Schep *et al.*, 2010; Panenka *et al.*, 2013). The peripheral toxicity

colloquially known “meth mouth”, xerostomia (dry mouth) and rampant dental caries, is one of the most widely known injuries that is publicized in many anti-drug campaigns (Shaner *et al.*, 2006). Little is currently known regarding the mechanisms leading to “meth mouth”. It has been speculated that methamphetamine reduces saliva flow through vasoconstriction of the capillaries around salivary glands (Hamamoto and Rhodus, 2009). However, a recent study in abusers indicated that xerostomia was not caused by a decreased saliva output but rather a change in saliva composition, suggesting direct toxicity to salivary glands (Ravenel *et al.*, 2012). In addition, methamphetamine abuse is associated with muscle toxicities. In severe cases a breakdown of muscle leads to rhabdomyolysis and injury of multiple organs (Carvalho *et al.*, 2012).

Elimination of methamphetamine is by both hepatic metabolism and renal secretion with approximately 40% excreted unchanged in the urine (Kim *et al.*, 2004). The polymorphic enzyme cytochrome P450 2D6 (CYP2D6) is the major liver enzyme that metabolizes methamphetamine to the primary circulating metabolites amphetamine and *p*-OHMA (Lin *et al.*, 1997; Shima *et al.*, 2008). We previously showed that methamphetamine and metabolites inhibit human organic cation transporters (hOCTs) and multidrug and toxin extrusion transporters (MATEs) and are selectively transported by these transporters (Wagner *et al.*, 2017). Renal excretion is another major elimination pathway for methamphetamine and its metabolites. We previously demonstrated that methamphetamine, amphetamine, and *p*-OHMA are all substrates of the human renal OCT2 and MATE transporters in vitro, suggesting that these transporters may play a role in the renal handling of methamphetamine and metabolites (Wright, 2005; Wagner *et al.*, 2017). OCT1, the major isoform in the liver, may be involved in the hepatic handling of *p*-OHMA as it is transported by hOCT1 in vitro; however, methamphetamine and amphetamine are not substrates (Wagner *et al.*, 2017).

Animal studies and human positron emission tomography (PET) studies showed that methamphetamine and metabolites are distributed into many organs with high accumulations (Rivière *et al.*, 2000; Volkow *et al.*, 2010). NET- and DAT-mediated high accumulation of methamphetamine and amphetamine in neuronal tissues is thought to at least partially contribute to neurotoxicity (de la Torre *et al.*, 2004; Carvalho *et al.*, 2012). In contrast, the role of transporters in peripheral distribution is poorly understood in vivo (Panenka *et al.*, 2013). As cations with reported or calculated LogD values of -0.38, -0.62, and -1.11; methamphetamine, amphetamine, and *p*-OHMA may have low passive permeability as protonated species (Fowler *et al.*, 2007). We and others have reported that OCT3 is highly expressed in a number of tissues including salivary glands and skeletal muscle in both human and rodents (Koepsell *et al.*, 2007; Lee *et al.*, 2013, 2014; Chen *et al.*, 2015). Using an *Oct3* knockout mouse model, we previously showed that OCT3 is responsible for the accumulation and secretion of metformin (an organic cation drug) in salivary glands (Lee *et al.*, 2014). Recently, we identified *p*-OHMA is an in vitro substrate of hOCT3, suggesting that OCT3 may play a role in tissue-specific accumulation of *p*-OHMA (Wagner *et al.*, 2017).

The goals of this study were to characterize the distribution of methamphetamine and its primary circulating metabolites amphetamine and *p*-OHMA in mice and determine the in vivo role of OCT3 in tissue disposition. We determined the pharmacokinetics and tissue partitioning of methamphetamine and metabolites in mice. The in vivo significance of Oct3 in methamphetamine, amphetamine, and *p*-OHMA tissue distribution was evaluated using a mouse model with a targeted deletion of the *Oct3/Slc22a3* gene.

4.2 Materials and Methods

4.2.1 *Materials.*

Analytical grade *d*-methamphetamine, *d*-amphetamine, *p*-OHMA, and ammonium formate were purchased from Sigma-Aldrich (St. Louis, MO). The *d*-methamphetamine isomer is the primary psychoactive entity, although racemic methamphetamine is produced by some synthesis methods (de la Torre *et al.*, 2004). We used the dextro isoform of methamphetamine in this study because it is the psychoactive form. Methamphetamine-D_{11} and amphetamine-D_{11} were purchased from Cerilliant Corporation (Round Rock, TX). [^{14}C]metformin (115 mCi/mmol) was purchased from Moravek Biochemicals, Inc. (Brea, CA). Optima grade acetonitrile, methanol, water, and formic acid were purchased from Fisher Scientific (Waltham, MA). Cell culture media and supplements were purchased from Invitrogen (Carlsbad, CA). All other chemicals were commercially available and of analytical grade or higher.

4.2.2 *Animals.*

Null *Oct3* (*Slc22a3*) mice were originally developed from the FVB inbred strain by Dr. Denise Barlow (Zwart *et al.*, 2001) and maintained by Dr. Alfred Schinkel (Netherlands Cancer Institute). Breeding pairs of both wild type *Oct3*$^{+/+}$ and *Oct3*$^{-/-}$ mice were generously provided by Dr. John Markowitz at the University of Florida after re-derivation at Charles River Laboratories (Zhu *et al.*, 2010). Mice were housed in specific pathogen-free facilities at the University of Washington with a 14/10-h light/dark cycle and a standard diet. All animal studies were approved by the Institutional Animal Care and Use Committee of the University of Washington.

4.2.3 *Uptake Experiments.*

Flp-in HEK293 cells stably expressing mOct3 were previously generated in our laboratory (Lee *et al.*, 2014). The cells were cultured in high glucose DMEM with 10% FBS, 1 mM L-glutamine, 100 U/mL penicillin, 100 μg/mL streptomycin, and 150 μg/mL hygromycin B supplementation at 37°C with 5% CO_2 and high humidity. Cell culture flasks and plates were coated with 0.01% poly-D-lysine to improve cell attachment. Uptake assays were performed as previously described (Wagner *et al.*, 2017). Briefly, cells were seeded in 96-well plates at 100,000 cells/well and grown overnight. Cells were washed with pre-warmed Hanks balanced salt solution (HBSS) and allowed to acclimate for 10 minutes at 37°C prior to uptake experiments. HBSS was removed and incubations initiated by the addition of 100 μL of HBSS at pH 7.4 containing substrate. Incubations were terminated by removing media and washing the cells three times with ice cold HBSS. Metformin, used as a reference substrate, was measured by liquid scintillation counting (LSC) (PerkinElmer, Tri-Carb B3110TR, Waltham, MA) after lysis with 100 μL of 1 M NaOH for one hour and neutralization with 100 μL of 1 M HCl. Methamphetamine, amphetamine, and *p*-OHMA were quantified by LC-MS/MS as described below. Briefly, cells were permeabilized with 100 μL/well of methanol containing 100 nM stable-labeled internal standards for 15 minutes followed by dilution into an equal volume of Optima water. Uptake was normalized to total protein measured in the lysate by the BCA Protein Assay Kit (Pierce Chemical, Rockford, IL). Kinetic experiments were performed during the initial rate period using a short incubation time (1 minute). Uptake experiments were performed in triplicate and repeated independently three times. Transporter specific uptake was calculated by subtracting uptake in vector-transfected cells from uptake in the mOct3-transfected cells. Transport experiments were performed in triplicate and repeated three independent times. Data representation and replicates with specific

numbers of observations are detailed in each figure legend. Since the Eadie-Hofstee plot indicated cooperativity, mOct3 transporter kinetics of *p*-OHMA were fitted to the Michaelis-Menten equation with a Hill slope (H) to obtain half maximal transport concentration ($K_{1/2}$ in place of K_m) and maximal transport rate (V_{max}) using GraphPad Prism 6.0 (GraphPad Software, Inc., La Jolla, CA) (Copeland, 2000):

$$v = \frac{V_{max} * S^H}{K_{1/2}{}^H + S^H} \quad (4\text{-}1)$$

4.2.4 *In vivo Pharmacokinetics Studies.*

All in vivo studies were carried out in male FVB mice 10-12 weeks old. Only male mice were used as we and others previously observed similar pharmacokinetics and tissue distribution of organic cations including amphetamine between male and female mice (Zhu *et al.*, 2010; Lee *et al.*, 2014). Mice were administered 10 mg/kg methamphetamine intravenously by retro orbital injection. This dose did not induce acute toxicity in mice and generated plasma concentrations of methamphetamine and metabolites that are within the ranges reported in methamphetamine abusers (Shima *et al.*, 2008). Mice (n=3 to 6 at each time point) were sacrificed by cardiac puncture with a heparinized syringe under isoflurane anesthesia at various time points (2, 15, 30, 60, 180, 300, and 480 min). Blood was centrifuged at 1700 *g* and the plasma was stored at -80°C until analysis. Tissues (submandibular salivary glands, brain, heart, liver, kidney, skeletal muscle, and adipose) were collected at each time point, snap frozen, and stored at -80°C until use. Methamphetamine, amphetamine, and *p*-OHMA concentrations in plasma and tissue homogenates were determined by LC-MS/MS analysis. Concentrations were expressed as nM for plasma and tissue assuming a density of 1 g/mL.

4.2.5 *LC-MS/MS Analysis of Methamphetamine and its Metabolites.*

Methamphetamine, amphetamine, and *p*-OHMA were quantified using a LC-MS/MS method adapted from our previously established procedures (Wagner *et al.*, 2017). In vitro samples were prepared by permeabilization of cells with 100 μL of methanol containing 100 nM stable-labeled internal standard and dilution into an equal volume of Optima water. Tissue samples were homogenized with 1:2 weight:volume phosphate buffered saline by an Omni Bead Ruptor (Omni International.; Kennesaw, GA). Tissue density was assumed to be 1 g/mL. In vivo plasma and tissue samples were prepared by protein precipitation with 5 volumes of 75% acetonitrile/25% methanol containing 100 nM internal standards followed by centrifugation at (20,000 *g*), evaporation under nitrogen, and reconstitution in 50% methanol in water. The LC-MS/MS system consisted of an AB-Sciex 5500 qTrap Q-LIT mass spectrometer (Foster City, CA) coupled with an Agilent 1290 UPLC (Santa Clara, CA), and a Phenomenex Synergi Hydro-RP column (50 x 2 mm; 2.5 μm). The Turbo Ion Spray interface was operated in positive ion mode. Gradient elution at 0.5 mL/min with 5 mM ammonium formate in water at pH 3 (A) and acetonitrile (B) was as follows: 10% B until 0.1 min, increased to 50% B by 1.5 min, then to 95% B by 1.51 min and held at 95% B until 2 min, returning to 10% B at 2.1 min with a total run time of 3 min. Mass transitions (*m/z*) for methamphetamine, amphetamine, *p*-OHMA, methamphetamine-d_{11}, and amphetamine-d_{11} were 150→119, 136→91, 166→135, 161→97, and 147→98, respectively. Data was analyzed with Analyst software version 1.6.3 (AB Sciex). Assay accuracy and precision were within 15% (20% for the lower limit of quantification).

4.2.6 *Pharmacokinetic Data Analysis.*

The mean and standard errors for pharmacokinetic parameters were estimated using a population-based bootstrap method previously described due to sampling plasma and tissue from

different animals at each time point (Mager and Göller, 1998; Lee *et al.*, 2014). Briefly, pseudo concentration-time data were created using the R package PK (RStudio version 1.1.383 with R version 3.4.2) (Jaki and Wolfsegger, 2011; R Studio, 2012; R Core Team, 2017) by resampling measured plasma or tissue concentrations 10,000 times with random replacement of individual animals. The pharmacokinetic parameters were determined with a non-compartmental approach using the equations defined below. The area under the concentration-time curve (AUC) was calculated using the linear trapezoidal rule. In order to normalize tissue AUC to any variability in systemic AUC, AUC ratios were calculated by dividing each tissue $AUC_{0\text{-}480min}$ by the plasma $AUC_{0\text{-}480min}$ as an estimate of tissue partition ratios.

The following equations were used to calculate exposure (AUC), clearance (CL), terminal half-life ($t_{½,\beta}$), and volume of distribution at steady state (V_{ss})

$$\mathrm{AUC_{0-t}} = \int_0^t \mathrm{C(t)dt} \tag{4-2}$$

$$\mathrm{AUC_{0-\infty}} = \mathrm{AUC_{0-t}} + \frac{\mathrm{C(T)}}{\beta} \tag{4-3}$$

$$\mathrm{CL} = \frac{\mathrm{Dose}}{\mathrm{AUC_{0-\infty}}} \tag{4-4}$$

$$\mathrm{t_{\frac{1}{2},\beta}} = \frac{\ln 2}{\beta} \tag{4-5}$$

$$\mathrm{V_{ss}} = \frac{\mathrm{Dose*AUMC}}{\mathrm{AUC^2}} \tag{4-6}$$

The terminal slope (β) was calculated by linear regression of log concentrations of the terminal phase of the concentration-time profile.

4.2.7 *Statistical Analysis.*

An unpaired Student's *t* test with multiple tests corrected by the Bonferroni method was used for in vitro studies to calculate *P* values. Standard errors around the point estimate for each

pharmacokinetic parameter were determined using the non-parametric bootstrap method (Efron and Tibshirani, 1994; Jaki and Wolfsegger, 2011; Lee *et al.*, 2014). Two-sided *P* values for pharmacokinetic parameters were calculated using permutation tests as described previously (Westfall and Young, 1993; Jaki and Wolfsegger, 2011; Lee *et al.*, 2014). Multiple comparisons were corrected using the Bonferroni method. A *P* value <0.05 was considered statistically significant.

4.3 RESULTS

4.3.1 *Transport of Methamphetamine and Metabolites by mOct3 Stably Expressed in HEK-293 Cells.*

We previously demonstrated that hOCT3 shows substrate specificity for amphetamines by transporting *p*-OHMA but not amphetamine or methamphetamine (Wagner *et al.*, 2017). To confirm mOct3 demonstrates similar substrate specificity, methamphetamine, amphetamine, and *p*-OHMA were screened for uptake in mOct3 and empty vector transfected cells (Figure 4-1 A). Similar to hOCT3, only *p*-OHMA demonstrated preferential uptake into mOct3 cells when compared with vector transfected cells (Figure 4-1 A & B). Initial rate uptake studies showed that mOct3-mediated transport of *p*-OHMA was sigmoidal (Figure 4-1 C) and the cooperativity was more clearly revealed by the Eadie-Hofstee plot (Figure 4-1 D). The half-maximal transport concentration ($K_{1/2}$) is 120 ± 26 μM and the maximal transport rate (V_{max}) is 3100 ± 1000 pmol/min/mg total protein. The fitted Hill slope is 1.29 ± 0.15, suggesting a mild cooperativity.

4.3.2 *Methamphetamine Pharmacokinetic Studies in Oct3$^{+/+}$ and Oct3$^{-/-}$ Mice.*

In order to determine the in vivo significance of OCT3 in the disposition of methamphetamine and metabolites, we determined plasma and tissue concentrations of methamphetamine,

amphetamine, and *p*-OHMA in *Oct3*$^{+/+}$ and *Oct3*$^{-/-}$ mice following intravenous injection of 10 mg/kg methamphetamine. The plasma concentration-time profiles for methamphetamine, amphetamine, and *p*-OHMA in *Oct3*$^{+/+}$ and *Oct*$^{-/-}$ mice are shown in Figure 4-2 with plasma methamphetamine pharmacokinetic parameters summarized in Table 4-1. The metabolite *p*-OHMA was rapidly observed in plasma with its peak concentration at the 2 minute time point. Conversely, amphetamine reached peak plasma concentrations at approximately 60 minutes. Plasma clearance, exposure, terminal half-life, and volume of distribution were comparable for methamphetamine in *Oct3*$^{+/+}$ and *Oct3*$^{-/-}$ mice (Table 4-1). Amphetamine and *p*-OHMA also displayed similar plasma AUCs in both *Oct3*$^{+/+}$ and *Oct3*$^{-/-}$ mice (Figure 4-2). The plasma concentrations and overall exposure of the two metabolites in both genotypes are much lower than the parent drug (Figure 4-1 and Table 4-2). These data suggest that Oct3 does not play a significant role in systemic exposure to methamphetamine and major metabolites following IV injection.

4.3.3 *Impact of Oct3 Deletion on Salivary Glands Exposure to Methamphetamine, Amphetamine and p-OHMA.*

In order to determine the in vivo significance of OCT3 in the salivary glands distribution of methamphetamine and metabolites, salivary glands were collected at each time point in the pharmacokinetic study and concentrations were determined in tissue homogenate (Figure 4-3). As we expected, we did not observe any significant genotype-dependent differences in salivary glands exposure for methamphetamine or amphetamine. In contrast, knock out mice had consistently lower concentrations of *p*-OHMA (Figure 4-3) in salivary glands with approximately a 50% reduction in salivary tissue AUC when compared with *Oct3*$^{+/+}$ mice (Table 4-2). These data suggest *p*-OHMA is actively transported by Oct3 from the blood into the salivary glands. The importance of Oct3 in salivary glands uptake of *p*-OHMA in vivo was further reflected by its high

partitioning ratio in salivary glands of *Oct3*$^{+/+}$ mice (9.4 ± 1.9), which was greatly reduced in the knockout mice (4.5 ± 0.89) (Table 4-3).

4.3.4 *Tissue Distribution of Methamphetamine, Amphetamine, and p-OHMA.*

In order to characterize the tissue distribution of methamphetamine and major metabolites, various tissues (muscle, brain, heart, adipose, liver, and kidney) were collected at each time point in the pharmacokinetic study. Methamphetamine, amphetamine, and *p*-OHMA in various tissue homogenates were quantified by LC-MS/MS and the overall exposure ($AUC_{0–480min}$) was determined (Figure 4-4 A; Table 4-2). The tissue partitioning ratio was calculated by normalizing tissue $AUC_{0–480min}$ to plasma $AUC_{0–480min}$ (Figure 4-4 B; Table 4-3). For methamphetamine and amphetamine, the kidney, liver, and brain had the highest exposure with tissue AUCs approximately 4-20 times higher than the plasma AUC (Figure 4-4; Table 4-2 & Table 4-3). Remarkably, salivary glands also showed very high exposures to methamphetamine and amphetamine with AUC and partitioning ratio comparable to those in organs of elimination (liver and kidney) and site of action (brain). The heart, muscle, and adipose tissues showed much lower exposures with partitioning ratios ranging from 0.24 to 2.3 (Table 4-3). Consistent with methamphetamine and amphetamine not being transported by Oct3 (Figure 4-1), there was no significant difference in tissue distribution of methamphetamine or amphetamine between *Oct3*$^{+/+}$ and *Oct3*$^{-/-}$ mice.

The concentrations of *p*-OHMA in various tissues in general are much lower than methamphetamine and amphetamine. In *Oct3*$^{+/+}$ mice, liver, kidney and salivary glands showed the highest exposure followed by brain, skeletal muscle, and heart. Adipose exposure to *p*-OHMA cannot be determined because the concentrations at most time points were below the quantification limit. In addition to salivary glands, muscle exposure to *p*-OHMA was significantly lower in *Oct3*$^{-}$

$^{/-}$ (Figure 4-3; Figure 4-4; Table 4-2), suggesting that Oct3 may also play a role in *p*-OHMA distribution into skeletal muscle. The mean AUC and tissue-to-plasma ratios of *p*-OHMA in the brain were ~2.6 fold higher in the *Oct3*$^{+/+}$ mice than in the *Oct3*$^{-/-}$ mice, although the *P* value corrected for multiple comparisons did not reach statistical significance (Table 4-2 and Table 4-3). Similar *p*-OHMA exposure was observed in the liver, kidney, and heart between *Oct3*$^{+/+}$ and *Oct3*$^{-/-}$ mice.

4.4 DISCUSSION

Methamphetamine is one of the most widely abused illicit drugs. While human intoxication and multiple tissue toxicities frequently occur in abusers, little is known about methamphetamine or its primary metabolites' distribution to their sites of toxicity (Volkow et al., 2010; Volkow, 2013). This study determined the pharmacokinetics, tissue exposure, and partition ratios of methamphetamine and major metabolites in various mouse tissues and investigated the impact of Oct3 on the tissue-specific accumulation of *p*-OHMA. Our data demonstrated that salivary glands are a novel site of high accumulation of methamphetamine, amphetamine, and *p*-OHMA (Table 4-2 & Table 4-3). Furthermore, our study identified Oct3 as an important determinant of tissue uptake of and exposure to *p*-OHMA in salivary glands and skeletal muscle (Figure 4-3; Figure 4-4). Our findings suggest that local tissue accumulation of methamphetamine and/or its metabolites may play a role in several of the reported peripheral toxicities of methamphetamine and Oct3 can significantly impact tissue exposure to drugs and drug metabolites independently from their systemic exposure.

The abuse of methamphetamine is associated with several negative effects on health. "Meth mouth", a condition characterized by xerostomia, rampant caries and excessive tooth loss,

represents a major health burden (Ravenel *et al.*, 2012). The salivary glands, which synthesize and secrete saliva, play a vital role in oral and dental health (Humphrey and Williamson, 2001). While the mechanisms leading to "meth mouth" are poorly understood, changes in saliva output and/or composition due to salivary glands dysfunction are believed to be the root cause (Hamamoto and Rhodus, 2009). A recent study indicated that xerostomia in methamphetamine abusers was not caused by a decreased saliva output but rather a change in the composition that may be caused by direct salivary glands toxicity (Ravenel *et al.*, 2012). The decreased saliva pH and buffering capacity may indicate damage to the intercalated ductal cells responsible for bicarbonate salivary secretion (Whelton, 1996). We previously showed that OCT3 is highly expressed in both acini and ductal cells of salivary glands, which are involved in the modification and buffering of saliva (Whelton, 1996; Lee *et al.*, 2014). We also demonstrated that Oct3 mediates active uptake and high accumulation of metformin, an OCT3 substrate, in salivary glands in vivo (Lee *et al.*, 2014). Recently, we identified that *p*-OHMA is a substrate of hOCT3 (Wagner *et al.*, 2017) and confirmed it is a substrate of mOct3 (Figure 4-1). These observations had led us to suspect that methamphetamine and/or metabolites may be actively transported into salivary glands by Oct3.

A novel finding of this study is that methamphetamine and metabolites are highly accumulated in salivary glands. Our data showed that in *Oct3*$^{+/+}$ mice, methamphetamine, amphetamine, and *p*-OHMA accumulated in the salivary glands at concentrations several fold higher than plasma levels (Figure 4-2 and Figure 4-3, Table 4-2). The greatest level of accumulation was of *p*-OHMA, which had 9.4-fold higher exposure in the salivary glands than the plasma (Figure 4-2; Figure 4-3; Table 4-3). This accumulation was mediated at least in part by Oct3 as demonstrated by the 50% reduction in the *p*-OHMA tissue AUC and partition ratio in

salivary glands of *Oct3*$^{-/-}$ mice (Table 4-3; Figure 4-4). The partition ratio of *p*-OHMA in *Oct3*$^{-/-}$ mice was similar to those observed for methamphetamine and amphetamine in both *Oct3*$^{+/+}$ and *Oct3*$^{-/-}$ mice (Table 4-3), which may be due to tissue binding, partitioning into subcellular compartments, or active uptake by an unidentified transporter. The high levels of accumulation of methamphetamine and metabolites in salivary glands suggest that one or more of these compounds may play a role in toxicity of salivary gland epithelial cells. As the toxicity of these compounds has not been examined, the main culprit(s) underlying salivary glands toxicity and "meth mouth" remain unclear. Future studies, such as chronic administration of each compound coupled with pathological examination of salivary glands in *Oct3*$^{+/+}$ and *Oct3*$^{-/-}$ mice, could be helpful for further understanding the toxicological mechanisms leading to meth mouth.

Methamphetamine abuse is also associated with skeletal muscle toxicities. In severe cases, the breakdown of muscle (e.g. rhabdomyolysis) can lead to kidney failure and injury to other organs (Carvalho *et al.*, 2012). Among the measured analytes, only *p*-OHMA is actively accumulated in skeletal muscle with a partitioning ratio of 3.9 (Table 4-2; Table 4-3). Muscle *p*-OHMA exposure in *Oct3*$^{-/-}$ mice (2.4 μM×min) was significantly less than in *Oct3*$^{+/+}$ mice (9.9 μM×min), indicating that Oct3 may play a role in distribution to muscle (Table 4-2; Figure 4-4). After normalizing to plasma AUC, the *p*-OHMA muscle partition ratio in *Oct3*$^{-/-}$ mice was reduced by ~ 4-fold, although the difference between *Oct3*$^{+/+}$ and *Oct3*$^{-/-}$ mice did not reach statistical significance (Table 4-3; Figure 4-4). Consistent with our observations, previous studies with metformin have provided evidences suggesting an in vivo role of Oct3 in muscle drug exposure in mice (Lee *et al.*, 2014; Chen *et al.*, 2015). While we have no evidence to link *p*-OHMA with methamphetamine-induced muscle toxicities, our data revealed that *p*-OHMA is the only analyte that showed active accumulation in skeletal muscle after methamphetamine injection.

Additional study is needed to elucidate whether OCT3 and *p*-OHMA is indeed involved in the peripheral toxicities of methamphetamine.

Oct3 is expressed in both neuronal and astroglial cells in multiple brain regions and is believed to act as part of the "uptake-2 system" for clearing released monoamine neurotransmitters (Cui *et al.*, 2009; Gasser *et al.*, 2009; Amphoux *et al.*, 2010; Duan and Wang, 2010; Klaassen and Aleksunes, 2010). Knockdown of Oct3 in mice was associated with altered methamphetamine-induced locomotor activity (Kitaichi *et al.*, 2005). While this study was unable to detect a significant difference in brain exposure of *p*-OHMA, the ~2.6-fold higher mean brain AUC and partition ratio of *p*-OHMA in $Oct^{+/+}$ mice (Table 4-2 and Table 4-3) warrants future examination. It is still possible that Oct3 plays a role in brain disposition of *p*-OHMA and other organic cations. Currently, there is no functional data to support a role of Oct3 in transporting organic cations at the blood-brain-barrier (André *et al.*, 2012). The seemingly higher AUC of *p*-OHMA in the $Oct3^{+/+}$ mice may be due to Oct3-mediated substrate uptake and retention in neuronal and astroglial cells. Analysis of *p*-OHMA disposition in discrete brain regions with high Oct3 expression and performing substrate uptake in isolated brain cells may provide additional clues.

Detailed methamphetamine and metabolite pharmacokinetics in humans who took methamphetamine recreationally are not available. Several opportunistic studies have measured plasma concentrations of methamphetamine, amphetamine, and *p*-OHMA in methamphetamine abusers, although the time of ingestion is often unknown (Römhild *et al.*, 2003; Shima *et al.*, 2008). The concentrations of methamphetamine, amphetamine, and *p*-OHMA observed in our study in mice were in the nanomolar to micromolar range, which are comparable to those reported in opportunistic studies in abusers (Römhild *et al.*, 2003; Shima *et al.*, 2008). Tissue concentrations and pharmacokinetics can be vastly different from those in the plasma. A previous human PET

study using labeled [^{11}C]methamphetamine identified the kidney, liver, and brain as high accumulation sites. However, because PET measures the total positron emission from the radionuclide, it could not differentiate between methamphetamine and metabolites containing the labeled carbon (Volkow *et al.*, 2010). To our knowledge, the current study is the first to comprehensively determine methamphetamine and both primary metabolites (amphetamine and *p*-OHMA) pharmacokinetics in plasma and multiple tissues. Similar to the results from the human PET imaging study (Volkow *et al.*, 2010), our study also found kidney, liver, and brain to be the major accumulation sites for methamphetamine. Furthermore, the metabolites (amphetamine and *p*-OHMA) are also highly accumulated in the kidney and liver (Figure 4-4, Table 4-2).

We previously identified methamphetamine, amphetamine, and *p*-OHMA as substrates of human OCT2, suggesting renal accumulation and elimination may partially be driven by Oct2 uptake (Wagner *et al.*, 2017). In contrast to OCT2, tissue expression and in vivo studies consistently suggest that OCT3 plays a major role in peripheral tissue uptake but appears to be less important for systemic elimination (Lee *et al.*, 2014; Chen *et al.*, 2015; Wagner *et al.*, 2016). Indeed, we observed little differences in plasma pharmacokinetics of methamphetamine and metabolites between *Oct3*$^{+/+}$ and *Oct3*$^{-/-}$ mice (Figure 4-2; Table 4-1; Table 4-2) but substantial differences in disposition of *p*-OHMA in tissues known to highly express Oct3 (Figure 4-3; Figure 4-4).

In summary, this study determined the pharmacokinetics, tissue exposure, and partition ratios of methamphetamine and major metabolites in various mouse tissues and investigated the impact of Oct3 on tissue-specific accumulation of *p*-OHMA. Our data demonstrated salivary glands as a novel site of high accumulation of methamphetamine, amphetamine, and *p*-OHMA (Figure 4-2; Table 4-2). Furthermore, our study identified Oct3 as an important determinant of tissue uptake

of and exposure to *p*-OHMA in salivary glands and skeletal muscle (Figure 4-4; Table 4-2; Table 4-3). Our findings suggest that local tissue accumulation of methamphetamine and/or its metabolites may play a role in several of the reported peripheral toxicities of methamphetamine and transporters can significantly impact tissue exposure to drugs and drug metabolites independently from their systemic exposure.

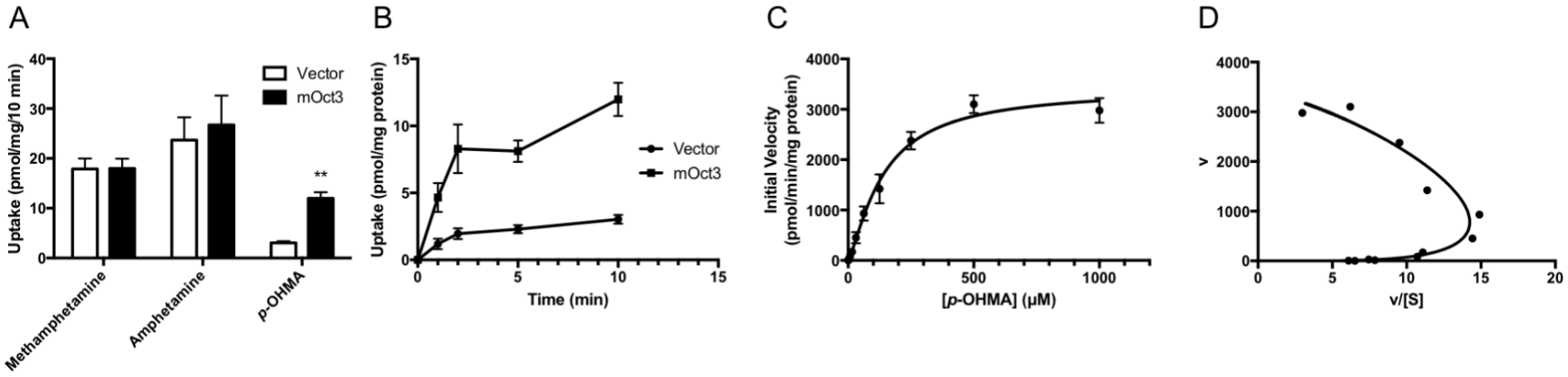

Figure 4-1. Uptake of methamphetamine, amphetamine, and *p* OHMA by vector or mOct3 transfected cells.

Uptake of 100 nM methamphetamine, amphetamine and *p*-OHMA was determined in mOct3 and pcDNA5 vector-transfected HEK293 cells after a 10 minute incubation at 37˚C (A). Data are illustrated as the mean and standard error from three independent experiments performed in triplicate. Uptake in transporter-expressing cells was compared with that in control cells (**P<0.01). Time dependent *p*-OHMA (100 nM) uptake (B) and concentration-dependent uptake (C) by mOct3 was determined in mOct3 and pcDNA5 vector-transfected HEK293 cells. The mOct3-specific uptake (C) was calculated by subtracting the transport activity in control cells. Based on the Eadie-Hofstee plot (D), mOct3-mediated uptake of *p*-OHMA was sigmoidal (C) with half-maximal transport concentration ($K_{1/2}$) of 120 ± 26 μM, a Hill slope of 1.29 ± 0.15, and maximal transport rate (V_{max}) of 3100 ± 1000 pmol/min/mg total protein from three independent experiments. Each data point in panes A, B, and C represents the mean and standard deviation from one representative experiment in triplicate. Each data point in pane D represents the mean transformed value; no error bar is shown due to uneven error propagation.

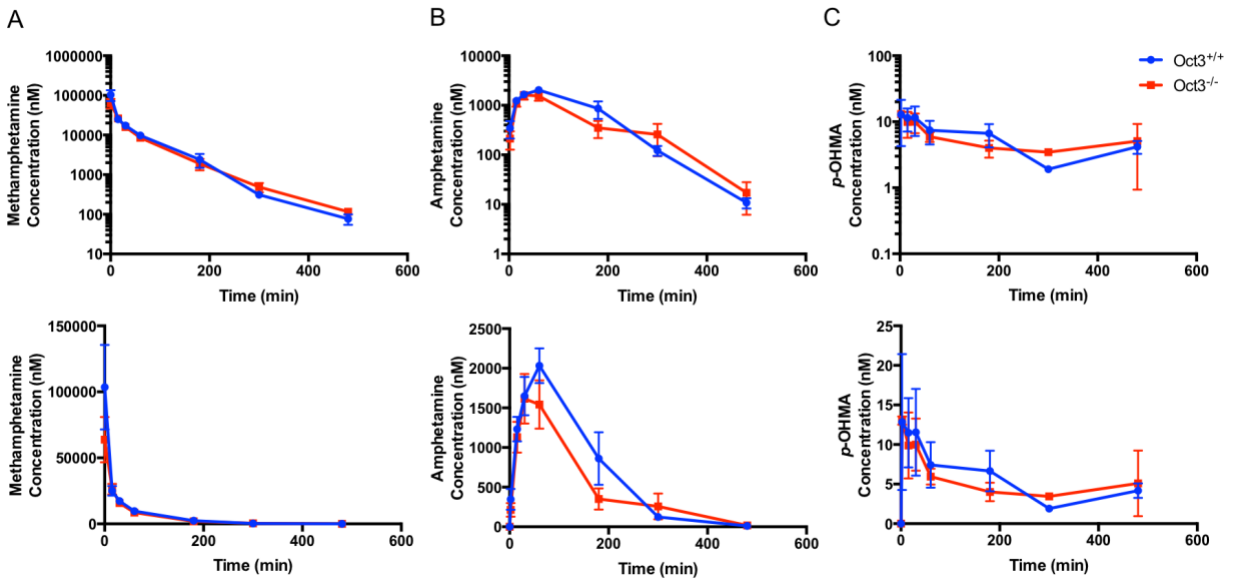

Figure 4-2. Methamphetamine, amphetamine, and p OHMA plasma concentration-time profiles in *Oct3*$^{+/+}$ and *Oct3*$^{-/-}$ mice.

Oct3$^{+/+}$ (blue circles) and *Oct3*$^{-/-}$ (red squares) mice were given a 10 mg/kg methamphetamine dose by retro-orbital IV administration. At various time points (0-480 minutes) after drug administration, animals were sacrificed with collection of blood and tissues. Methamphetamine (A), amphetamine (B), and *p*-OHMA (C) plasma concentrations were measured by LC-MS/MS analysis. Data represents mean and standard error from 3-6 mice per time point. The top graph of each pane displays the log-linear concentration-time profile while the bottom graph displays the linear-linear profile.

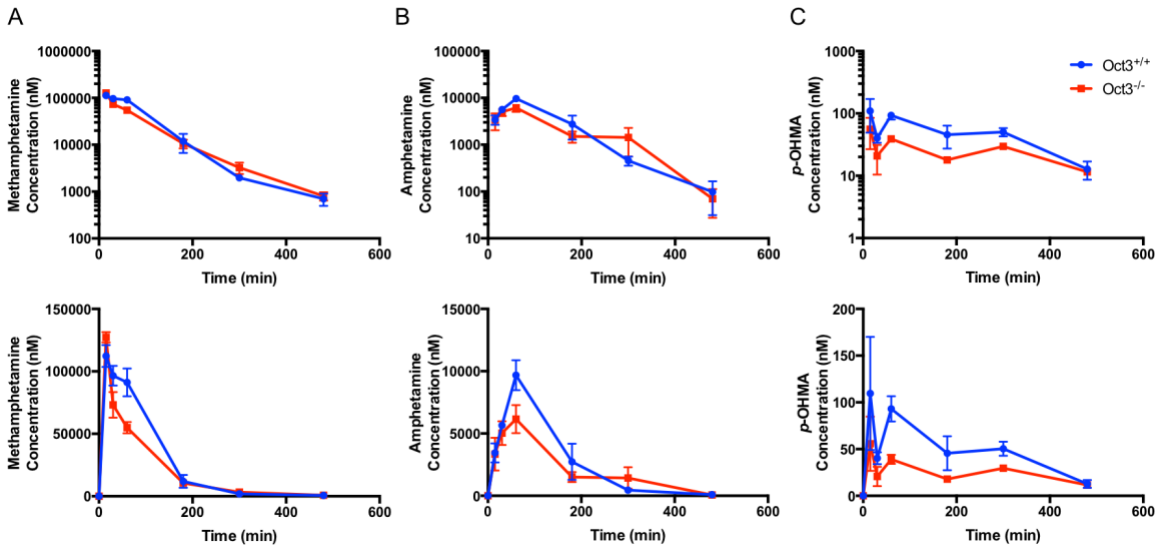

Figure 4-3. Methamphetamine, amphetamine, and *p* OHMA salivary glands concentration-time profiles in Oct3$^{+/+}$ and Oct3$^{-/-}$ mice.

Oct3$^{+/+}$ (blue circles) and *Oct3*$^{-/-}$ (red squares) mice were given a 10 mg/kg methamphetamine dose by retro-orbital IV administration. At various time points (0-480 minutes) after drug administration, animals were sacrificed with collection of blood and tissues. Methamphetamine (A), amphetamine (B), and *p*-OHMA (C) salivary glands concentrations were measured by LC-MS/MS analysis. Data represents mean and standard error from 3-6 mice per time point. The top graph of each pane displays the log-linear concentration-time profile while the bottom graph displays the linear-linear profile.

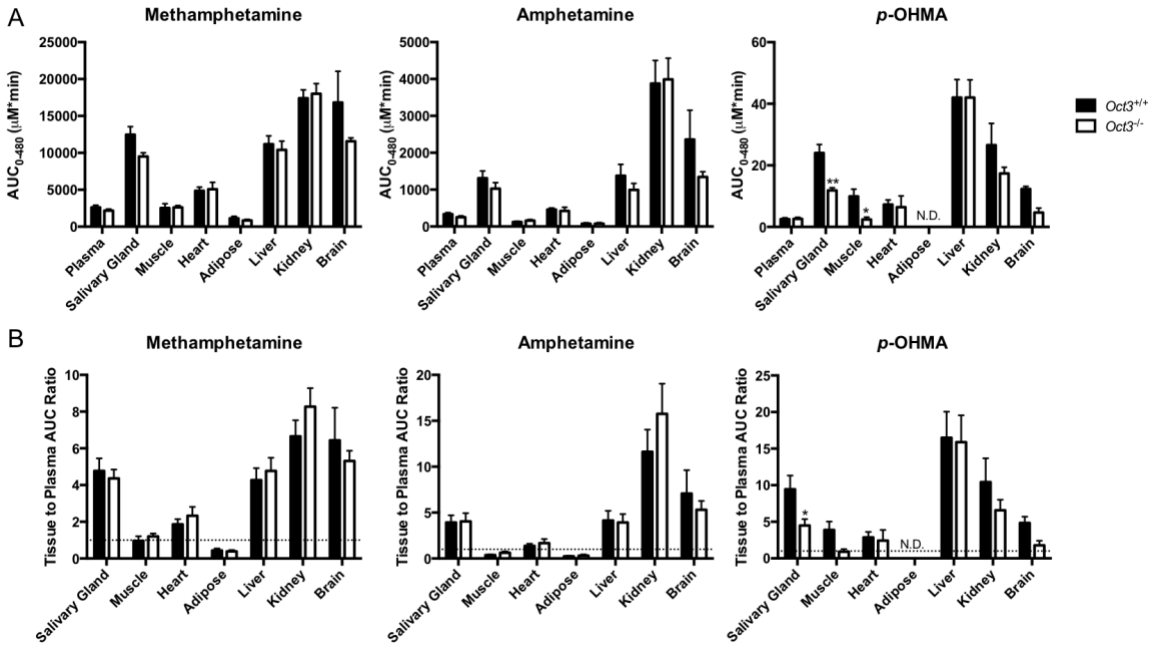

Figure 4-4. Methamphetamine, amphetamine, and p OHMA tissue AUC and AUC ratios in Oct3+/+ and Oct3-/- mice.

Oct3$^{+/+}$ (■) and *Oct3*$^{-/-}$ (□) mice were given a 10 mg/kg methamphetamine dose by retro-orbital IV administration. At various time points (0-480 min) after drug administration, animals were sacrificed with collection of blood and tissues. Methamphetamine, amphetamine, and *p*-OHMA concentrations were measured by LC-MS/MS analysis and the AUC (A) or tissue to plasma AUC ratio (B) were calculated. The dotted line denotes a ratio of one in panel B. Data represent mean and standard error estimated using a bootstrap approach from 3-6 mice per time point. Two-sided *P* values were calculated using permutation tests for each analyte in each tissue with multiple comparisons corrected using the Bonferroni method as described under Materials and Methods (*P<0.05, **P<0.01).

Table 4-1. Methamphetamine plasma pharmacokinetic parameters in *Oct3*$^{+/+}$ and *Oct3*$^{-/-}$ mice

Parameters	*Oct3*$^{+/+}$	*Oct3*$^{-/-}$
AUC_{inf} (μM×min)	2600 ± 270	2200 ± 210
Terminal $t_{1/2}$ (min)	35 ± 4.2	59 ± 5.2
Clearance (mL/min/kg)	26 ± 2.6	31 ± 3.0
V_{ss} (L/kg)	1.3 ± 0.23	1.8 ± 0.26

Data are presented as mean ± standard error. No statistically significant differences were determined between genotypes for each pharmacokinetic parameter using a permutation test with multiple comparisons corrected using the Bonferroni method as detailed in the Materials and Methods.

Table 4-2. Methamphetamine, amphetamine and *p*-OHMA tissue AUC0-480 (μM×min) in *Oct3*$^{+/+}$ and *Oct3*$^{-/-}$ mice

Tissue	Methamphetamine		Amphetamine		*p*-OHMA	
	Oct3$^{+/+}$	*Oct3*$^{-/-}$	*Oct3*$^{+/+}$	*Oct3*$^{-/-}$	*Oct3*$^{+/+}$	*Oct3*$^{-/-}$
Plasma	2600 ± 300	2200 ± 210	330 ± 44	250 ± 38	2.5 ± 0.42	2.6 ± 0.49
Salivary Glands	12000 ± 1100	9500 ± 510	1300 ± 200	1000 ± 160	24 ± 2.7	12 ± 0.85**
Muscle	2500 ± 580	2600 ± 240	120 ± 21	160 ± 28	9.9 ± 2.4	2.4 ± 0.77*
Heart	4900 ± 500	5100 ± 950	460 ± 44	420 ± 99	7.3 ± 1.5	6.4 ± 3.6
Adipose	1100 ± 260	851 ± 140	79 ± 21	78 ± 31	N.D.	N.D.
Liver	11000 ± 1100	10000 ± 1200	1400 ± 310	990 ± 180	42 ± 5.9	42 ± 5.7
Kidney	17000 ± 1100	18000 ± 1400	3900 ± 620	4000 ± 570	27 ± 7.1	17 ± 2.0
Brain	17000 ± 4200	12000 ± 560	2400 ± 790	1300 ± 140	12 ± 0.84	4.7 ± 1.4

Data are presented as mean ± standard error. Statistical significance was determined between genotypes for each analyte in each tissue using a permutation test with multiple comparisons corrected using the Bonferroni method as detailed in the Materials and Methods. N.D. Not determined, *P<0.05, **P<0.01

Table 4-3. Methamphetamine, amphetamine, and *p*-OHMA tissue to plasma AUC_{0-480} ratios in *Oct3*$^{+/+}$ and *Oct3*$^{-/-}$ mice

Tissue	Methamphetamine		Amphetamine		*p*-OHMA	
	Oct3$^{+/+}$	*Oct3*$^{-/-}$	*Oct3*$^{+/+}$	*Oct3*$^{-/-}$	*Oct3*$^{+/+}$	*Oct3*$^{-/-}$
Salivary Glands	4.8 ± 0.68	4.4 ± 0.48	3.9 ± 0.78	4.0 ± 0.89	9.4 ± 1.9	4.5 ± 0.89*
Muscle	0.97 ± 0.25	1.2 ± 0.16	0.37 ± 0.078	0.63 ± 0.15	3.9 ± 1.1	0.91 ± 0.34
Heart	1.9 ± 0.29	2.3 ± 0.49	1.4 ± 0.22	1.7 ± 0.46	2.9 ± 0.75	2.4 ± 1.4
Adipose	0.44 ± 0.11	0.39 ± 0.075	0.24 ± 0.071	0.31 ± 0.13	N.D.	N.D.
Liver	4.3 ± 0.65	4.8 ± 0.71	4.1 ± 1.1	3.9 ± 0.91	17 ± 3.5	16 ± 3.7
Kidney	6.7 ± 0.87	8.3 ± 1.0	12 ± 2.4	16 ± 3.3	10 ± 3.3	6.6 ± 1.4
Brain	6.4 ± 1.8	5.3 ± 0.55	7.1 ± 2.5	5.3 ± 0.98	4.8 ± 0.86	1.8 ± 0.64

Data are presented as mean ± standard error. Statistical significance was determined between genotypes for each analyte in each tissue using a permutation test with multiple comparisons corrected using the Bonferroni method as detailed in the Materials and Methods. N.D. Not determined, *P<0.05

Chapter 5. POTENT INHIBITION OF HUMAN ORGANIC CATION TRANSPORTER 2 (HOCT2) BY β-CARBOLINE ALKALOIDS

(A version of this chapter was published in *Xenobiotica* 47.12 (2017): 1112-1120.)

5.1 INTRODUCTION

Many drugs and toxins are hydrophilic organic cations that rely on membrane transporters to cross biological membranes. The polyspecific organic cation transporters 1-3 (OCT1-3) in the solute carrier 22 (SLC22) family play important roles in systemic elimination and tissue-specific disposition of organic cations including many clinically used drugs (Koepsell *et al.*, 2007; Giacomini *et al.*, 2010). OCT1-3 (SLC22A1-3) possess largely overlapping substrate and inhibitor specificities and are differentially expressed in various tissues. In humans, OCT1 is abundantly expressed in the liver, and represents a major transporter for hepatic uptake of cationic drugs such as metformin (Koepsell, 2013). OCT2, on the other hand, is predominantly expressed in the kidney and plays a key role in renal secretion of organic cations (Koepsell, 2013; Yin *et al.*, 2015). OCT3 is broadly distributed in many tissues (brain, heart, placenta, skeletal muscle, liver, kidney etc.) and has been suggested to play a role in tissue-specific uptake of both endogenous biogenic amines as well as xenobiotic organic cations (Chen *et al.*, 2010; Duan and Wang, 2010). Among the OCTs, OCT2 is of particular relevance to pharmacokinetics and drug-drug interactions (DDIs). Localized on the basolateral membrane of renal proximal tubule cells, OCT2 actively transports organic cations from blood into renal epithelial cells, where they can be further effluxed into the urine by the apically localized multidrug and toxin extrusion protein 1 and 2-K (MATE1 and MATE2-K) (Giacomini *et al.*, 2010; Hillgren *et al.*, 2013). OCT2 is thought to be involved in

many clinical relevant drug-drug interactions (DDIs) (Li *et al.*, 2006; Morrissey *et al.*, 2013), and is one of the seven drug transporters that are recommended by FDA and International Transporter Consortium for consideration in drug development based on their demonstrated relevance in clinical pharmacokinetics and drug interactions (Giacomini *et al.*, 2010; Zhang *et al.*, 2010).

Beta-carbolines, characterized by a core indole structure fused with a pyridine ring (Figure 5-1), are a class of naturally occurring indole alkaloids found in plants and animal tissues. Originally identified from the plant *Peganum harmala* (Syria rue), these alkaloids are widespread in our environment and diets and may also be produced endogenously (Robinson *et al.*, 2003; Pfau and Skog, 2004). They can be found in well-cooked meats and fish, coffee, chocolate, alcoholic beverages, tobacco smoke, as well as in herbal products used in traditional medicine or for recreational purpose (Nussberger *et al.*, 1987; Totsuka *et al.*, 1999; Herraiz, 2000a; b, 2004; Herraiz *et al.*, 2010). In humans, there are many potential sources of β-carboline exposure including foods, beverages, and cigarette smoking (Totsuka *et al.*, 1999; Herraiz, 2000a; b, 2004). They have been detected in human body fluids (blood, urine, cerebrospinal fluid) and tissues including brain, liver and kidney (Airaksinen and Kari, 1981; Matsubara *et al.*, 1993, 1995; Louis *et al.*, 2010). Beta-carbolines have a broad spectrum of biological, pharmacological and toxicological activities, including antitumor, antimicrobial, anti-inflammatory, cardiovascular, neuroactive, psychoactive or neurotoxic actions (Du *et al.*, 1997; Glennon *et al.*, 2000; Gockler *et al.*, 2009; Herraiz *et al.*, 2010). Of particular note, the 2N-methylated β-carboline compounds (i.e. β-carbolinium cations), which can be produced through endogenous N-methyltransferase activity, are structurally similar to the neurotoxin MPP+ (Storch *et al.*, 2004). Several β-carbolinium cations have been suggested as environmental neurotoxins underlying idiopathic Parkinson's disease (Gearhart *et al.*, 2002; Hamann *et al.*, 2006; Yang *et al.*, 2008).

Many β-carbolines are extensively metabolized in vivo whereas others are significantly excreted into urine (Fekkes and Bode, 1993; Fekkes *et al.*, 2001; Riba *et al.*, 2003, 2012). While the bioactivation pharmacological activity, and toxicological action of various β-carbolines have long been areas of active research; much less is known regarding their disposition and potential interactions with drug metabolizing enzymes and transporters (Fekkes and Bode, 1993; Fekkes *et al.*, 2001; Riba *et al.*, 2012). Several β-carbolines undergo *O*-demethylation mediated by the cytochrome P450 enzymes, especially CYP2D6 (Wu *et al.*, 2009; Herraiz *et al.*, 2013; Jiang *et al.*, 2013). A recent study also suggested significant inhibition of CYP3A4 (Zhao *et al.*, 2011). These studies have raised the concern of possible pharmacokinetic interactions between Beta-carboline rich natural products and CYP substrate drugs (Yu, 2008; Zhao *et al.*, 2011; Jiang *et al.*, 2013). Currently, little is known about the effect of β-carbolines on renal or hepatic drug transporters. Beta-carbolines are structurally related to MPP+, a known substrate of the OCTs (Figure 5-1) (Koepsell *et al.*, 2007). Several β-carbolines have been shown to be transported by the dopamine transporter (DAT) (Storch *et al.*, 2004) and the plasma membrane monoamine transporter (PMAT) (Ho *et al.*, 2011), which share a substantial overlap of substrates and inhibitors with the OCTs (Engel and Wang, 2005; Koepsell *et al.*, 2007; Duan and Wang, 2010). Hence, we hypothesized that β-carbolines are inhibitors and/or substrates of the OCTs. Given their increasing prominence as targets for clinical DDIs, we analyzed the interaction of five commercially available β-carbolines with human OCT1-3 using Flp-in HEK293 cells stably expressing these transporters. The transportability of β-carbolines by OCT1-3 was assessed by uptakes assays followed by LC-MS/MS quantification; and the impact of transport on β-carboline cytotoxicity was examined by MTT assay.

5.2 MATERIALS AND METHODS

5.2.1 *Materials*

Harmaline (4,9-dihydro-7-methoxy-1-methyl-3*H*-pyrido[3,4-*b*]indole), harmine (7-methoxy-1-methyl-9*H*-pyrido[3,4-*b*]indole), harmane methosulfate (1-methyl-9*H*-pyrido[3,4-b]indole, methosulfate), norharmanium methiodide (2-methyl-9*H*-β-carboline-2-ium, iodide), 2,9-dimethyl-4,9-dihydro-3*H*-β-carbolin-2-ium, iodide], and MTT (thiazolyl blue tetrazolium, bromide) were obtained from Sigma-Aldrich (St. Louis, MO). [^{3}H]MPP+ (85 Ci/mmol) was purchased from American Radiolabelled Chemicals (St. Louis, MO). ASP+ (4-(4-(diethylamino)styryl)-N-methylpyridinium, iodide) and trypan blue were purchased from Life Technologies, Inc. (Carlsbad, CA). Cell culture media and reagents were from Life Technologies, Inc. LC-MS/MS grade acetonitrile, water, and formic acid were purchased from Fisher Scientific (Waltham, MA).

5.2.2 *Cell Culture*

Flp-in HEK293 cell lines stably expressing hOCT1, hOCT2 and hOCT3 at isogenic locations were previously generated in our laboratory (Duan and Wang, 2010; Duan *et al.*, 2015). A HEK293 cell line stably transfected with the empty pcDNA5/FRT vector served as control. The cells were cultured in D-MEM (high glucose) media supplemented with 10% FBS, 2 mM L-glutamine, 100 U/ml penicillin, 100 µg/ml streptomycin and 150 µg/ml hygromycin B in a 37˚C humidified incubator with 5% CO_2. For better attachment of cells, all cell culture plastic surfaces were coated with 0.01% poly L-ornithine (MW 30,000 ~ 70,000) in phosphate buffered saline solution before plating.

5.2.3 *β-Carboline Inhibition Studies*

Interaction between β-carbolines and hOCT1-3 were assessed with a fluorescent ASP+-based uptake assay as we described previously (Duan *et al.*, 2015). The assay uses ASP+ as substrate and trypan blue as extracellular fluorescence-quenching dye. The uptake cocktail consists of 2 µM ASP+ and 10 µM trypan blue in uptake buffer (1X Hank's Balanced Salt Solution and 20 mM HEPES, pH 7.4). Cells were seeded at a density of 100,000 cells/well in 96-well plates and grown overnight. Uptake assays was performed at 37°C. All reagents were pre-warmed to 37°C. Immediately before the assay, cells were washed once and 100 µl of uptake buffer containing β-carbolines at graded concentrations was transferred to the wells. Uptake was initiated by adding 100 µl of ASP+ uptake cocktail. Relative fluorescence (RFU) was recorded for each well immediately after adding ASP+ (time 0) and at the end of the uptake experiment (5 min). Specific uptake was calculated by subtracting the fluorescence readings at time 0 from the end point (RFU_{end}-RFU_{time0}). Specific uptake in the absence of any inhibitors was normalized as 100%. Florescence measurements were done from a bottom-read position in a Perkin-Elmer Wallac 1420 Multilabel Counter capable of precise temperate control and kinetic measurements. For ASP+, the excitation/emission wavelengths are 475 nm/609 nm. Excitation and emission filters were configured within 10 nm of these wavelengths. Uptake experiments were repeated independently three times.

5.2.4 *β-Carbolines Uptake Assay*

Uptake assays were performed as previously described with modification for analysis of β-carbolines by liquid chromatography tandem mass spectrometry analysis (Duan and Wang, 2010; Duan *et al.*, 2015; Yin *et al.*, 2015). Cells were seeded in 96-well plates at 100,000 cells/well and grown overnight. Uptake assays were performed at 37°C. All reagents were pre-warmed to

37°C. Immediately before the assay, cells were washed twice with HBSS and allowed to acclimate for 10 minutes at 37°C. Media was emptied and incubations initiated by addition of HBSS containing substrate (1 μM). Uptake was terminated at 30 minutes by removing media and washing three times with ice cold HBSS. Cells were lysed by addition of acetonitrile containing an internal standard and β-carbolines were quantified by LC-MS/MS. For [^{3}H]MPP+ uptake, cells were lysed with 1 M NaOH and neutralized with 1 M HCl; and intracellular MPP+ was quantified by liquid scintillation counting (PerkinElmer, Tri-Carb B3110TR, Waltham, MA). Uptake was normalized to total protein measured using a BCA Protein Assay Kit (Pierce Chemical, Rockford, IL).

5.2.5 *Quantification of β-Carbolines by LC-MS/MS*

Beta-carbolines were quantified in cell lysate by LC-MS/MS using published methods with modification (Richling *et al.*, 1996; Oliveira *et al.*, 2012; Meyer *et al.*, 2014). Glyburide was used as the internal standard. An AB Sciex 4000 QTRAP Mass Spectrometer (AB Sciex, Framingham, MA) coupled to an Acquity UPLC system (Waters corporation, Milford, MA) was operated in electrospray ionization (ESI) positive mode. An Agilent Zorbax Eclipse plus C18 column (1.8 um, 2.1 x 50 mm) was used with a mobile phase consisting of 0.1% v/v formic acid in water (A) 0.1% formic acid in acetonitrile (B). A box gradient with 0.45 ml/min flow starting with 10% B until 0.1 minutes and 90% B from 0.1 to 1.5 minutes followed by 0.5 minutes at 10% B eluted β-carbolines at 0.9 minutes. Mass transitions (m/z) were 213.2→170.1 for harmine, 215.1→176.1 for harmaline, 183.2→114.9 for harmane, 183.2→114.9 for norharmanium, 185.1→139.2 for 2,9-dimethyl-4,9-dihydro-3*H*-β-carbolin-2-ium, and 494.1→369 for the internal standard glyburide. Instrument control and data processing were performed using Analyst software version 1.6.2. Accuracy was within 15% (20% for the lower limit of quantification).

5.2.6 *β-Carboline Toxicity Assay*

The MTT assay was used to determine cytotoxicity of β-carbolines toward pcDNA5 and hOCT1-3 stably transfected HEK293 cells as we described previously (Ho *et al.*, 2011). Cells were seeded in 96-well plates at a density of 14,000 cells/well and grown overnight to reach ~20% confluency. The cells were then incubated with fresh media containing β-carbolines at graded concentrations for an additional 72 hrs. The cells were then washed once with warm Dulbecco's phosphate-buffered saline, and 0.1 ml/well of MTT working solution (0.5 mg/ml MTT in 1X Hank's Balanced Salt Solution with 20 mM HEPES) was added into each well. After incubation at 37°C for 1 hr, the MTT solution was aspirated away, and 0.1 ml/well acidic isopropanol (0.04 M HCl in absolute isopropanol) was added. The plate was mixed on a rotating platform vigorously for 15 minutes to completely dissolve MTT formazan precipitates (Ho *et al.*, 2011). Absorbance was measured at a wavelength of 570 nm to determine cell viability. Because we observed a systematic increase (10–25%) in optical intensity in cells treated with all β-carbolines at low and nontoxic concentrations, which is probably due to additional optical absorbance by residual β-carbolines, the survival rate in cells treated with the lowest drug concentration was set to 100% and used as a control to normalize cell viability across the entire concentration range.

5.2.7 *Data Analysis*

The half maximum inhibition concentration (IC_{50}) and the half maximum toxic concentration (TC_{50}) were determined by non-linear regression fit of uptake or cell viability data with the log(inhibitor) versus response—variable slope (four parameters) model in GraphPad Prism® v5.0. The equation is: Y=Bottom + (Top-Bottom)/(1+10^((LogIC_{50}-X)*H)), where Y is the % specific uptake or cell survival, Bottom is the residual uptake or survival, Top is the maximal uptake or survival, X is β-carboline concentration, and H is the hill slope. For cell viability, TC_{50} replaces

IC_{50}. The constraints were set as Bottom ≥ 0. Data are expressed as Mean ± S.D. of independent experiments and repeated at least three times. The *p* values were determined by student's t-test in GraphPad Prism® 5.0.

5.3 RESULTS

5.3.1 *β -Carbolines Inhibit hOCT1-3 Mediated ASP+ Uptake*

The ASP+ uptake assay is a rapid, non-radioactive, fluorescent substrate-based method that has been previously used to characterize compound interaction with the OCTs (Ciarimboli *et al.*, 2005; Mason *et al.*, 2005; Kido *et al.*, 2011; Duan *et al.*, 2015). We previously demonstrated that the IC_{50} values obtained by the fluorescence assay correlate well with IC_{50} values determined by traditional radiotracer assays (Duan *et al.*, 2015). Here we applied the assay to study hOCT interaction with commercially available β-carbolines. The structures of the five tested β-carbolines are shown in Figure 1. These include two methoxy harmala alkaloids (harmine, harmaline), a non-methoxy substituted analogue (harmane), and two β-carbolinium cations (norharmanium, 2,9-dimethyl-4,9-dihydro-3*H*-β-carbolinium). Concentration-dependent inhibition of ASP+ uptake was observed for all five β-carbolines towards hOCT1-3 (Figure 2). The fitted IC_{50} values are summarized in Table 1. No apparent relationship was observed between the molecular structures of β-carbolines (Figure 1) and their inhibition potencies (Table 1) for a specific transporter. The 2N-methylated β-carbolinium cations (norharmanium, 2,9-dimethyl-4,9-dihydro-3*H*-β-carbolinium) showed comparable potencies to the non-permanently charged β-carbolines (harmine, harmaline, harmane). The 3,4-carbon saturation on the pyridine ring (harmaline versus harmine), and the methoxyl substitution on position 7 of the indole ring (harmine versus harmane) also did not have a major effect on the β-carboline interaction with the OCTs.

For all five β-carbolines, hOCT2 showed much greater sensitivity with IC_{50} values in sub- or low micromolar range. Harmaline, a psychoactive alkaloid present in *Peganum harmala* as well as in the hallucinogenic drink ayahuasca, showed the most potent inhibition towards hOCT2 (IC_{50} = 0.479 ± 0.077 μM). In contrast, hOCT1 was 1-2 orders of magnitude less sensitive to β-carboline inhibition. hOCT3 showed an intermediate sensitivity. These data suggest that β-carbolines are potent inhibitors of hOCT2, a major transporter involved in the elimination of cationic drugs in the kidney.

5.3.2 *Permanently Charged β-carbolines are Substrates of hOCT1-3*

Direct determination of β-carbolines (1 μM) hOCT substrate potential was performed by measuring accumulation in vector and hOCT1-3-transfected cells by LC-MS/MS quantification (Figure 3). The positive control MPP+ accumulated 4- to 10-fold relative to vector cells in hOCT1-3 transfected cells at 30 minutes. Substantially higher accumulation (5- to 7-fold) was observed in hOCT1-3 transfected cells with norharmanium and 2,9-dimethyl-4,9-dihydro-3H-β-corbolin-2-ium, suggesting these two permanently charged cations are substrates of all three hOCT isoforms. Harmaline demonstrated ~ 2-fold higher accumulation in hOCT1 and hOCT3 transfected cells. Harmine and harmane did not show significantly higher accumulation in hOCT1-3 transfected cells as compared with vector controls at 1 μM.

5.3.3 *Impact of hOCT1-3 Expression on β-carboline Cytotoxicity*

Beta-carbolines are structurally related to MPP+, which exerts mitochondrial toxicity by inhibiting complex I of the mitochondrial respiratory chain. To test whether expression of hOCTs would impact intracellular toxicity of β-carbolines, we examined if the apparent toxicity of these compounds to HEK293 cells are altered using an MTT assay. The dose-dependent toxic response

curves of the five β-carbolines in pcDNA5- (control) and hOCT1-, hOCT2-, and hOCT3-transfected cell lines are shown in Figure 4. The fitted TC_{50} values are summarized in Table 2. MPP+ and all five tested β-carbolines showed innate toxicity in control HEK293 cells (Table 2). As expected, expression of hOCT1, hOCT2, and hOCT3 increased HEK293 cell sensitivity to MPP+ by 16.4, 8.9 and 10.9 folds respectively (Table 2). Similar to MPP+, harmane and norharmanium exhibited greatly increased toxicity in all three transporter-transfected cells. These data suggest that transport mediated accumulation of norharmanium by hOCT1, 2 and 3 in HEK293 cells increased its apparent potency. Compared to vector-transfected HEK293 cells, expression of hOCT1-3 had no significant effect on cellular response to harmine, harmaline, and 2,9-dimethyl-4,9-dihydro-3*H*-β-carbolin-2-ium.

5.4 DISCUSSION

Naturally occurring in plants, foods, and animal tissues, β-carboline alkaloids have been found in human tissues and body fluids. They are a major form of alkaloid in the seeds of *Peganum harmala* (Syria rue), which has been used in traditional medicine and for recreational purposes (Nussberger *et al.*, 1987; Herraiz *et al.*, 2010). Some β-carbolines, such as harmine and harmaline, are also the major psychotropic ingredients in Ayahuasca, a tea used for a religious and recreational purposes that was originally used by indigenous Amazonia tribes but has also spread to the United States and elsewhere (Riba *et al.*, 2003; McKenna, 2004). The psychotropic effect of harmine and harmaline in Ayahuasca is largely due to their potent inhibition of monoamine oxidase A (MAO-A), which metabolically inactivates other psychedelic indolealkylamines co-present in Ayahuasca (Rommelspacher *et al.*, 1994; Kim *et al.*, 1997; Smith *et al.*, 2013). Recent studies have revealed interactions between β-carbolines and CYP2D6 (Wu *et al.*, 2009; Herraiz *et al.*, 2013; Jiang *et al.*, 2013), raising the concern of possible pharmacokinetic interactions (Yu, 2008; Zhao *et al.*, 2011;

Jiang *et al.*, 2013). Because β-carbolines are structurally related to the OCT substrate MPP+, the goal of this study is to determine if β-carbolines are inhibitors and/or substrates for human OCT1-3.

In the human kidney, the basolateral hOCT2 and apical hMATEs sequentially mediate tubular secretion of many organic cation drugs (Wagner *et al.*, 2016). According to the recent draft FDA guidance (Food and Drug Administration, 2012a), OCT2 is one of three drug transporters in the human kidney recommended for evaluation for potential DDIs during drug development. Our results (Table 1 and Figure 2) showed that while hOCT1-3 are all inhibited by β-carbolines, hOCT2 is most sensitive to these indole alkaloids with IC_{50} values in nanomolar to low micromolar range. Although several synthetic compounds, such as decynium 22, tetrapentylammonium, and N-butyl-N-methylpyrrolidinium, are identified as potent hOCT2 inhibitors with reported IC_{50} or K_i values in the same range as the β-carbolines (Gorboulev *et al.*, 1997; Cheng *et al.*, 2011), their use is limited to in vitro assays and animal studies. In contrast, most clinically used hOCT2 inhibitors are much less potent, with affinities in mid- to high micromolar range (Morrissey *et al.*, 2013; Motohashi and Inui, 2013). For example, cimetidine, the classic blocker of OCT2, has a reported K_i of 95–146 μM for hOCT2 expressed in HEK293 cells (Ito *et al.*, 2012). In contrast, the apically localized MATEs proteins are more sensitive to cimetidine (K_i = 1-4 μM). Because clinically encountered concentrations of cimetidine in plasma is about 2.0-3.6 μM, it has been suggested that inhibition of hMATEs, rather than hOCT2, underlines renal cimetidine-drug interactions (Ito *et al.*, 2012). Here we show that β-carbolines, which occur both endogenously and exogenously in diets and herbal products, are much more potent in vivo inhibitors for hOCT2. The most potent inhibitor is harmaline (IC_{50} ~ 500 nM), a major psychotropic ingredient in the Amazonia tea Ayahuasca. The reported endogenous β-carboline concentrations in human body

and fluids are generally in the low nanomolar range (Matsubara *et al.*, 1993; Gearhart *et al.*, 2002; Parker *et al.*, 2004), and therefore will not affect the function of hOCT2. Unfortunately, the blood levels of β-carbolines in self-administered religious or recreational users is unknown. In healthy volunteers, a 0.5 mg/kg dose of harmine - which has an IC_{50} of 6.14 μM for hOCT2 - reached an unbound C_{max} of approximately 1.6 μM suggesting the potential for inhibition (Slotkin *et al.*, 1970; Zetler *et al.*, 1974; Food and Drug Administration, 2017). Additionally, after a single ingestion of Ayahuasca in healthy volunteers, plasma β-carbolines, including harmaline, reportedly reached mid nanomolar to mid micromolar concentrations (Riba *et al.*, 2012), which may lead to significant inhibition of hOCT2. This interaction may be further aggregated by multiple Ayahuasca ingestions and/or in CYP2D6 poor metabolizers since harmaline is metabolized primarily via *O*-demethylation by CYP2D6. Thus, our study suggests potential herb- or food-drug interactions at the site of hOCT2 as a result of potent inhibition of the transporter by β-carbolines in diets and natural products.

Beta-carbolines exhibit a broad spectrum of biological and pharmacological activities due to their binding to benzodiazepine, imidazoline, and serotonin receptors as well as reversible inhibition of intracellular MAO (Glennon *et al.*, 2000; Robinson *et al.*, 2003; Parker *et al.*, 2004; Herraiz *et al.*, 2010). Many β-carbolines are readily absorbed and distributed in body tissues and brain (Matsubara *et al.*, 1993, 1995; Louis *et al.*, 2010). β-carbolines (e.g. harmine, harmaline, norharman) are extensively metabolized by the liver while others are excreted into urine. Our finding that norharmanium, 2,9-dimethyl-4,9-dihydro-3*H*-β-carbolin-2-ium, and harmaline are accepted as substrates by hOCT1-3 suggests that hOCTs are likely to play a role in the disposition and action of these β-carbolines (Figure 3). Transport mediated disposition may be particularly important for the permanently charged norharmanium and 2,9-dimethyl-4,9-dihydro-3*H*-β-

carbolin-2-ium which are less membrane permeable. For example, hOCT1, which is expressed on the sinusoidal membrane of hepatocytes (Koepsell *et al.*, 2007; Nies *et al.*, 2011), may mediate β-carboline uptake into the liver, where they can be further metabolized by CYP2D6 or other liver enzymes. The kidney-specific hOCT2, on the other hand, may play a role in renal excretion of certain β-carbolines. hOCT3, which is broadly expressed in many neuronal tissues and astrocytes (Cui *et al.*, 2009), could play a role in brain distribution and neurotoxicity of β-carbolines. The non-charged β-carbolines (harmine, harmaline, harmane) had much higher passive diffusion (~5-fold higher accumulation in control cells) and showed minimal enhanced accumulation in hOCT1-3 transfected cells (Figure 5-3). Therefore, hOCTs may play a minor role in the disposition of these non-charged β-carbolines in vivo.

We found that expression of hOCT1-3 greatly sensitized HEK293 cells to MPP+, norharmanium and harmane cytotoxicity (Figure 4). Norharmanium and 2,9-dimethyl-4,9-dihydro-3*H*-β-carbolin-2-ium were both good substrates of hOCT1-3 but only norharmanium showed increased cytotoxicity. It is important to note that overall toxic response depends on the innate cytotoxicity of these compounds and is also influenced by their passive diffusion across the cell membranes. It is possible that the toxic effect of 2,9-dimethyl-4,9-dihydro-3*H*-β-carbolin-2-ium towards HEK293 cells involves multiple cellular activation steps and cellular uptake of these compounds is not a rate-limiting step. Surprisingly, hOCT-expressing cells also showed significantly increased sensitivity to harmane, which is not a substrate of the hOCT (Figure 3). The reason for this observation is unknown. Previous studies suggest that the 2N-methylated β-carbolinium cations are the active toxic species (Storch *et al.*, 2004; Hamann *et al.*, 2006; Yang *et al.*, 2008). It is possible that harmane itself is not toxic, but undergoes 2N-methylation in HEK293 cells to generate a cytotoxic carbolinium species, which could be a substrate of the

hOCTs. Expression of the hOCTs may increase the retention of the toxic species, enhancing its cytotoxic effect in these cells. The disagreement between substrate status and cytotoxicity highlights the importance of directly confirming transporter substrates by uptake assays.

In summary, we show that β-carbolines interact with human OCT1-3 with differential inhibition potencies towards these transporters. We also confirmed that harmaline, norharmanium, and 2,9-dimethyl-4,9-dihydro-3*H*-β-carbolin-2-ium are transportable substrates of hOCT1-3. Together, our data support a role of hOCT1-3 in tissue uptake and disposition of β-carbolines. More importantly, the potent inhibition of hOCT2 by β-carbolines also raises a concern of potential drug interactions between naturally occurring β-carboline alkaloids and drugs that are renally eliminated via hOCT2.

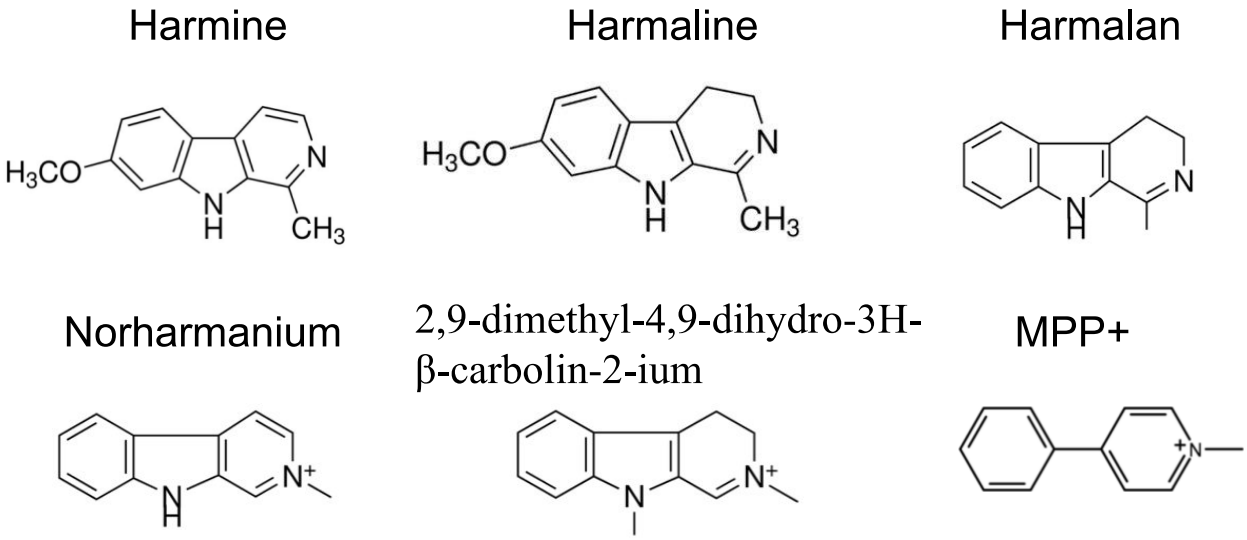

Figure 5-1. Molecular structure of β-carbolines used in the current study and MPP+.

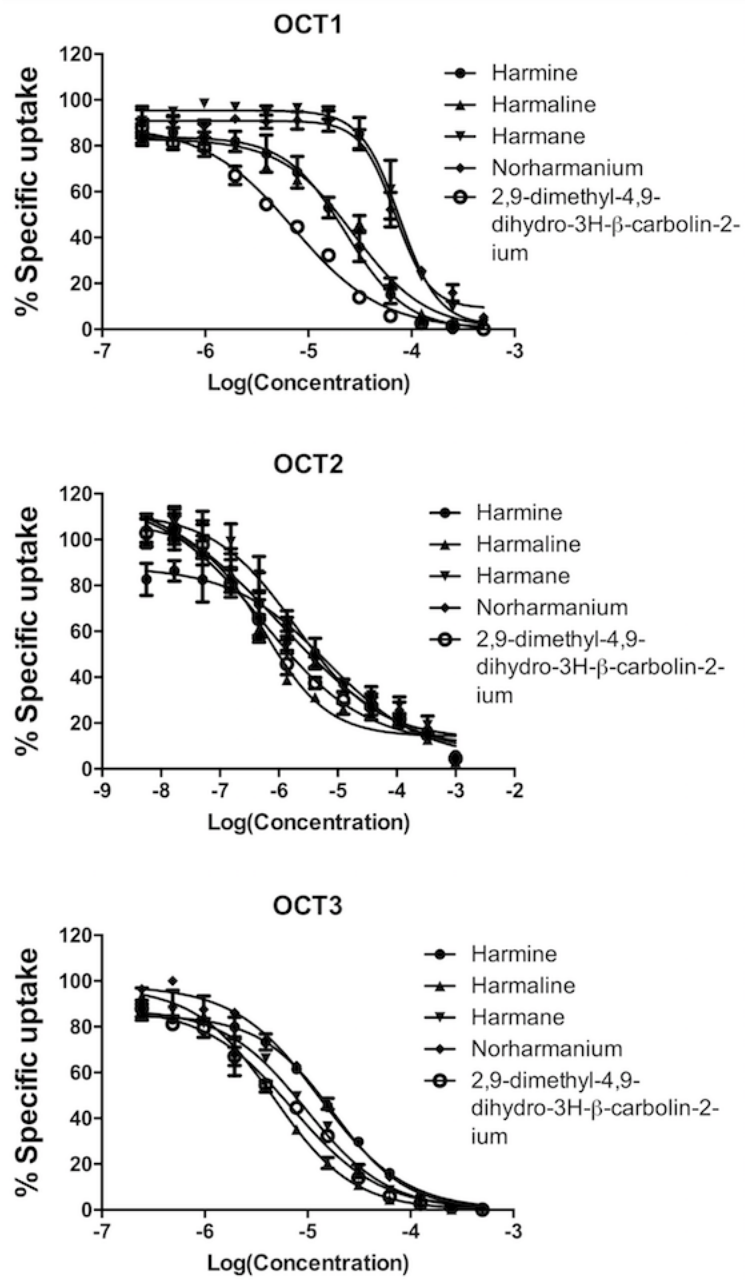

Figure 5-2. Interaction of β-carbolines with hOCT1 3.

Concentration-dependent inhibition of hOCT1-3 was determined with ASP+-based fluorescence uptake assay. Data represent Mean ± S.D. of three independent experiments.

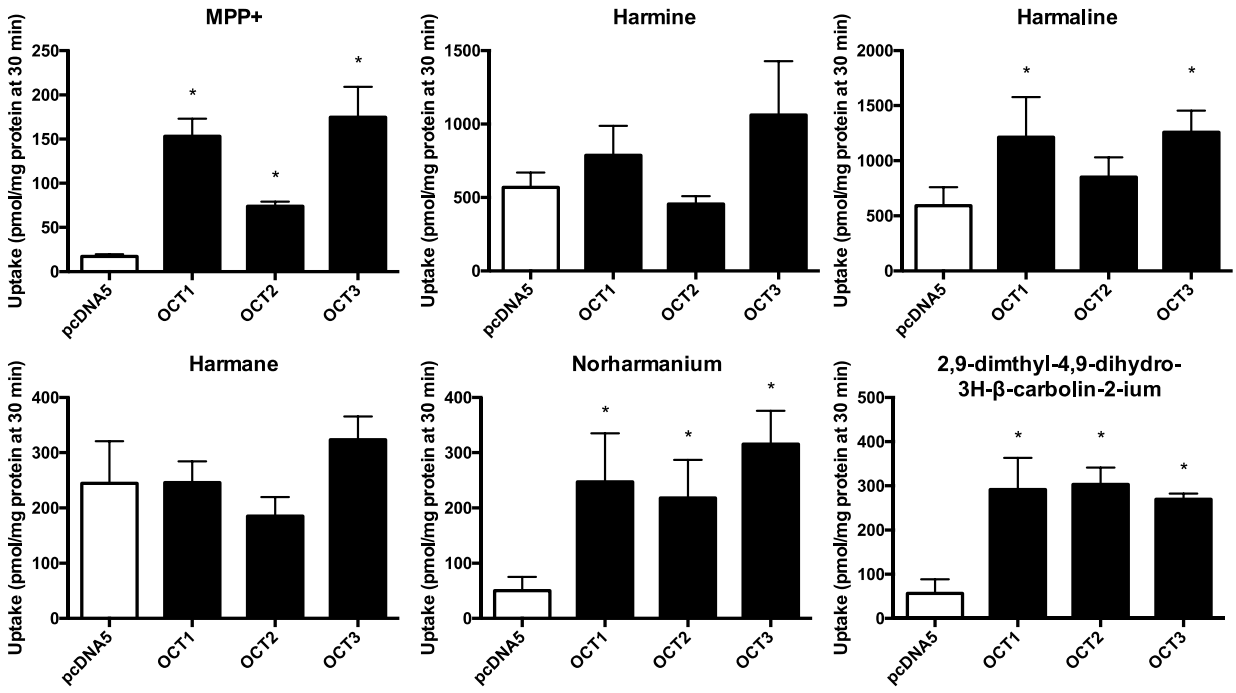

Figure 5-3. Uptake of 1 μM MPP+ (positive control) and β-carbolines in vector (pcDNA5) or hOCT1 3 stably transfected Flp-in HEK293 cells.

Data represent Mean ± S.D. of three independent experiments. *Indicates values in transporter-expressing cells significantly different from those in pcDNA5 control cells ($p<0.005$)

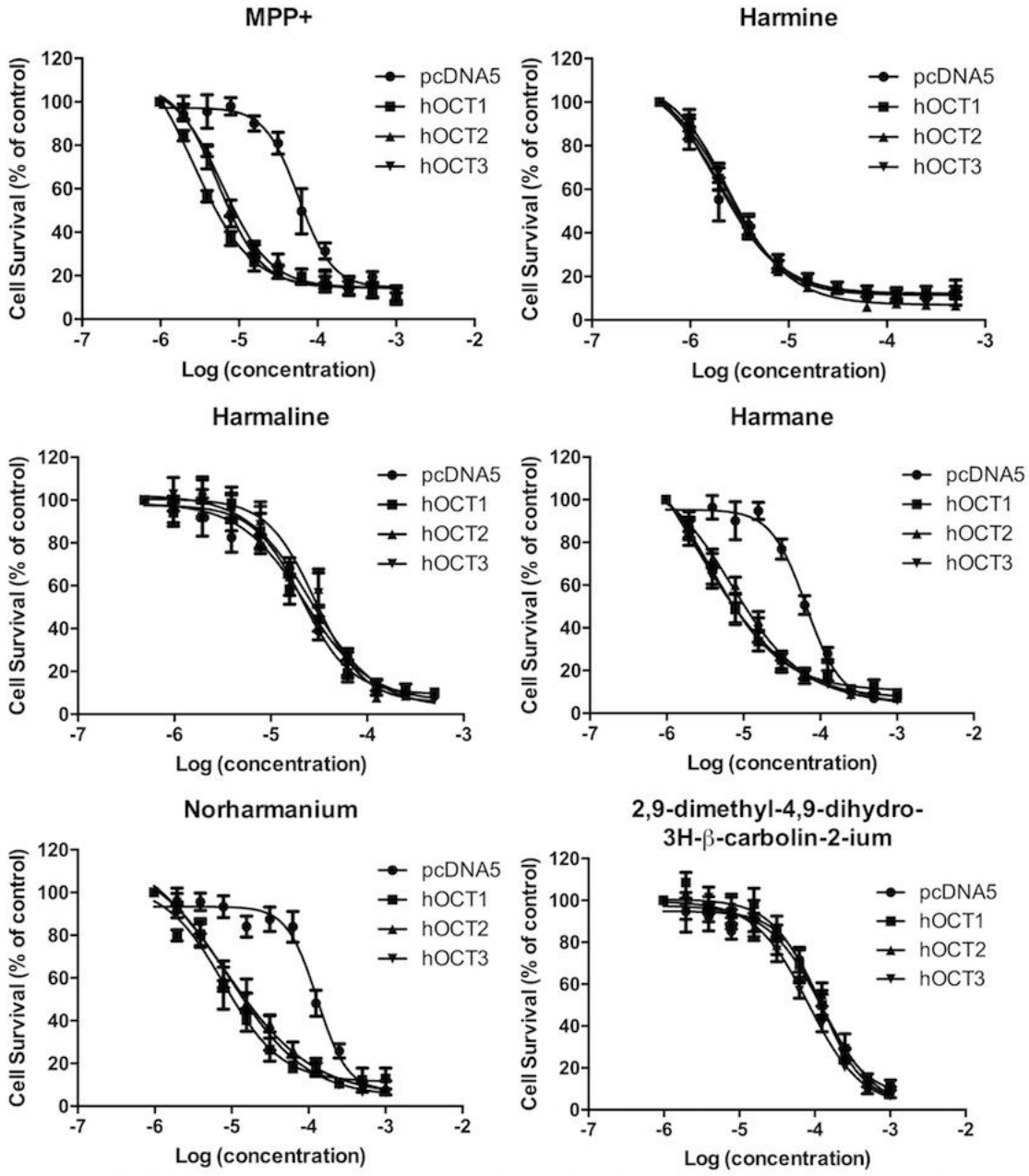

Figure 5-4. Concentration-dependent toxicity of MPP+ (positive control) and β-carbolines in vector (pcDNA5) or hOCT1 3 stably transfected Flp-in HEK293 cells.

Concentration-dependent toxicity was determined with an MTT-based absorbance assay. Data represent Mean ± S.D. of six independent experiments.

Table 5-1. IC_{50} values of β-carbolines for hOCT1 3 as determined by the ASP+-based uptake assay.

Compound	IC_{50} (μM)		
	OCT1	OCT2	OCT3
Harmine	23.1 ± 2.8	6.14 ± 0.70	17.7 ± 1.0
Harmaline	27.6 ± 3.8	0.497 ± 0.077	4.76 ± 0.46
Harmane	75.5 ± 10.2	2.04 ± 0.35	10.1 ± 0.6
Norharmanium	70.5 ± 6.6	1.05 ± 0.06	13.1 ± 0.1
2,9-dimethyl-4,9-dihydro-3H-β-carbolin-2-ium	40.4 ± 2.4	0.524 ± 0.088	7.30 ± 0.50

Results represent Mean ± S.D. of three independent experiments.

Table 5-2. TC_{50} values of β-carboline toxicity towards pcDNA5 (control) and OCT1 3 transfected cells, as determined with the MTT cytotoxicity assay.

Compound	TC_{50} (μM)				Fold increase over pcDNA5		
	pcDNA5	OCT1	OCT2	OCT3	OCT1	OCT2	OCT3
MPP+	63.6 ± 12.7	3.88 ± 0.38*	7.16 ± 0.75*	5.86 ± 0.68*	16.4	8.9	10.9
Harmine	2.87 ± 0.47	2.55 ± 0.26	3.01 ± 0.41	2.81 ± 0.23	1.1	0.95	1.0
Harmaline	23.0 ± 3.6	23.0 ± 5.1	35.5 ± 3.8	33.1 ± 8.2	1.0	0.65	0.69
Harmane	66.6 ± 4.6	7.16 ± 1.96*	10.3 ± 1.5*	8.88 ± 2.76*	9.3	6.5	7.5
Norharmanium	119 ± 18	9.05 ± 2.54*	13.4 ± 2.4*	10.8 ± 1.4*	13.1	8.9	11.0
2,9-dimethyl-4,9-dihydro-3H-β-carbolin-2-ium	127 ± 18	119 ± 33	117 ± 22	80.6 ± 7.2	1.1	1.1	1.6

Data represent Mean ± S.D. of six independent experiments. *Indicates values in transporter-expressing cells significantly different from those in pcDNA5 control cells ($p<0.005$)

Chapter 6. CONCLUSIONS AND FUTURE DIRECTIONS

This dissertation research aimed to elucidate the roles of organic cation transporters in the disposition, drug-drug interactions, and toxicity of methamphetamine. Work conducted in this dissertation research has elucidated the molecular mechanisms involved in transport and disposition of methamphetamine and its metabolites and provided novel insights into the in vivo significance of OCTs in the disposition, potential drug-drug interactions, and toxicities of this widely abused drug.

In Chapter 2, I showed that methamphetamine and its metabolites interact with hOCT1-3 and hMATE1/2-K at clinically relevant concentrations (Melega *et al.*, 2007; Shima *et al.*, 2009; Wagner *et al.*, 2017). I further demonstrated that methamphetamine and amphetamine are substrates of hOCT2, hMATE1, and hMATE2-K, suggesting that the hOCT2/hMATEs pathway is involved in renal secretion of methamphetamine and its metabolites, and that inhibition of hOCT2 and hMATEs by methamphetamine may lead to potential DDIs for drugs that are eliminated by the hOCT2/hMATE pathway. The role of the hOCT2/hMATE pathway in active renal secretion can be further tested in vivo using preclinical animal models such as transporter knockout mice or with specific inhibitors. Ultimately, a human study would be needed to understand the clinical significance of hOCT2/hMATE in methamphetamine disposition and drug interactions. The pH dependence of methamphetamine and amphetamine renal clearance has long been known and was mostly attributed to the pH effect on ionization and membrane partitioning (Beckett and Rowland, 1965a, c; b). In my view, the potential for urinary pH to modulate MATE transport activities in vivo should also be considered and studied further. Physiologically based pharmacokinetic modeling may offer a first step in predicting the in vivo implications before

moving into animal models. Dissecting the role of pH on passive diffusion and MATE transport in vivo may be particularly challenging. Performing preclinical work using a MATE substrate with negligible passive diffusion (e.g. metformin, MPP+) under acidified and alkaline urine conditions may represent the first step to gauge the pH effect on MATE activity in vivo.

Complex kinetics and substrate dependent inhibition of OCTs has gained increasing attention and has hindered in vitro to in vivo extrapolation. Chapter 3 demonstrated that the apparent mechanism of inhibition (i.e. competitive or noncompetitive) depends on the substrate transport kinetics and sidedness of the inhibitory interaction. These findings suggest some hOCT2 substrates have spatially distinct binding sites within the binding region and may likely be transported simultaneously. This work highlights the need to consider intracellular unbound concentrations when examining inhibition of transporters. Emerging studies suggest that using plasma inhibitor concentrations may lead to significant under-prediction of hOCT2-mediated DDIs. For example, PBPK modeling of the cimetidine-metformin inhibition required a 1000-fold fudge factor increasing the in vitro apparent potency of cimetidine for OCT2 (Burt *et al.*, 2016). Incorporation of trans inhibition and equilibrium exchange from in vitro data to estimate intracellular inhibition potency could be the next steps to narrow the in vitro-to-in vivo gap of poorly predicted clinical DDIs. High throughput screening of transporter inhibitors with multiple substrates are beginning to empirically classify probe substrates based on sensitivity (Chen *et al.*, 2017). Leveraging the high throughput data with additional mechanistic studies could support the rational selection of in vitro probe substrates for DDI assessment.

Chapter 4 determined the pharmacokinetics, tissue exposure, and partition ratios of methamphetamine and major metabolites in various mouse tissues and investigated the impact of Oct3 on the tissue-specific accumulation of *p*-OHMA. The data demonstrated that salivary glands

are a novel site of exceedingly high accumulation of methamphetamine, amphetamine, and *p*-OHMA. Furthermore, Chapter 4 identified Oct3 as an important determinant of tissue uptake of and exposure to *p*-OHMA in salivary glands and skeletal muscle. These findings suggest that local tissue accumulation of methamphetamine and/or its metabolites may play a direct role in several of the reported peripheral toxicities of methamphetamine, and Oct3 can significantly impact tissue exposure to drugs and drug metabolites independently from their systemic exposure. Future toxicological studies examining the effect of chronic administration of methamphetamine or *p*-OHMA on salivary glands and skeletal muscle tissues in wild type and knockout mice will help further elucidate the drivers of toxicity. The very high salivary accumulation of methamphetamine and amphetamine was surprising considering they are not substrates of OCT3. In vitro binding studies with salivary tissue homogenate or slices could help determine if the partitioning is primarily due to tissue binding or a yet-to be identified transporter could be involved.

Chapter 5 showed that β-carbolines interact with human OCT1-3 with differential inhibition potencies towards these transporters. The research also confirmed that harmalan and norharmanium are transportable substrates of hOCT1, 2 and 3. Together, these data support a role of hOCT1-3 in tissue uptake and disposition of β-carbolines. More importantly, the potent inhibition of hOCT2 by β-carbolines also raises a concern of potential drug interactions between naturally occurring β-carboline alkaloids and drugs that are renally eliminated via hOCT2. Food-drug interactions mediated by dietary β-carbolines may be further examined in vivo as this has implications for inhibition of renal OCT2 which is not typically considered in food-drug interactions. Interestingly, hOCT-expressing cells showed significantly increased sensitivity to harmane, which is not a substrate of the hOCTs. The disagreement between substrate status and cytotoxicity highlights the importance of directly confirming transporter substrates by uptake

assays. Possible harmane intracellular metabolism and subsequent metabolite transport by hOCTs highlighted the interplay between metabolism, transport, and toxicity which could be further investigated in systematic metabolism, transport, and toxicity studies.

In summary, this dissertation research has contributed greatly to our understanding of transporter mediated disposition, drug-drug interactions, and toxicity of the drugs of abuse methamphetamine and β-carbolines. Taken together, this research provides useful information that may be considered when prescribing medications to methamphetamine users to mitigate the risk of DDIs that may potentially compromise therapeutic efficacy and drug safety. There are still significant gaps and challenges left to be addressed in this field. In particular, the extrapolation from in vitro to in vivo transporter inhibition and substrate kinetics is still difficult. The integration of the carrier-specific kinetic model into these extrapolations as was eluded to in Chapter 3 may be a potential path forward. As highlighted in Chapter 2, the potential modulation of the MATE transporters by physiological conditions (e.g. urinary pH) in vivo may play a surprising role in overall activity that requires future investigation. The incorporation of membrane sidedness, physiological driving forces, and carrier-specific kinetics into modeling and simulation approaches offers promising paths towards the understanding and accurate prediction of transporter-mediated drug disposition, drug-drug interactions and adverse effects.

BIBLIOGRAPHY

Ackerman BH, and Kasbekar N (1996) Disturbances of taste and smell induced by drugs. *Pharmacotherapy* **17**:482–496.

Airaksinen MM, and Kari I (1981) Beta-carbolines, psychoactive compounds in the mammalian body. Part I: Occurrence, origin and metabolism. *Med Biol* **59**:21–34.

Amphoux A, Millan MJ, Cordi A, Bönisch H, Vialou V, Mannoury la Cour C, Dupuis DS, Giros B, and Gautron S (2010) Inhibitory and facilitory actions of isocyanine derivatives at human and rat organic cation transporters 1, 2 and 3: A comparison to human ??1- and ??2-adrenoceptor subtypes. *Eur J Pharmacol* **634**:1–9, Elsevier B.V.

Amphoux A, Vialou V, Drescher E, Bruss M, Mannoury La Cour C, Rochat C, Millan MJ, Giros B, Bonisch H, Gautron S, Brüss M, La Cour CM, Rochat C, Millan MJ, Giros B, Bönisch H, and Gautron S (2006) Differential pharmacological in vitro properties of organic cation transporters and regional distribution in rat brain. *Neuropharmacology* **50**:941–952.

André P, Saubaméa B, Cochois-Guégan V, Marie-Claire C, Cattelotte J, Smirnova M, Schinkel AH, Scherrmann JM, and Cisternino S (2012) Transport of biogenic amine neurotransmitters at the mouse blood-retina and blood-brain barriers by uptake1 and uptake2. *J Cereb Blood Flow Metab* **32**:1989–2001.

Atkins WM (2006) Current views on the fundamental mechanisms of cytochrome P450 allosterism. *Expert Opin Drug Metab Toxicol* **2**:573–579.

Atkins WM (2005) Non-Michaelis-Menten kinetics in cytochrome P450-catalyzed reactions. *Annu Rev Pharmacol Toxicol* **45**:291–310.

Beckett AH, and Rowland M (1965a) Urinary excretion kinetics of amphetamine in man. *J Pharm Pharmacol* **17**:628–639.

Beckett AH, and Rowland M (1965b) Urinary excretion kinetics of methylamphetamine in man. *J Pharm Pharmacol* **17**:109S–114S.

Beckett AH, and Rowland M (1965c) Urinary excretion of methylamphetamine in man. *Nature* **206**:1260–1261.

Belzer M, Morales M, Jagadish B, Mash EA, and Wright SH (2013) Substrate-dependent ligand inhibition of the human organic cation transporter OCT2. *J Pharmacol Exp Ther* **346**:300–310.

Bobulescu IA, and Moe OW (2009) Luminal Na+/H+ exchange in the proximal tubule. *Pflügers Arch - Eur J Physiol* **458**:5–21.

Bracchi M, Stuart D, Castles R, Khoo S, Back D, and Boffito M (2015) Increasing use of 'party drugs' in people living with HIV on antiretrovirals. *AIDS* **29**:1585–1592.

Brouwer KLR, Keppler D, Hoffmaster K a, Bow D a J, Cheng Y, Lai Y, Palm JE, Stieger B, Evers R, and International Transporter Consortium (2013) In vitro methods to support transporter evaluation in drug discovery and development. *Clin Pharmacol Ther* **94**:95–112.

Budiman T, Bamberg E, Koepsell H, and Nagel G (2000) Mechanism of electrogenic cation transport by the cloned organic cation transporter 2 from rat. *J Biol Chem* **275**:29413–29420.

Burt HJ, Neuhoff S, Almond L, Gaohua L, Harwood M, Jamei M, Rostami-Hodjegan A, Tucker GT, and Rowland-Yeo K (2016) Metformin and cimetidine: Physiologically based pharmacokinetic modelling to investigate transporter mediated drug–drug interactions. *Eur J Pharm Sci*, doi: 10.1016/j.ejps.2016.03.020, Elsevier B.V.

Caldwell J, Dring LG, and Williams RT (1972) Metabolism of (14 C)methamphetamine in man, the guinea pig and the rat. *Biochem J* **129**:11–22.
Carvalho M, Carmo H, Costa VM, Capela JP, Pontes H, Remião F, Carvalho F, and De Lourdes Bastos M (2012) Toxicity of amphetamines: An update. *Arch Toxicol* **86**:1167–1231.
Cashman JR, Xiong YN, Xu L, and Janowsky A (1999) N-oxygenation of amphetamine and methamphetamine by the human flavin-containing monooxygenase (form 3): role in bioactivation and detoxication. *J Pharmacol Exp Ther* **288**:1251–1260.
Cassolato SF, and Turnbull RS (2003) Xerostomia: clinical aspects and treatment. *Gerodontology* **20**:64–77.
Chen EC, Khuri N, Liang X, Stecula A, Chien H-C, Yee SW, Huang Y, Sali A, and Giacomini KM (2017) Discovery of Competitive and Noncompetitive Ligands of the Organic Cation Transporter 1 (OCT1; SLC22A1). *J Med Chem* **1**.
Chen EC, Liang X, Yee SW, Geier EG, Stocker SL, Chen L, and Giacomini KM (2015) Targeted Disruption of Organic Cation Transporter 3 Attenuates the Pharmacologic Response to Metformin. *Mol Pharmacol* **88**:75–83.
Chen L, Pawlikowski B, Schlessinger A, More SS, Stryke D, Johns SJ, Portman MA, Chen E, Ferrin TE, Sali A, and Giacomini KM (2010) Role of organic cation transporter 3 (SLC22A3) and its missense variants in the pharmacologic action of metformin. *Pharmacogenet Genomics* **20**:687–699.
Cheng Y, Martinez-Guerrero LJ, Wright SH, Kuester RK, Hooth MJ, and Sipes IG (2011) Characterization of the inhibitory effects of N-butylpyridinium chloride and structurally related ionic liquids on organic cation transporters 1/2 and human toxic extrusion transporters 1/2-k in vitro and in vivo. *Drug Metab Dispos* **39**:1755–1761.
Chien H-C, Zur AA, Maurer TS, Yee S-W, Tolsma J, Jasper P, Scott DO, and Giacomini KM (2015) Rapid Method to Determine Intracellular Drug Concentrations in Cellular Uptake Assays: Application to Metformin in OCT1-transfected HEK Cells. *Drug Metab Dispos* dmd.115.066647-.
Choi CI, Bae JW, Keum SK, Lee YJ, Lee HI, Jang CG, and Lee SY (2013) Effects of OCT2 c.602C > T genetic variant on the pharmacokinetics of lamivudine. *Xenobiotica* **43**:636–640.
Chu X, Korzekwa K, Elsby R, Fenner K, Galetin A, Lai Y, Matsson P, Moss A, Nagar S, Rosania GR, Bai JPF, Polli JW, Sugiyama Y, Brouwer KLR, and International Transporter Consortium (2013) Intracellular drug concentrations and transporters: measurement, modeling, and implications for the liver. *Clin Pharmacol Ther* **94**:126–41.
Ciarimboli G (2011) Role of organic cation transporters in drug-induced toxicity. *Expert Opin Drug Metab Toxicol* **7**:159–174.
Ciarimboli G, Koepsell H, Iordanova M, Gorboulev V, Durner B, Lang D, Edemir B, Schroter R, Van Le T, and Schlatter E (2005) Individual PKC-phosphorylation sites in organic cation transporter 1 determine substrate selectivity and transport regulation. *J Am Soc Nephrol* **16**:1562–1570.
Cook CE, Jeffcoat AR, Hill JM, Pugh DE, Patetta PK, Sadler BM, White WR, and Perez-Reyes M (1993) Pharmacokinetics of methamphetamine self-administered to human subjects by smoking S-(+)-methamphetamine hydrochloride. *Drug Metab Dispos* **21**:717–23.
Cook CE, Jeffcoat AR, Sadler BM, Hill JM, Voyksner RD, Pugh DE, White WR, and Perez-Reyes M (1992) Pharmacokinetics of oral methamphetamine and effects of repeated daily dosing in humans. *Drug Metab Dispos* **20**:856–862.

Copeland a. R (2000) *Enzymes: A Practical Introduction to Structure, Mechanism, and Data Analysis*.

Cui M, Aras R, Christian W V, Rappold PM, Hatwar M, Panza J, Jackson-Lewis V, Javitch JA, Ballatori N, Przedborski S, and Tieu K (2009) The organic cation transporter-3 is a pivotal modulator of neurodegeneration in the nigrostriatal dopaminergic pathway. *Proc Natl Acad Sci U S A* **106**:8043–8048.

de la Torre R, Farré M, Navarro M, Pacifici R, Zuccaro P, and Pichini S (2004) Clinical pharmacokinetics of amfetamine and related substances: monitoring in conventional and non-conventional matrices. *Clin Pharmacokinet* **43**:157–85.

DeGorter MK, Xia CQ, Yang JJ, and Kim RB (2012) Drug transporters in drug efficacy and toxicity. *Annu Rev Pharmacol Toxicol* **52**:249–273.

Deves R (1991) Kinetics of Transport: Characterizing the Interaction of Substrates and Inhibitors with Carrier Systems, in *Cell Membrane Transport: Experimental Approaches and Methodologies* (Yudilevich DL, Devés R, Perán S, and Cabantchik ZI eds) pp 3–19, Springer US, Boston, MA.

Deves R, and Krupka RM (1990) A simple test for the sidedness of binding of transport inhibitors. *Biochim Biophys Acta* **1030**:24–31.

Du W, Aloyo VJ, and Harvey JA (1997) Harmaline competitively inhibits [3H]MK-801 binding to the NMDA receptor in rabbit brain. *Brain Res* **770**:26–29.

Duan H, Hu T, Foti RS, Pan Y, Swaan PW, and Wang J (2015) Potent and Selective Inhibition of Plasma Membrane Monoamine Transporter by HIV Protease Inhibitors. *Drug Metab Dispos* **43**:1773–1780.

Duan H, and Wang J (2010) Selective transport of monoamine neurotransmitters by human plasma membrane monoamine transporter and organic cation transporter 3. *J Pharmacol Exp Ther* **335**:743–753.

Efron B, and Tibshirani RJ (1994) *An introduction to the bootstrap*, CRC press.

Engel K, and Wang J (2005) Interaction of organic cations with a newly identified plasma membrane monoamine transporter. *Mol Pharmacol* **68**:1397–1407.

Engel K, Zhou M, and Wang J (2004) Identification and characterization of a novel monoamine transporter in the human brain. *J Biol Chem* **279**:50042–50049.

European Medicines Agency (2012) *Guideline on the investigation of drug interactions*.

Fekkes D, and Bode WT (1993) Occurrence and partition of the beta-carboline norharman in rat organs. *Life Sci* **52**:2045–2054.

Fekkes D, Tuiten A, Bom I, and Pepplinkhuizen L (2001) Pharmacokinetics of the beta-carboline norharman in man. *Life Sci* **69**:2113–2121.

Food and Drug Administration (2012a) Draft guidance for industry: drug interaction studies—study design, data analysis, implications for dosing, and labeling recommendations. http://www.fda.gov/downloads/Drugs/GuidanceComplianceRegulatoryInformation/Guidances/UCM292362.pdf. *Food Drug Adm*, Silver Spring, MD.

Food and Drug Administration (2012b) *Guidance for industry. Drug interaction studies study design, data analysis, implications for dosing, and labeling recommendations*.

Food and Drug Administration (2017) *In Vitro Metabolism- and Transporter- Mediated Drug-Drug Interaction Studies Guidance for Industry*.

Fowler JS, Kroll C, Ferrieri R, Alexoff D, Logan J, Dewey SL, Schiffer W, Schlyer D, Carter P, King P, Shea C, Xu Y, Muench L, Benveniste H, Vaska P, and Volkow ND (2007) PET studies of d-methamphetamine pharmacokinetics in primates: comparison with l-

methamphetamine and (--)-cocaine. *J Nucl Med* **48**:1724–32.
Gasser PJ, Orchinik M, Raju I, and Lowry CA (2009) Distribution of organic cation transporter 3, a corticosterone-sensitive monoamine transporter, in the rat brain. *J Comp Neurol* **512**:529–555.
Gearhart DA, Neafsey EJ, and Collins MA (2002) Phenylethanolamine N-methyltransferase has beta-carboline 2N-methyltransferase activity: hypothetical relevance to Parkinson's disease. *Neurochem Int* **40**:611–620.
Giacomini KM, Tweedie DJ, Huang SM, Tweedie DJ, Benet LZ, Brouwer KL, Chu X, Dahlin A, Evers R, Fischer V, Hillgren KM, Hoffmaster KA, Ishikawa T, Keppler D, Kim RB, Lee CA, Niemi M, Polli JW, Sugiyama Y, Swaan PW, Ware JA, Wright SH, Yee SW, Zamek-Gliszczynski MJ, and Zhang L (2010) Membrane transporters in drug development. *Nat Rev Drug Discov* **9**:215–236.
Glennon RA, Dukat M, Grella B, Hong S, Costantino L, Teitler M, Smith C, Egan C, Davis K, and Mattson M V (2000) Binding of beta-carbolines and related agents at serotonin (5-HT(2) and 5-HT(1A)), dopamine (D(2)) and benzodiazepine receptors. *Drug Alcohol Depend* **60**:121–132.
Gockler N, Jofre G, Papadopoulos C, Soppa U, Tejedor FJ, and Becker W (2009) Harmine specifically inhibits protein kinase DYRK1A and interferes with neurite formation. *FEBS J* **276**:6324–6337.
Gong L, Goswami S, Giacomini KM, Altman RB, and Klein TE (2012) Metformin pathways.
Gorboulev V, Ulzheimer JC, Akhoundova A, Ulzheimer-Teuber I, Karbach U, Quester S, Baumann C, Lang F, Busch AE, and Koepsell H (1997) Cloning and characterization of two human polyspecific organic cation transporters. *DNA Cell Biol* **16**:871–881.
Gorboulev V, Volk C, Arndt P, Akhoundova A, and Koepsell H (1999) Selectivity of the polyspecific cation transporter rOCT1 is changed by mutation of aspartate 475 to glutamate. *Mol Pharmacol* **56**:1254–1261.
Gorbunov D, Gorboulev V, Shatskaya N, Mueller T, Bamberg E, Friedrich T, and Koepsell H (2008) High-affinity cation binding to organic cation transporter 1 induces movement of helix 11 and blocks transport after mutations in a modeled interaction domain between two helices. *Mol Pharmacol* **73**:50–61.
Graham GG, Punt J, Arora M, Day RO, Doogue MP, Duong JK, Furlong TJ, Greenfield JR, Greenup LC, Kirkpatrick CM, Ray JE, Timmins P, and Williams KM (2011) Clinical pharmacokinetics of metformin. *Clin Pharmacokinet* **50**:81–98.
Grundemann D, Gorboulev V, Gambaryan S, Veyhl M, Koepsell H, Gründemann D, Gorboulev V, Gambaryan S, Veyhl M, and Koepsell H (1994) Drug excretion mediated by a new prototype of polyspecific transporter. *Nature* **372**:549–552.
Grundemann D, Schechinger B, Rappold GA, and Schomig E (1998) Molecular identification of the corticosterone-sensitive extraneuronal catecholamine transporter. *Nat Neurosci* **1**:349–351.
Hacker K, Maas R, Kornhuber J, Fromm MF, and Zolk O (2015) Substrate-dependent inhibition of the human organic cation transporter OCT2: A comparison of metformin with experimental substrates. *PLoS One* **10**:1–16.
Hagenbuch B (2010) Drug uptake systems in liver and kidney: a historic perspective. *Clin Pharmacol Ther* **87**:39–47.
Hamamoto DT, and Rhodus NL (2009) Methamphetamine abuse and dentistry. *Oral Dis* **15**:27–37.

Hamann J, Rommelspacher H, Storch A, Reichmann H, and Gille G (2006) Neurotoxic mechanisms of 2,9-dimethyl-beta-carbolinium ion in primary dopaminergic culture. *J Neurochem* **98**:1185–1199.

Harper JN, and Wright SH (2012) Multiple Mechanisms of Ligand Interaction with the Human Organic Cation Transporter, OCT2. *AJP Ren Physiol* 56–67.

Harris DS, Boxenbaum H, Everhart ET, Sequeira G, Mendelson JE, and Jones RT (2003) The bioavailability of intranasal and smoked methamphetamine. *Clin Pharmacol Ther* **74**:475–486.

Herraiz T (2004) Relative exposure to beta-carbolines norharman and harman from foods and tobacco smoke. *Food Addit Contam* **21**:1041–1050.

Herraiz T (2000a) Tetrahydro-beta-carboline-3-carboxylic acid compounds in fish and meat: possible precursors of co-mutagenic beta-carbolines norharman and harman in cooked foods. *Food Addit Contam* **17**:859–866.

Herraiz T (2000b) Tetrahydro-beta-carbolines, potential neuroactive alkaloids, in chocolate and cocoa. *J Agric Food Chem* **48**:4900–4904.

Herraiz T, Gonzalez D, Ancin-Azpilicueta C, Aran VJ, and Guillen H (2010) beta-Carboline alkaloids in Peganum harmala and inhibition of human monoamine oxidase (MAO). *Food Chem Toxicol* **48**:839–845.

Herraiz T, Guillen H, and Galisteo J (2013) Metabolite profile resulting from the activation/inactivation of 1-methyl-4-phenyl-1,2,3,6-tetrahydropyridine and 2-methyltetrahydro-beta-carboline by oxidative enzymes. *Biomed Res Int* **2013**:248608.

Higgins JW, Bedwell DW, and Zamek-Gliszczynski MJ (2012) Ablation of both organic cation transporter (oct)1 and oct2 alters metformin pharmacokinetics but has no effect on tissue drug exposure and pharmacodynamics. *Drug Metab Dispos* **40**:1170–1177.

Hillgren KM, Keppler D, Zur AA, Giacomini KM, Stieger B, Cass CE, Zhang L, and International Transporter C (2013) Emerging transporters of clinical importance: an update from the International Transporter Consortium. *Clin Pharmacol Ther* **94**:52–63.

Ho HTB, Pan Y, Cui Z, Duan H, Swaan PW, and Wang J (2011) Molecular analysis and structure-activity relationship modeling of the substrate/inhibitor interaction site of plasma membrane monoamine transporter. *J Pharmacol Exp Ther* **339**:376–385.

Holsinger F, and Bui D (2007) Anatomy, function, and evaluation of the salivary glands. *Salivary Gland Disord pittsburgh Springer*.

Humphrey SP, and Williamson RT (2001) A review of saliva: Normal composition, flow, and function. *J Prosthet Dent* **85**:162–169.

Ishiguro N, Shimizu H, Kishimoto W, Ebner T, and Schaefer O (2013) Evaluation and prediction of potential drug-drug interactions of linagliptin using in vitro cell culture methods. *Drug Metab Dispos* **41**:149–158.

Itagaki S, Ganapathy V, Ho HT, Zhou M, Babu E, and Wang J (2012) Electrophysiological characterization of the polyspecific organic cation transporter plasma membrane monoamine transporter. *Drug Metab Dispos* **40**:1138–1143.

Ito S, Kusuhara H, Kuroiwa Y, Wu C, Moriyama Y, Inoue K, Kondo T, Yuasa H, Nakayama H, Horita S, and Sugiyama Y (2010) Potent and specific inhibition of mMate1-mediated efflux of type I organic cations in the liver and kidney by pyrimethamine. *J Pharmacol Exp Ther* **333**:341–350.

Ito S, Kusuhara H, Yokochi M, Toyoshima J, Inoue K, Yuasa H, and Sugiyama Y (2012) Competitive inhibition of the luminal efflux by multidrug and toxin extrusions, but not

basolateral uptake by organic cation transporter 2, is the likely mechanism underlying the pharmacokinetic drug-drug interactions caused by cimetidine in the kidney. *J Pharmacol Exp Ther* **340**:393–403.
Ivanyuk A, Livio F, Biollaz J, and Buclin T (2017) Renal Drug Transporters and Drug Interactions. *Clin Pharmacokinet*, doi: 10.1007/s40262-017-0506-8.
Iwai M, Minematsu T, Li Q, Iwatsubo T, and Usui T (2011) Utility of P-glycoprotein and organic cation transporter 1 double-transfected LLC-PK1 cells for studying the interaction of YM155 monobromide, novel small-molecule survivin suppressant, with P-glycoprotein. *Drug Metab Dispos* **39**:2314–2320.
Jaki T, and Wolfsegger MJ (2011) Estimation of pharmacokinetic parameters with the R package PK. *Pharm Stat* **10**:284–288.
Jiang XL, Shen HW, Mager DE, and Yu AM (2013) Pharmacokinetic interactions between monoamine oxidase A inhibitor harmaline and 5-methoxy-N,N-dimethyltryptamine, and the impact of CYP2D6 status. *Drug Metab Dispos* **41**:975–986.
Jung N, Lehmann C, Rubbert a., Schömig E, Fätkenheuer G, Hartmann P, and Taubert D (2013) Organic cation transporters OCT1 and OCT2 determine the accumulation of lamivudine in CD4 cells of HIV-infected patients. *Infection* **41**:379–385.
Jung N, Lehmann C, Rubbert A, Knispel M, Hartmann P, van Lunzen J, Stellbrink H-JJ, Faetkenheuer G, and Taubert D (2008) Relevance of the organic cation transporters 1 and 2 for antiretroviral drug therapy in human immunodeficiency virus infection. *Drug Metab …* **36**:1616–1623.
Kekuda R, Prasad PD, Wu X, Wang H, Fei YJ, Leibach FH, and Ganapathy V (1998) Cloning and functional characterization of a potential-sensitive, polyspecific organic cation transporter (OCT3) most abundantly expressed in placenta. *J Biol Chem* **273**:15971–15979.
Kenworthy KE, Bloomer JC, Clarke SE, and Houston JB (1999) CYP3A4 drug interactions: Correlation of 10 in vitro probe substrates. *Br J Clin Pharmacol* **48**:716–727.
Kido Y, Matsson P, and Giacomini KM (2011) Profiling of a prescription drug library for potential renal drug-drug interactions mediated by the organic cation transporter 2. *J Med Chem* **54**:4548–4558.
Kim H, Sablin SO, and Ramsay RR (1997) Inhibition of monoamine oxidase A by beta-carboline derivatives. *Arch Biochem Biophys* **337**:137–142.
Kim I, Oyler JM, Moolchan ET, Cone EJ, and Huestis MA (2004) Urinary pharmacokinetics of methamphetamine and its metabolite, amphetamine following controlled oral administration to humans. *Ther Drug Monit* **26**:664–672.
Kirpichnikov D, Mcfarlane SI, and Sowers JR (2002) Metformin: An Update. *Ann Intern Med*.
Kitaichi K, Fukuda M, Nakayama H, Aoyama N, Ito Y, Fujimoto Y, Takagi K, Takagi K, and Hasegawa T (2005) Behavioral changes following antisense oligonucleotide-induced reduction of organic cation transporter-3 in mice. *Neurosci Lett* **382**:195–200.
Kitaichi K, Morishita Y, Doi Y, Ueyama J, Matsushima M, Zhao Y-L, Takagi K, and Hasegawa T (2003) Increased plasma concentration and brain penetration of methamphetamine in behaviorally sensitized rats. *Eur J Pharmacol* **464**:39–48.
Klaassen CD, and Aleksunes LM (2010) Xenobiotic, Bile Acid, and Cholesterol Transporters: Function and Regulation. *Pharmacol Rev* **62**:1–96.
Koepsell H (2004) Polyspecific organic cation transporters: their functions and interactions with drugs. *Trends Pharmacol Sci* **25**:375–381.
Koepsell H (2015) Role of organic cation transporters in drug–drug interaction. *Expert Opin*

Drug Metab Toxicol **11**:1619–1633.
Koepsell H (2011) Substrate recognition and translocation by polyspecific organic cation transporters. *Biol Chem* **392**:95–101.
Koepsell H (2013) The SLC22 family with transporters of organic cations, anions and zwitterions. *Mol Asp Med* **34**:413–435.
Koepsell H, Busch A, Gorboulev V, and Arndt P (1998) Structure and Function of Renal Organic Cation Transporters. *News Physiol Sci* **13**:11–16.
Koepsell H, and Endou H (2004) The SLC22 drug transporter family. *Pflugers Arch* **447**:666–676.
Koepsell H, Lips K, and Volk C (2007) Polyspecific organic cation transporters: Structure, function, physiological roles, and biopharmaceutical implications. *Pharm Res* **24**:1227–1251.
Koepsell H, Schmitt BM, and Gorboulev V (2003) Organic cation transporters. *Rev Physiol Biochem Pharmacol* **150**:36–90.
Komatsu T, Hiasa M, Miyaji T, Kanamoto T, Matsumoto T, Otsuka M, Moriyama Y, and Omote H (2011) Characterization of the human MATE2 proton-coupled polyspecific organic cation exporter. *Int J Biochem Cell Biol* **43**:913–918, Elsevier Ltd.
Krupka RM, and Devés R (1980) Asymmetric binding of steroids to internal and external sites in the glucose carrier of erythrocytes. *Biochim Biophys Acta* **598**:134–44.
Krupka RM, and Devés R (1983) Kinetics of inhibition of transport systems. *Int Rev Cytol* **84**:303–52.
Lai Y, Sampson KE, Balogh LM, Brayman TG, Cox SR, Adams WJ, Kumar V, and Stevens JC (2010) Preclinical and clinical evidence for the collaborative transport and renal secretion of an oxazolidinone antibiotic by organic anion transporter 3 (OAT3/SLC22A8) and multidrug and toxin extrusion protein 1 (MATE1/SLC47A1). *J Pharmacol Exp Ther* **334**:936–944.
Lee N, Duan H, Hebert MF, Liang CJ, Rice KM, and Wang J (2014) Taste of a Pill: ORGANIC CATION TRANSPORTER-3 (OCT3) MEDIATES METFORMIN ACCUMULATION AND SECRETION IN SALIVARY GLANDS. *J Biol Chem* **289**:27055–27064.
Lee N, Hebert MF, Prasad B, Easterling TR, Kelly EJ, Unadkat JD, and Wang J (2013) Effect of gestational age on mRNA and protein expression of polyspecific organic cation transporters during pregnancy. *Drug Metab Dispos* **41**:2225–2232.
Li M, Anderson GD, and Wang J (2006) Drug-drug interactions involving membrane transporters in the human kidney. *Expert Opin Drug Metab Toxicol* **2**:505–532.
Li Q, and Shu Y (2014) Role of solute carriers in response to anticancer drugs. *Mol Cell Ther* **2**:15.
Lin LY, Di Stefano EW, Schmitz DA, Hsu L, Ellis SW, Lennard MS, Tucker GT, and Cho AK (1997) Oxidation of methamphetamine and methylenedioxymethamphetamine by CYP2D6. *Drug Metab Dispos* **25**:1059–64.
Lips KS, Volk C, Schmitt BM, Pfeil U, Arndt P, Miska D, Ermert L, Kummer W, and Koepsell H (2005) Polyspecific cation transporters mediate luminal release of acetylcholine from bronchial epithelium. *Am J Respir Cell Mol Biol* **33**:79–88.
Louis ED, Jiang W, Gerbin M, Mullaney MM, and Zheng W (2010) Relationship between blood harmane and harmine concentrations in familial essential tremor, sporadic essential tremor and controls. *Neurotoxicology* **31**:674–679.
Maeda K, Tian Y, Fujita T, Ikeda Y, Kumagai Y, Kondo T, Tanabe K, Nakayama H, Horita S, Kusuhara H, and Sugiyama Y (2014) Inhibitory effects of p-aminohippurate and probenecid

on the renal clearance of adefovir and benzylpenicillin as probe drugs for organic anion transporter (OAT) 1 and OAT3 in humans. *Eur J Pharm Sci* **59**:94–103, Elsevier B.V.
Mager H, and Göller G (1998) Resampling methods in sparse sampling situations in preclinical pharmacokinetic studies. *J Pharm Sci* **87**:372–378.
Mason JN, Farmer H, Tomlinson ID, Schwartz JW, Savchenko V, DeFelice LJ, Rosenthal SJ, and Blakely RD (2005) Novel fluorescence-based approaches for the study of biogenic amine transporter localization, activity, and regulation. *J Neurosci Methods* **143**:3–25.
Masuda S, Terada T, Yonezawa A, Tanihara Y, Kishimoto K, Katsura T, Ogawa O, and Inui K (2006) Identification and functional characterization of a new human kidney-specific H+/organic cation antiporter, kidney-specific multidrug and toxin extrusion 2. *J Am Soc Nephrol* **17**:2127–2135.
Matsubara K, Collins MA, Akane A, Ikebuchi J, Neafsey EJ, Kagawa M, and Shiono H (1993) Potential bioactivated neurotoxicants, N-methylated beta-carbolinium ions, are present in human brain. *Brain Res* **610**:90–96.
Matsubara K, Kobayashi S, Kobayashi Y, Yamashita K, Koide H, Hatta M, Iwamoto K, Tanaka O, and Kimura K (1995) beta-Carbolinium cations, endogenous MPP+ analogs, in the lumbar cerebrospinal fluid of patients with Parkinson's disease. *Neurology* **45**:2240–2245.
Maxwell JC, and Rutkowski B a (2008) The prevalence of methamphetamine and amphetamine abuse in North America: a review of the indicators, 1992-2007. *Drug Alcohol Rev* **27**:229–235.
McKenna DJ (2004) Clinical investigations of the therapeutic potential of ayahuasca: rationale and regulatory challenges. *Pharmacol Ther* **102**:111–129.
Meijer DK, Mol WE, Muller M, and Kurz G (1990) Carrier-mediated transport in the hepatic distribution and elimination of drugs, with special reference to the category of organic cations. *J Pharmacokinet Biopharm* **18**:35–70.
Melega WP, Cho AK, Harvey D, and Laćan G (2007) Methamphetamine blood concentrations in human abusers: Application to pharmacokinetic modeling. *Synapse* **61**:216–220.
Meyer MR, Caspar A, Brandt SD, and Maurer HH (2014) A qualitative/quantitative approach for the detection of 37 tryptamine-derived designer drugs, 5 ??-carbolines, ibogaine, and yohimbine in human urine and plasma using standard urine screening and multi-analyte approaches. *Anal Bioanal Chem* **406**:225–237.
Miners JO, Yang X, Knights KM, and Zhang L (2017) The Role of the Kidney in Drug Elimination: Transport, Metabolism, and the Impact of Kidney Disease on Drug Clearance. *Clin Pharmacol Ther* **102**:436–449.
Minuesa G, Purcet S, Erkizia I, Molina-Arcas M, Bofill M, Izquierdo-Useros N, Casado FJ, Clotet B, Pastor-Anglada M, and Martinez-Picado J (2008) Expression and functionality of anti-human immunodeficiency virus and anticancer drug uptake transporters in immune cells. *J Pharmacol Exp Ther* **324**:558–567.
Minuesa G, Volk C, Molina-Arcas M, Gorboulev V, Erkizia I, Arndt P, Clotet B, Pastor-Anglada M, Koepsell H, and Martinez-Picado J (2009) Transport of lamivudine [(-)-beta-L-2',3'-dideoxy-3'-thiacytidine] and high-affinity interaction of nucleoside reverse transcriptase inhibitors with human organic cation transporters 1, 2, and 3. *J Pharmacol Exp Ther* **329**:252–61.
Moaddel R, Yamaguchi R, Ho PC, Patel S, Hsu CP, Subrahmanyam V, and Wainer IW (2005) Development and characterization of an immobilized human organic cation transporter based liquid chromatographic stationary phase. *J Chromatogr B Anal Technol Biomed Life*

Sci **818**:263–268.
Morrissey KM, Stocker SL, Wittwer MB, Xu L, and Giacomini KM (2013) Renal transporters in drug development. *Annu Rev Pharmacol Toxicol* **53**:503–29.
Motohashi H, and Inui K (2013) Organic cation transporter OCTs (SLC22) and MATEs (SLC47) in the human kidney. *AAPS J* **15**:581–588.
Motohashi H, Sakurai Y, Saito H, Masuda S, Urakami Y, Goto M, Fukatsu A, Ogawa O, and Inui K (2002) Gene expression levels and immunolocalization of organic ion transporters in the human kidney. *J Am Soc Nephrol* **13**:866–874.
Moule SK, and McGivan JD (1990) Regulation of the plasma membrane potential in hepatocytes--mechanism and physiological significance. *Biochim Biophys Acta* **1031**:383–397.
Müller F, König J, Hoier E, Mandery K, and Fromm MF (2013) Role of organic cation transporter OCT2 and multidrug and toxin extrusion proteins MATE1 and MATE2-K for transport and drug interactions of the antiviral lamivudine. *Biochem Pharmacol* **86**:808–815.
Neuhoff S, Ungell AL, Zamora I, and Artursson P (2003) pH-dependent bidirectional transport of weakly basic drugs across Caco-2 monolayers: implications for drug-drug interactions. *Pharm Res* **20**:1141–1148.
Newton TF, Roache JD, De La Garza R, Fong T, Wallace CL, Li S-H, Elkashef A, Chiang N, and Kahn R (2005) Safety of intravenous methamphetamine administration during treatment with bupropion. *Psychopharmacology (Berl)* **182**:426–435.
Nies AT, Damme K, Schaeffeler E, and Schwab M (2012) Multidrug and toxin extrusion proteins as transporters of antimicrobial drugs. *Expert Opin Drug Metab Toxicol* **8**:1565–1577.
Nies AT, Koepsell H, Damme K, and Schwab M (2011) Organic cation transporters (OCTs, MATEs), in vitro and in vivo evidence for the importance in drug therapy., in *Handbook of experimental pharmacology* pp 105–67.
Nies AT, Koepsell H, Winter S, Burk O, Klein K, Kerb R, Zanger UM, Keppler D, Schwab M, and Schaeffeler E (2009) Expression of organic cation transporters OCT1 (SLC22A1) and OCT3 (SLC22A3) is affected by genetic factors and cholestasis in human liver. *Hepatology* **50**:1227–1240.
Nishimura M, and Naito S (2005) Tissue-specific mRNA expression profiles of human ATP-binding cassette and solute carrier transporter superfamilies. *Drug Metab Pharmacokinet* **20**:452–477.
Nussberger J, Fasanella d'Amore T, Porchet M, Waeber B, Brunner DB, Brunner HR, Kler L, Brown AN, and Francis RJ (1987) Repeated administration of the converting enzyme inhibitor cilazapril to normal volunteers. *J Cardiovasc Pharmacol* **9**:39–44.
Ohta KY, Inoue K, Yasujima T, Ishimaru M, and Yuasa H (2009) Functional characteristics of two human MATE transporters: kinetics of cimetidine transport and profiles of inhibition by various compounds. *J Pharm Pharm Sci* **12**:388–396.
Okuda M, Saito H, Urakami Y, Takano M, and Inui K (1996) cDNA cloning and functional expression of a novel rat kidney organic cation transporter, OCT2. *Biochem Biophys Res Commun* **224**:500–507.
Oliveira CD, Okai GG, da Costa JL, de Almeida RM, Oliveira-Silva D, and Yonamine M (2012) Determination of dimethyltryptamine and beta-carbolines (ayahuasca alkaloids) in plasma samples by LC-MS/MS. *Bioanalysis* **4**:1731–1738.

Otsuka M, Matsumoto T, Morimoto R, Arioka S, Omote H, and Moriyama Y (2005) A human transporter protein that mediates the final excretion step for toxic organic cations. *Proc Natl Acad Sci U S A* **102**:17923–17928.

Panenka WJ, Procyshyn RM, Lecomte T, MacEwan GW, Flynn SW, Honer WG, and Barr AM (2013) Methamphetamine use: a comprehensive review of molecular, preclinical and clinical findings. *Drug Alcohol Depend* **129**:167–79, Elsevier Ireland Ltd.

Parker CA, Anderson NJ, Robinson ES, Price R, Tyacke RJ, Husbands SM, Dillon MP, Eglen RM, Hudson AL, Nutt DJ, Crump MP, and Crosby J (2004) Harmane and harmalan are bioactive components of classical clonidine-displacing substance. *Biochemistry* **43**:16385–16392.

Pfau W, and Skog K (2004) Exposure to beta-carbolines norharman and harman. *J Chromatogr B Anal Technol Biomed Life Sci* **802**:115–126.

Popp C, Gorboulev V, Müller TD, Gorbunov D, Shatskaya N, and Koepsell H (2005) Amino acids critical for substrate affinity of rat organic cation transporter 1 line the substrate binding region in a model derived from the tertiary structure of lactose permease. *Mol Pharmacol* **67**:1600–1611.

Pritchard JB, and Miller DS (1993) Mechanisms Mediating Renal Secretion of Organic-Anions and Cations. *Physiol Rev* **73**:765–796.

Pritzker D, Kanungo A, Kilicarslan T, Tyndale RF, and Sellers EM (2002) Designer drugs that are potent inhibitors of CYP2D6. *J Clin Psychopharmacol* **22**:330–2.

R Core Team (2017) R: A language and environment for statistical computing., R Foundation for Statistical Computing, Vienna, Austria.

R Studio (2012) R Studio: integrated development environment for R, Boston, MA.

Ravenel MC, Salinas CF, Marlow NM, Slate EH, Evans ZP, and Miller PM (2012) Methamphetamine abuse and oral health: a pilot study of "meth mouth". *Quintessence Int* **43**:229–237.

Reese MJ, Savina PM, Generaux GT, Tracey H, Humphreys JE, Kanaoka E, Webster LO, Harmon KA, Clarke JD, and Polli JW (2013) In vitro investigations into the roles of drug transporters and metabolizing enzymes in the disposition and drug interactions of dolutegravir, a hiv integrase inhibitor. *Drug Metab Dispos* **41**:353–361.

Riba J, McIlhenny EH, Valle M, Bouso JC, and Barker SA (2012) Metabolism and disposition of N,N-dimethyltryptamine and harmala alkaloids after oral administration of ayahuasca. *Drug Test Anal* **4**:610–616.

Riba J, Valle M, Urbano G, Yritia M, Morte A, and Barbanoj MJ (2003) Human pharmacology of ayahuasca: subjective and cardiovascular effects, monoamine metabolite excretion, and pharmacokinetics. *J Pharmacol Exp Ther* **306**:73–83.

Richling E, Herderich M, and Schreier P (1996) High performance liquid chromatography — Electrospray tandem mass spectrometry (HPLC-ESI-MS-MS) for the analysis of heterocyclic aromatic amines (HAA). *Chromatographia* **42**:7–11.

Rivière GJ, Gentry WB, and Owens SM (2000) Disposition of methamphetamine and its metabolite amphetamine in brain and other tissues in rats after intravenous administration. *J Pharmacol Exp Ther* **292**:1042–1047.

Robinson ES, Anderson NJ, Crosby J, Nutt DJ, and Hudson AL (2003) Endogenous beta-carbolines as clonidine-displacing substances. *Ann N Y Acad Sci* **1009**:157–166.

Römhild W, Krause D, Bartels H, Ghanem a., Schöning R, and Wittig H (2003) LC-MS/MS analysis of pholedrine in a fatal intoxication case. *Forensic Sci Int* **133**:101–106.

Rommelspacher H, May T, and Salewski B (1994) Harman (1-methyl-beta-carboline) is a natural inhibitor of monoamine oxidase type A in rats. *Eur J Pharmacol* **252**:51–59.
Saadatmand AR, Tadjerpisheh S, Brockmoller J, and Tzvetkov M V (2012) The prototypic pharmacogenetic drug debrisoquine is a substrate of the genetically polymorphic organic cation transporter OCT1. *Biochem Pharmacol* **83**:1427–1434.
Sala-Rabanal M, Li DC, Dake GR, Kurata HT, Inyushin M, Skatchkov SN, and Nichols CG (2013) Polyamine transport by the polyspecific organic cation transporters OCT1, OCT2, and OCT3. *Mol Pharm* **10**:1450–1458.
Sata R, Ohtani H, Tsujimoto M, Murakami H, Koyabu N, Nakamura T, Uchiumi T, Kuwano M, Nagata H, Tsukimori K, Nakano H, and Sawada Y (2005) Functional analysis of organic cation transporter 3 expressed in human placenta. *J Pharmacol Exp Ther* **315**:888–895.
Scheen AJ (1996) Clinical pharmacokinetics of metformin. *Clin Pharmacokinet* **30**:359–371.
Schep LJ, Slaughter RJ, and Beasley DMG (2010) The clinical toxicology of metamfetamine. *Clin Toxicol* **48**:675–694.
Segel IH (1976) *Enzyme kinetics: Behavior and analysis of rapid equilibrium and steady-state enzyme systems*.
Shaner JW, Kimmes N, Saini T, and Edwards P (2006) "Meth mouth": rampant caries in methamphetamine abusers. *AIDS Patient Care STDS* **20**:146–150.
Shang T, Uihlein A V, Van Asten J, Kalyanaraman B, and Hillard CJ (2003) 1-Methyl-4-phenylpyridinium accumulates in cerebellar granule neurons via organic cation transporter 3. *J Neurochem* **85**:358–367.
Shima N, Kamata HT, Katagi M, and Tsuchihashi H (2006) Urinary excretion of the main metabolites of methamphetamine, including p-hydroxymethamphetamine-sulfate and p-hydroxymethamphetamine-glucuronide, in humans and rats. *Xenobiotica* **36**:259–267.
Shima N, Katagi M, Kamata H, Zaitsu K, Kamata T, Miki A, Tsuchihashi H, Sakuma T, and Nemoto N (2008) Conjugates of p-hydroxymethamphetamine and 4-hydroxy-3-methoxymethamphetamine in blood obtained from methamphetamine and 3,4-methylenedioxymethamphetamine users: Analysis by LC-MS-MS. *Forensic Toxicol* **26**:58–65.
Shima N, Katagi M, and Tsuchihashi H (2009) Direct Analysis of Conjugate Metabolites of and Their Designer Drugs in Biological Fluids. *J Heal Sci* **55**:495–502.
Shirasaka Y, Lee N, Zha W, Wagner D, and Wang J (2016) Involvement of Organic Cation Transporter 3 (Oct3/Slc22a3) in the Bioavailability and Pharmacokinetics of Antidiabetic Metformin in Mice. *Drug Metab Pharmacokinet* **3**:385–388, Elsevier Ltd.
Shu Y, Brown C, Castro RA, Shi RJ, Lin ET, Owen RP, Sheardown SA, Yue L, Burchard EG, Brett CM, and Giacomini KM (2008) Effect of genetic variation in the organic cation transporter 1, OCT1, on metformin pharmacokinetics. *Clin Pharmacol Ther* **83**:273–280.
Shu Y, Sheardown SAS, Brown C, Owen RP, Zhang S, Castro RA, Ianculescu AG, Yue L, Lo JC, Burchard EG, Brett CM, and Giacomini KM (2007) Effect of genetic variation in the organic cation transporter 1 (OCT1) on metformin action. *J Clin …* **117**:1422–31.
Slotkin TA, DiSTEFANO V, and AU WYW (1970) Blood levels and urinary excretion of harmine and its metabolites in man and rats. *J Pharmacol Exp Ther* **173**:26–30.
Smith D a, Di L, and Kerns EH (2010) The effect of plasma protein binding on in vivo efficacy: misconceptions in drug discovery. *Nat Rev Drug Discov* **9**:929–939.
Smith KL, Ford GK, Jessop DS, and Finn DP (2013) Behavioural, neurochemical and neuroendocrine effects of the endogenous beta-carboline harmane in fear-conditioned rats. *J*

Psychopharmacol **27**:162–170.
Song IS, Shin HJ, Shim EJ, Jung IS, Kim WY, Shon JH, and Shin JG (2008) Genetic variants of the organic cation transporter 2 influence the disposition of metformin. *Clin Pharmacol Ther* **84**:559–62.
Staud F, Cerveny L, Ahmadimoghaddam D, and Ceckova M (2013) Multidrug and toxin extrusion proteins (MATE/SLC47); role in pharmacokinetics. *Int J Biochem Cell Biol* **45**:2007–2011, Elsevier Ltd.
Stein WD (1986) *Transport and diffusion across cell membranes*, Academic Press Inc.
Stein WD, and Litman T (2014) *Channels, carriers, and pumps : an introduction to membrane transport*, Elsevier.
Storch A, Hwang YI, Gearhart DA, Beach JW, Neafsey EJ, Collins MA, and Schwarz J (2004) Dopamine transporter-mediated cytotoxicity of beta-carbolinium derivatives related to Parkinson's disease: relationship to transporter-dependent uptake. *J Neurochem* **89**:685–694.
Strazzabosco M, Sakisaka S, Hayakawa T, and Boyer JL (1991) Effect of UDCA on intracellular and biliary pH in isolated rat hepatocyte couplets and perfused livers. *Am J Physiol* **260**:G58-69.
Takane H, Shikata E, Otsubo K, Higuchi S, and Ieiri I (2008) Polymorphism in human organic cation transporters and metformin action. *Pharmacogenomics* **9**:415–422.
Tanihara Y, Masuda S, Sato T, Katsura T, Ogawa O, and Inui KI (2007) Substrate specificity of MATE1 and MATE2-K, human multidrug and toxin extrusions/H+-organic cation antiporters. *Biochem Pharmacol* **74**:359–371.
Thévenod F, Ciarimboli G, Leistner M, Wolff NA, Lee WK, Schatz I, Keller T, Al-Monajjed R, Gorboulev V, Koepsell H, Thevenod F, Ciarimboli G, Leistner M, Wolff NA, Lee WK, Schatz I, Keller T, Al-Monajjed R, Gorboulev V, and Koepsell H (2013) Substrate- and cell contact-dependent inhibitor affinity of human organic cation transporter 2: studies with two classical organic cation substrates and the novel substrate cd2+. *Mol Pharm* **10**:3045–3056.
Totsuka Y, Ushiyama H, Ishihara J, Sinha R, Goto S, Sugimura T, and Wakabayashi K (1999) Quantification of the co-mutagenic beta-carbolines, norharman and harman, in cigarette smoke condensates and cooked foods. *Cancer Lett* **143**:139–143.
Volkow ND (2013) *Research Report Series: Methamphetamine*, Rockville, MD.
Volkow ND, Fowler JS, Wang GJ, Shumay E, Telang F, Thanos PK, and Alexoff D (2010) Distribution and pharmacokinetics of methamphetamine in the human body: Clinical implications. *PLoS One* **5**:1–6.
Wagner DJ, Hu T, and Wang J (2016) Polyspecific organic cation transporters and their impact on drug intracellular levels and pharmacodynamics. *Pharmacol Res* **111**:237–246, Elsevier Ltd.
Wagner DJ, Sager JE, Duan H, Isoherranen N, and Wang J (2017) Interaction and Transport of Methamphetamine and its Primary Metabolites by Organic Cation and Multidrug and Toxin Extrusion Transporters. *Drug Metab Dispos* **45**:770–778.
Wang D-SS, Jonker JW, Kato Y, Kusuhara H, Schinkel AH, and Sugiyama Y (2002) Involvement of organic cation transporter 1 in hepatic and intestinal distribution of metformin. *J Pharmacol Exp Ther* **302**:510–515.
Wang ZJ, Yin OQ, Tomlinson B, and Chow MS (2008) OCT2 polymorphisms and in-vivo renal functional consequence: studies with metformin and cimetidine. *Pharmacogenet Genomics* **18**:637–645.

Westfall PH, and Young SS (1993) *Resampling-based multiple testing: Examples and methods for p-value adjustment*, John Wiley & Sons.
Whelton H (1996) Introduction: The Anatomy and Physiology of Salivary Glands, in *Saliva and Oral Health* pp 1–36.
Wright SH (2005) Role of organic cation transporters in the renal handling of therapeutic agents and xenobiotics. *Toxicol Appl Pharmacol* **204**:309–319.
Wright SH, and Dantzler WH (2004) Molecular and cellular physiology of renal organic cation and anion transport. *Physiol Rev* **84**:987–1049.
Wright SH, and Wunz TM (1987) Transport of tetraethylammonium by rabbit renal brush-border and basolateral membrane vesicles. *Am J Physiol* **253**:F1040-50.
Wu C, Jiang XL, Shen HW, and Yu AM (2009) Effects of CYP2D6 status on harmaline metabolism, pharmacokinetics and pharmacodynamics, and a pharmacogenetics-based pharmacokinetic model. *Biochem Pharmacol* **78**:617–624.
Wu D, Victoria Otton S, Inaba T, Kalow W, and Sellers EM (1997) Interactions of amphetamine analogs with human liver CYP2D6. *Biochem Pharmacol* **53**:1605–1612.
Wu X, Huang W, Ganapathy ME, Wang H, Kekuda R, Conway SJ, Leibach FH, and Ganapathy V (2000) Structure, function, and regional distribution of the organic cation transporter OCT3 in the kidney. *Am J Physiol Ren Physiol* **279**:F449-58.
Wu X, Kekuda R, Huang W, Fei YJ, Leibach FH, Chen J, Conway SJ, and Ganapathy V (1998) Identity of the Organic Cation Transporter OCT3 as the Extraneuronal Monoamine Transporter (uptake2) and Evidence for the Expression of the Transporter in the Brain. *J Biol Chem* **273**:32776–32786.
Xia L, Engel K, Zhou M, and Wang J (2007) Membrane localization and pH-dependent transport of a newly cloned organic cation transporter (PMAT) in kidney cells. *Am J Physiol Ren Physiol* **292**:F682-90.
Yang YJ, Lee JJ, Jin CM, Lim SC, and Lee MK (2008) Effects of harman and norharman on dopamine biosynthesis and L-DOPA-induced cytotoxicity in PC12 cells. *Eur J Pharmacol* **587**:57–64.
Yin J, Duan H, Shirasaka Y, Prasad B, and Wang J (2015) Atenolol Renal Secretion Is Mediated by Human Organic Cation Transporter 2 and Multidrug and Toxin Extrusion Proteins. *Drug Metab Dispos* **43**:1872–1881.
Yin J, Duan H, and Wang J (2016) Impact of Substrate-Dependent Inhibition on Renal Organic Cation Transporters hOCT2- and hMATE1/2-K-mediated Drug Transport and Intracellular Accumulation. *J Pharmacol Exp Ther* **359**:401–410.
Yin J, and Wang J (2016) Renal drug transporters and their significance in drug-drug interactions. *Acta Pharm Sin B* **6**:363–373, Elsevier.
Yokoo S, Yonezawa A, Masuda S, Fukatsu A, Katsura T, and Inui KI (2007) Differential contribution of organic cation transporters, OCT2 and MATE1, in platinum agent-induced nephrotoxicity. *Biochem Pharmacol* **74**:477–487.
Yonezawa A, and Inui KI (2011) Organic cation transporter OCT/SLC22A and H+/organic cation antiporter MATE/SLC47A are key molecules for nephrotoxicity of platinum agents. *Biochem Pharmacol* **81**:563–568, Elsevier Inc.
Yonezawa A, Masuda S, Yokoo S, Katsura T, and Inui K-I (2006) Cisplatin and oxaliplatin, but not carboplatin and nedaplatin, are substrates for human organic cation transporters (SLC22A1-3 and multidrug and toxin extrusion family). *J Pharmacol Exp Ther* **319**:879–886.

Yoon H, Cho H-Y, Yoo H-D, Kim S-M, and Lee Y-B (2013) Influences of organic cation transporter polymorphisms on the population pharmacokinetics of metformin in healthy subjects. *AAPS J* **15**:571–80.

Yu AM (2008) Indolealkylamines: biotransformations and potential drug-drug interactions. *AAPS J* **10**:242–253.

Zamek-Gliszczynski MJ, Bao JQ, Day JS, and Higgins JW (2013) Metformin sinusoidal efflux from the liver is consistent with negligible biliary excretion and absence of enterohepatic cycling. *Drug Metab Dispos* **41**:1967–1971.

Zamek-Gliszczynski MJ, Lee C a, Poirier a, Bentz J, Chu X, Ellens H, Ishikawa T, Jamei M, Kalvass JC, Nagar S, Pang KS, Korzekwa K, Swaan PW, Taub ME, Zhao P, and Galetin a (2013) ITC Recommendations for Transporter Kinetic Parameter Estimation and Translational Modeling of Transport-Mediated PK and DDIs in Humans. *Clin Pharmacol Ther* 1–16.

Zetler G, Back G, and Iven H (1974) PHARMACOKINETICS In the rat of the hallucinogenic alkaloids harmine and harmaline. *Naunyn Schmiedebergs Arch Pharmacol* **285**:273–92.

Zhang L, Dresser MJ, Gray AT, Yost SC, Terashita S, and Giacomini KM (1997) Cloning and functional expression of a human liver organic cation transporter. *Mol Pharmacol* **51**:913–921.

Zhang L, Reynolds KS, Zhao P, and Huang SM (2010) Drug interactions evaluation: an integrated part of risk assessment of therapeutics. *Toxicol Appl Pharmacol* **243**:134–145.

Zhao T, He YQ, Wang J, Ding KM, Wang CH, and Wang ZT (2011) Inhibition of human cytochrome P450 enzymes 3A4 and 2D6 by beta-carboline alkaloids, harmine derivatives. *Phytother Res* **25**:1671–1677.

Zhou M, Engel K, and Wang J (2007) Evidence for significant contribution of a newly identified monoamine transporter (PMAT) to serotonin uptake in the human brain. *Biochem Pharmacol* **73**:147–154.

Zhou M, Xia L, and Wang J (2007) Metformin transport by a newly cloned proton-stimulated organic cation transporter (plasma membrane monoamine transporter) expressed in human intestine. *Drug Metab Dispos* **35**:1956–1962.

Zhou Z, Rodman JH, Flynn PM, Robbins BL, Wilcox CK, and D'Argenio DZ (2006) Model for intracellular lamivudine metabolism in peripheral blood mononuclear cells ex vivo and in human immunodeficiency virus type 1-infected adolescents. *Antimicrob Agents Chemother* **50**:2686–2694.

Zhu HJ, Appel DI, Gründemann D, and Markowitz JS (2010) Interaction of organic cation transporter 3 (SLC22A3) and amphetamine. *J Neurochem* **114**:142–149.

Zwart R, Verhaagh S, Buitelaar M, Barlow DP, and Popp-snijders C (2001) Impaired Activity of the Extraneuronal Monoamine Transporter System Known as Uptake-2 in Orct3 / Slc22a3-Deficient Mice Impaired Activity of the Extraneuronal Monoamine Transporter System Known as Uptake-2 in Orct3 / Slc22a3- Deficient Mice. *Mol Cell Biol* **21**:4188–4196.

VITA

David James Wagner was born and raised in Minnesota where he attended St. Croix Lutheran High School. He received a Bachelor of Science in Biology with a minor in Environmental Studies from Boston College in Chestnut Hill, Massachusetts. In his free time, he enjoys reading and rock climbing.